FLUORESCENT POLYMER BASED POST-TRANSLATIONAL DIFFERENTIATION AND SUBTYPING OF CANCER CELLS

A Dissertation
Submitted to the Graduate Faculty
of the
North Dakota State University
of Agriculture and Applied Sciences

By

Michael David Scott

In Partial Fulfillment
For the Degree of
DOCTOR OF PHILOSOPHY

Major Department:
Pharmaceutical Sciences

July 2012

Fargo, North Dakota

North Dakota State University
Graduate School

Title

FLUORESCENT POLYMER BASED POST-TRANSLATIONAL DIFFERENTIATION AND SUBTYPING OF CANCER CELLS

By

Michael David Scott

The Supervisory Committee certifies that this ***disquisition*** complies with North Dakota State University's regulations and meets the accepted standards for the degree of

DOCTOR OF PHILOSOPHY

SUPERVISORY COMMITTEE:

Dr. Sanku Mallik
Chair

Dr. Benedict Law

Dr. Chengwen Sun

Dr. Katie Reindl

Dr. Daniel Friesner

Approved:

6/17/2012
Date

Dr. Jagdish Singh
Department Chair

ABSTRACT

The field of personalized medicine is focused on gathering information at a pre-translational level. Although this information is useful, it is becoming increasingly apparent that post-translational expression is not always consistent with that of the DNA or mRNA. Thus to advance personalized medicine, the development of additional technologies to gather disease state information at post-translational levels are necessary.

This dissertation is focused on the advancement of fluorescent polymer technology to monitor at a secretomics level. Secretomics is a subset of proteomics that is focused on secreted proteins/enzymes from the cell. To monitor these secreted proteins, polymers were synthesized from the monomer state, with a polymerizable moiety of 4-vinylbenzoic acid. This compound was conjugated to various amino acids, alcohol derivatives, fluorophores, and metalloproteinase inhibitors. The monomer composition was thus varied to generate a library of polymers capable of forming unique interactions with proteins and enzymes.

This polymeric library was screened against recombinant human MMP-7, -9, and -10. The fluorescent emissions data was subsequently evaluated using statistical analysis. This analysis provided information regarding an optimal polymer formulation for MMP isozyme specific interactions.

This polymer was subsequently screened against both breast and prostate cancer cell conditioned media. This media were prepared such that the polymers would only interact with secreted proteins/enzymes (*i.e.* secretomics). Again fluorescence emissions data were evaluated using statistical analysis (linear discriminate analysis [LDA]) to demonstrate the polymer could distinguish between the subtypes, or sub-classification of the cancerous cells.

Replacement of the fluorophore with a more hydrophilic pyranine improved the water solubility of the polymer. This polymer was thus screened against both the prostate and breast cancer conditioned media and evaluated using LDA. The results demonstrate an enhanced ability to distinguish and subtype the cancer cells.

This dissertation will discuss an alternative mythology for the advancement of post-translational sub-typing with the intent to advance the field of personalized medicine.

ACKNOWLEDGEMENTS

I would like to thank the Department of Pharmaceutical Sciences, the College of Pharmacy, Nursing, and Allied Sciences, the Graduate School, and North Dakota State University for providing me with the opportunity and tools to better my education.

I would like to thank my graduate advisor, Dr. Sanku Mallik for his guidance and support. My committee members: Dr. Daniel Friesner, Dr. Benedict Law, Dr. Katie Reindl, and Dr. Chengwen Sun for their helpful suggestions. Additionally, I would like to thank all my instructors and faculty members who have helped me develop the foundation for my education.

I would like to thank Dr. Kalpana Katti and her graduate student Avinash Ambre for their assistance in obtaining the AFM images. Scott Payne and Jayma Moore for their assistance with generating the TEM images. Buddhadev Layek for his assistance with obtaining molecular weights of the polymers. Dr. Bin Guo's lab for his assistance in the prostate cancer project. I would like to thank Dr. D.K. Srivastava and Dr. Bratati Ganguly for providing the recombinant MMPs. I would like to thank several graduate students who provided helpful suggestions during my development of cell culturing techniques.

I would like to thank our departmental chairman Dr. Jagdish Singh, our college dean Dr. Charles Peterson, and our graduate school dean Dr. David Wittrock for providing me an educational home and the opportunity to demonstrate my abilities and professional utility.

I would like to thank my past and current labmates including: Dr. Rinku Dutta, Dr. Manas K. Haldar, Dr. Jayati Banerjee, Dr. Rajesh Subramaniam, Erin Nyren-Erickson, Rahul Nahire, and Prajakta Kulkarni. I would like to thank my students I have had the good fortune to oversee and assist in the lab: Edna Lampkin, Jane Loueng, Rob Sieg, Chantal Vance, Hannah Walbroch, and Lee Schwan.

I would like to thank the NDSU staff in particular Ms. Janet Krom and Ms. Jean Trautmann for providing assistance in multiple different areas essential for my development at NDSU.

I would like to thank Bill and Dianna Makens and their family for providing me with the "tools" to recover after UNL. I would like to thank the University of Minnesota-Twin Cities for providing me an undergraduate "home" and North Dakota State University for allowing me to "pursue" my Masters degree and allowing me to continue such that I could "earn" my Ph.D.

I would like to thank Dr. Richa Nagar who was my women studies professor at the University of Minnesota-Twin Cities for encouraging me talk in the lecture halls. I would also like to thank Dr. Ann Mai May who was my economics professor at the University of Nebraska-Lincoln for having the courage to share with her class the story of her earlier educational setbacks as an undergraduate student.

Most importantly I would like to thank those that have chosen to support me including my family, friends, and those with the courage to love me.

DEDICATION

I would like to dedicate this work to all those who have shown instruction, support, and love during my development as a person.

TABLE OF CONTENTS

LIST OF TABLES

LIST OF FIGURES

Figure Page

LIST OF SCHEMES

LIST OF ABBREVIATIONS

ADAM…….A Disintegrin and a Metalloproteinase

AFM…….Atomic force microscopy

AIBN……Azoisobutyronitrile

Ala……Alanine

Asp……Aspartic acid

BG…….Biotinylated gelatin

BOP……...Benzotriazol-1-yl-oxy-tris(dimethylamino)phosphonium hexafluorophosphate

CO_2……Carbon dioxide

DMEM……..Dulbecco's modified eagle medium

DMF……..Dimethylformamide

ELISA……Enzyme-linked immunosorbent assay

FBS……Fetal bovine serum

FITC……..Fluorescein isothiocyanate

fTHP……..Fluorogenic triple-helical peptide

GPC……Gel permeation chromatography

GSK-3……Glycogen synthase kinase-3

HBSS…….Hank's balanced salt solution

HBTU……O-benzotriazole-N,N,N',N'-tetramthyluronium hexafluorophosphate

HOBT……1-Hydroxybenzotriazole

IFETS……Intra-molecular fluorescence energy transfer substrates

IPA……Isopropyl alcohol

iPr_2NEt...…..N-ethyldiisopropylamine

LDA……..Linear discriminant analysis

Lys……Lysine

MEM…….Minimum essential medium Eagle's

MeOH……Methanol

MMP……..Matrix metalloproteinase

M_n……..Number average molecular weight

M_w…….Weight average molecular weight

NMM…….4-Methylmorpholine

PI……Polydispersity

PSA……Prostate-specific antigen

RI……Refractive index

RPM……Revolutions per minute

RPMI……..Roswell Park Memorial Institute medium

TEM……...Transmission electron microscopy

TFA……Trifluoroacetic acid

TIMP……..Tissue inhibitor of metalloproteinases

TIPS……Triisopropylsilane

UTIINE……..Urinary type II collagen neoepitope assay

LIST OF APPENDIX FIGURES

LIST OF APPENDIX SCHEMES

CHAPTER 1. INTRODUCTION

Abstract

The general topics of this thesis include: matrix metalloproteinases (MMPs), polymers, and cell subtyping. MMPs have been shown to be over-expressed at various levels in different cancer types and subtypes. There are various methodologies to detect them by use of a fluorimetric method that used a polymer based detection system.

Introduction to Matrix Metalloproteinase (MMPs)

Matrix metalloproteinases (MMPs) are a group of zinc-dependent, metalloenzymes that were discovered in 1962 by Jerome Gross and Charles Lapiere.[1] This discovery was made during the metamorphism of the tale of tadpole.[1] Since the initial discovery several other MMPs have been identified and categorized.

Currently, we know of more than 23 different MMPs isozymes.[2-4] MMP-1 was initial discovered in the tails of tadpoles before they metamorphed into frogs illustrates the general underling function of MMPs. MMPs belong to a family of endopeptidases (zinc-dependent) that are involved in normal physiological processes such as organogenesis,[5, 6] wound healing,[7-9] and apoptosis of amniotic fibroblasts during pregnancy.[6] They are also involved in pathological conditions and are implicated with inflammatory disorders,[10, 11] carcinogenesis,[12-14] and other diseases that involve degradation (**Table 1**).

Expression of MMPs

MMPs are synthesized in the inactive form within the cell (**Figure 1**).[3, 6] They are then bound to the membrane or secreted into the extracellular environment as pro-MMP where they are cleaved and activated into MMPs.[15] The pro-MMPs are catalytically inactive due to an

interaction between a thiol of the prodomain cysteine and the Zn^{2+} ion in the catalytic site of the MMP.[16]

Table 1. Leading causes of death in U.S. 2010 (http://www.cdc.gov/nchs/fastats/lcod.htm) (accessed on 7/15/12). All but accidents have been associated in some way with MMPs.

Leading Causes of Death in U.S. 2010		
1	Heart disease	599,413
2	Cancer	567,628
3	Chronic lower respiratory disease	137,353
4	Stroke	128,842
5	Accidents (unintentional injuries)	118,021
6	Alzheimer's disease	79,003

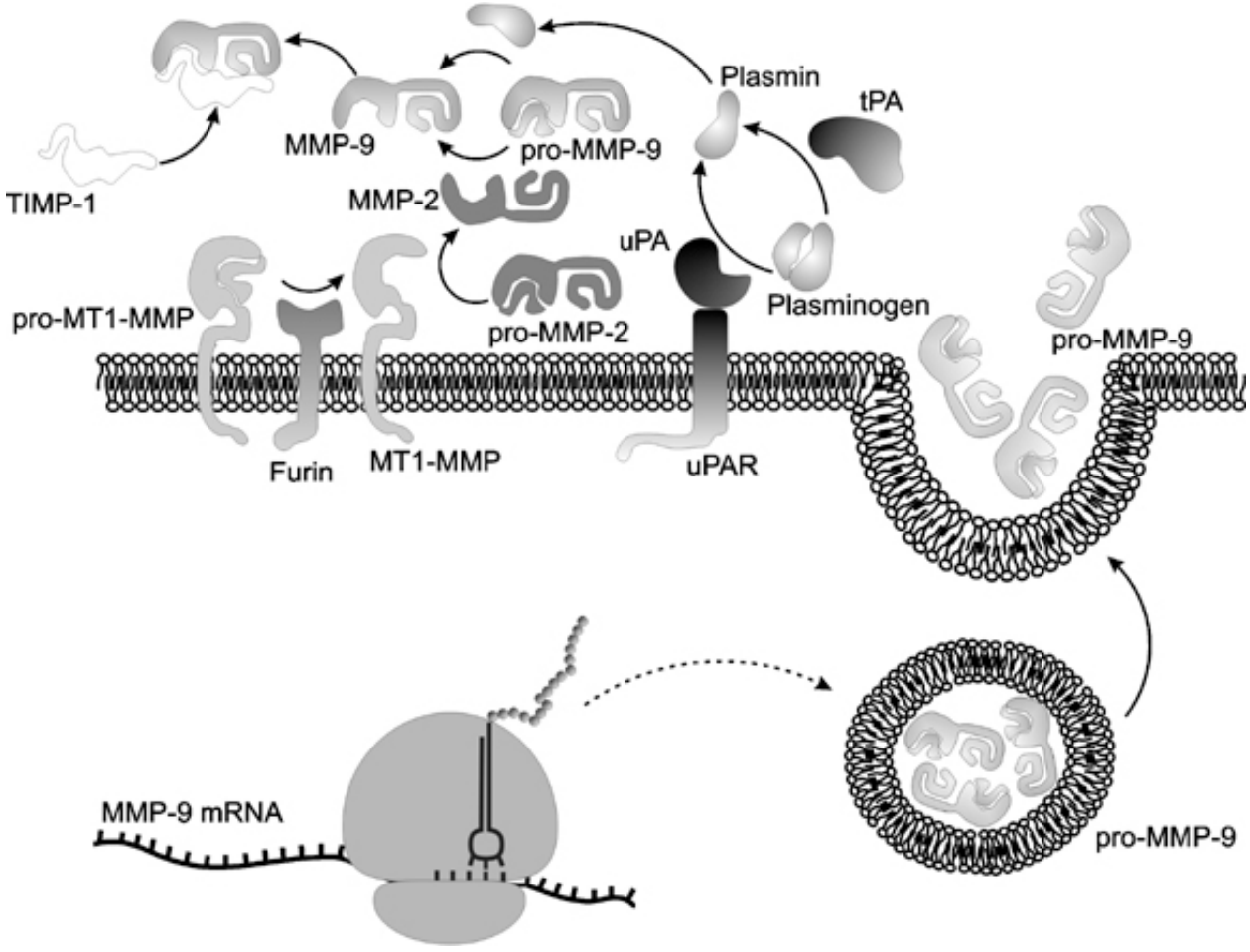

Figure 1. Inactive pro-MMP is activated at a post-translational level.[17] This figure was taken with permission from P. Michaluk, L. Kaczmarek; Cell Death and Differentiation. **2007**, *14*, 1252. doi:10.1038/sj.cdd.4402141

The prodomain of the MMPs is cleaved during activation. Upon activation, the thiol-Zn^{2+} interaction (or cysteine switch) is removed due to post-translational modification of the thiol group, or potential interactions between other macromolecules.[16] Current detection techniques such as ELISA cannot distinguish between the pro and active forms of the MMPs. Because they are unable to distinguish between the active and inactive (or pro-MMP) it is difficult to understand the actual physiological effect the MMPs are playing.

MMP Inhibitors

MMPs inhibitors were promising targets for cancer therapy due to MMPs ability of cancer cells to degrade the basement membrane.[8, 15] Thus, the development of several MMP inhibitors (**Table 2**) occurred with nearly all of them failing in clinical trials.[18, 19] The exact reason for this failure has been the subject of considerable scientific debate.

Table 2. A few MMP inhibitors and the isozymes they inhibit.[20] Note Neovastat (AE-941) is a natural product taken from shark cartilage that so far has performed well in clinical trails.

Inhibitor's Name	Enzyme Inhibited
Batimastat	-1, -2, -3, -7, -9
Bisphosphonates	-1, -2, -7, -9, MT1-MMP, MT2MMP
BMS-275291	-2, -9
CGS27023A	-1, -2, -3
Genistein	-2, -9, MT1-MMP, MT2-MMP, MT3-MMP
Letrozole	-2, -9
Neovastat (AE-941)	-1, -2, -7, -9, -13
Marimastat	Broad spectrum
Metastat (COL-3)	-1, -2, -8, -9, -13
Minocycline	-1, -2, -3
Prinomastat	-2, -3, -7, -9, -13
SB-3CT	-2, -9
Tanomastat (BAY12-9666)	-2, -3, -9

MMPs are over-expressed in cancerous cells, however, this is the result of both the cancer cells but also the neighboring stromal cells.[20-22] This recent discovery that the

neighboring stromal cells over-express MMPs to act as a paracrine defensive mechanism to control cancer cellular growth.[20] Thus, administration of early broad spectrum inhibitors have limited the ability of the stromal cells to defend themselves against the invading cancerous cells.[22]

An additional complication is MMP's role in cancer progression and apoptosis, changes at different times, roles, or stages of cancerous development. Thus, MMPs have a dichotomist's functionality in progression and apoptosis of cancer. Knockout studies of MMP's suggested, that they promote or inhibit the development of cancer cells based upon tumor stage. For example, MMP-8 decreases the metastatic potential of breast cancer and thus acts as a tumor suppressor.[23] In knockout studies, MMP-9 was shown to promote the growth of cancerous cells and is thus an oncogene.[24] MMP-1 and MMP-7 cleave E-cadherin which may allow for morphological transition and cell migration.[25]

MMP Detection Techniques

Despite broad spectrum MMP inhibitors limitations as safe anti-cancer drugs, they are effective enzymes (particularly MMP-9 and -7) to target for the development of new approaches to detect, stage, and subtype cancerous cells.[26] This is due to their over expression by both the cancerous cells and neighboring stromal cells. However, practical use of MMPs for this purpose is currently limited by techniques (*i.e.* ELISA) for their detection.[26, 27]

ELISA does not distinguish between pre-MMP and active MMP. Additionally, ELISA is time consuming and can take up to eight hours to complete using skilled labor. Due to these technical limitations, performing ELISA for MMP quantification within the clinic is currently

not desirable. However, if these major limitations (**Table 3**) to MMP detection are corrected they may have a future in the clinical setting.

Table 3. Limitations of current MMP detection techniques.

Limitations to MMP Detection Techniques	
1	Ability to distinguish between pre-MMP and active MMP.
2	Time consuming process.
3	Involves skilled personal working many hours.

Additional techniques for the detection of MMPs include the following: bioassay, zymography assay, immunoassay, fluorimetric assay, and other techniques.[2] These are discussed below.

Bioassay

Bioassays are generally used to determine the biological activity of substrates. They include assays using biotinylated gelatin (BG)[28-30] and assays using succinylated gelatin.[31] Both techniques have only been applied to testing inhibitor activity.[2]

Zymography Assay

This technique is a variation on the acrylamide gel electrophoresis that is used to evaluate matrix metalloproteinases and its inhibitors.[2] This method contains gel that is polymerized with gelatin or some other protease substrate directly into it. Inhibitor activity is determined with the presence (no inhibitor activity) or absence (inhibitor activity) of the protein staining.

This quantitative technique has accuracy, but doubts have been raised in regards to its limits of detection.[5] Variations on this technique include: gelatin zymography, casein zymography, collagen zymography, in situ zymography, reverse zymography, real-time

zymography, and *in vivo* zymography.[2, 3] This assay is limited by poor inter-laboratory comparisons.[2, 32]

Immunoassay

These assays are used to develop MMP-TIMP complexes.[2] They are dependent on the utilization of biological antibodies. Due to their ability to detect both pro- and active MMPs, they do not discriminate well between active and inactive MMPs.[2] These techniques include: enzyme-linked immunosorbent assay (ELISA),[33, 34] immuno capture assay,[35-38] sandwich enzyme immunoassay,[39-43] and urinary type II collagen neoepitope assay (uTIINE assay)[2, 32, 44] and western blotting.[45]

Fluorimetric Assay

These assays are good for detecting low concentrations of MMPs, but are very limited by time, high background, or limited solubility.[32, 46] These techniques include: fluorescein isothiocyanate (FITC) labeled proteins,[47] fluorogenic triple-helical peptide (fTHP),[32, 48] intra-molecular fluorescence energy transfer substrates (IFETS).[49-52] My proposed research is based upon an extension of this area, but will address solubility, time, and background issues.

Other Techniques

Akizawa *et. al.* reported the application of flow injection analysis for the measurement of MMP-7 activity.[8] This group focused on the development of a screening mechanism for inhibitor development utilizing recombinant MMP-7.[8] To the best of our knowledge, this system has not been applied past this focus. Other techniques include radio isotopic assay, phage-displayed assay, multiple-enzyme/multiple-reagent assay, and activity-based profiling assay.[2, 48] These techniques are problematic due to cost, or inability to distinguish between pro- and active

MMP levels.[2] Additionally, all of these systems are generally limited by their inability to provide fast and accurate cancer cell subtyping techniques.

Cancer Subtyping Techniques

Cancer subtyping techniques have developed an important role for the development of target chemotherapeutic strategies. The aim of these subtypes allows primary health care providers to match the most successful clinical agent to the mechanism of cancerous development. Researchers can develop agents to target specific biological targets. Pharmaceutical companies that utilize personalized medicine subtyping technologies, lower the risk of having new agents from failing clinical trials.

Traditional subtyping techniques come from the field of Molecular Biology and include PCR and RT-QPCR, *etc*. These techniques are limited by cost and a general lack of understanding of genetics by physicians.[53] Genomic approaches are further limited by variations between predicted mRNA levels and actual proteins levels as is the case with MMP-2 and -9 mRNA expression or proteins.[54, 55] To avoid these issues, we developed a protein-based system, that works within a knowledge framework that the physicians already use.[53]

Polymer Based Detection

Polymers are extremely fast and non-selective means of detection. They have been used by different groups to achieve protein identification and differentiation.[27, 56-61] Such groups have utilized polymers abilities to form multivalent interactions along the surface of the proteins/enzymes.[61-63] Such multivalent interactions mimic protein-protein interactions that

occur *in vivo*.[64] To make polymers useful for detection the issue of specificity must be addressed.[59] Towards this end the following specific aims were explored.

Specific Aims

First Specific Aim

The first hurdle that was addressed was the polymer's lack of specificity in enzyme specific detection system. The ability of the polymer system to distinguish between active recombinant human MMP-7, -9, and -10 was evaluated. This polymeric system used a design to generate multivalent interactions along with a specific zinc binding inhibitor to enhance detection specificity. This inhibitor will function *in vitro* and thus will avoid limitations that result from current toxicity with MMP inhibitors.

Second Specific Aim

To investigate the ability of the optimal polymer to distinguish between different prostate cancer cells, which require different clinical treatment methods. This was accomplished with the optimal polymer from *First Specific Aim*. Current polymeric technologies have not previously been investigated for their ability to do this. This aim investigated the utilization of polymers for a rapid post-translational differentiation and subtyping based upon secretomics, of secreted proteins.

Third Specific Aim

To expand *Second Specific Aim* towards the investigation of the ability of the optimal polymer to distinguish between different breast cancer cells. Again the breast cancer cell lines chosen have unique clinical treatment options. This was accomplished by using the optimal polymer from *First Specific Aim*.

Fourth Specific Aim

Enhanced detection ability of the optimal polymer formulation towards both breast and prostate cancer cell lines. Towards this an alteration of the fluorophore was made from a hydrophobic dansyl to a more hydrophilic pyranine. The more hydrophilic polymer showed an enhanced differentiation and subtype between the cell lines.

References

1. Gross, J. & Lapiere, C.M. Collagenolytic activity in amphibian tissues: a tissue culture assay. *Proceedings of the National Academy of Sciences of the United States of America* **48**, 1014-1022 (1962).
2. Cheng, X.C., Fang, H. & Xu, W.F. Advances in assays of matrix metalloproteinases (MMPs) and their inhibitors. *J Enzyme Inhib Med Chem* **23**, 154-167 (2008).
3. Offersen, B.V. et al. Matrix metalloproteinase-9 measured in urine from bladder cancer patients is an independent prognostic marker of poor survival. *Acta Oncol* **49**, 1283-1287 (2010).
4. Kohrmann, A., Kammerer, U., Kapp, M., Dietl, J. & Anacker, J. Expression of matrix metalloproteinases (MMPs) in primary human breast cancer and breast cancer cell lines: New findings and review of the literature. *BMC Cancer* **9**, 188 (2009).
5. Neumann, U., Kubota, H., Frei, K., Ganu, V. & Leppert, D. Characterization of Mca-Lys-Pro-Leu-Gly-Leu-Dpa-Ala-Arg-NH2, a fluorogenic substrate with increased specificity constants for collagenases and tumor necrosis factor converting enzyme. *Anal Biochem* **328**, 166-173 (2004).

6. Chung, L. et al. Collagenase unwinds triple-helical collagen prior to peptide bond hydrolysis. *The EMBO journal* **23**, 3020-3030 (2004).

7. Page-McCaw, A., Ewald, A.J. & Werb, Z. Matrix metalloproteinases and the regulation of tissue remodelling. *Nat Rev Mol Cell Biol* **8**, 221-233 (2007).

8. Itoh, M. et al. Flow injection analysis for measurement of activity of matrix metalloproteinase-7 (MMP-7). *J Pharm Biomed Anal* **15**, 1417-1426 (1997).

9. Puerta, D.T., Lewis, J.A. & Cohen, S.M. New beginnings for matrix metalloproteinase inhibitors: identification of high-affinity zinc-binding groups. *Journal of the American Chemical Society* **126**, 8388-8389 (2004).

10. Parks, W.C., Wilson, C.L. & Lopez-Boado, Y.S. Matrix metalloproteinases as modulators of inflammation and innate immunity. *Nat Rev Immunol* **4**, 617-629 (2004).

11. Minond, D., Lauer-Fields, J.L., Nagase, H. & Fields, G.B. Matrix metalloproteinase triple-helical peptidase activities are differentially regulated by substrate stability. *Biochemistry* **43**, 11474-11481 (2004).

12. Egeblad, M. & Werb, Z. New functions for the matrix metalloproteinases in cancer progression. *Nature reviews. Cancer* **2**, 161-174 (2002).

13. Basset, P. et al. A novel metalloproteinase gene specifically expressed in stromal cells of breast carcinomas. *Nature* **348**, 699-704 (1990).

14. Liotta, L.A., Steeg, P.S. & Stetler-Stevenson, W.G. Cancer metastasis and angiogenesis: an imbalance of positive and negative regulation. *Cell* **64**, 327-336 (1991).

15. Jani, M., Tordai, H., Trexler, M., Banyai, L. & Patthy, L. Hydroxamate-based peptide inhibitors of matrix metalloprotease 2. *Biochimie* **87**, 385-392 (2005).

16. Ra, H.J. et al. Control of promatrilysin (MMP7) activation and substrate-specific activity by sulfated glycosaminoglycans. *The Journal of biological chemistry* **284**, 27924-27932 (2009).

17. Michaluk, P. & Kaczmarek, L. Matrix metalloproteinase-9 in glutamate-dependent adult brain function and dysfunction. *Cell Death Differ* **14**, 1255-1258 (2007).

18. Cheng, X.C., Wang, Q., Fang, H. & Xu, W.F. Role of sulfonamide group in matrix metalloproteinase inhibitors. *Current medicinal chemistry* **15**, 368-373 (2008).

19. Chen, E.I. et al. A unique substrate recognition profile for matrix metalloproteinase-2. *The Journal of biological chemistry* **277**, 4485-4491 (2002).

20. Gialeli, C., Theocharis, A.D. & Karamanos, N.K. Roles of matrix metalloproteinases in cancer progression and their pharmacological targeting. *Febs J* **278**, 16-27 (2011).

21. Coussens, L.M., Fingleton, B. & Matrisian, L.M. Matrix metalloproteinase inhibitors and cancer: trials and tribulations. *Science* **295**, 2387-2392 (2002).

22. Kessenbrock, K., Plaks, V. & Werb, Z. Matrix metalloproteinases: regulators of the tumor microenvironment. *Cell* **141**, 52-67 (2010).

23. Decock, J. et al. Plasma MMP1 and MMP8 expression in breast cancer: protective role of MMP8 against lymph node metastasis. *BMC Cancer* **8**, 77 (2008).

24. Deryugina, E.I. & Quigley, J.P. Matrix metalloproteinases and tumor metastasis. *Cancer Metastasis Rev* **25**, 9-34 (2006).

25. Noe, V. et al. Release of an invasion promoter E-cadherin fragment by matrilysin and stromelysin-1. *Journal of cell science* **114**, 111-118 (2001).

26. Leelawat, K., Sakchinabut, S., Narong, S. & Wannaprasert, J. Detection of serum MMP-7 and MMP-9 in cholangiocarcinoma patients: evaluation of diagnostic accuracy. *BMC Gastroenterol* **9**, 30 (2009).

27. You, C.C. et al. Detection and identification of proteins using nanoparticle-fluorescent polymer 'chemical nose' sensors. *Nature nanotechnology* **2**, 318-323 (2007).

28. Paemen, L. et al. The gelatinase inhibitory activity of tetracyclines and chemically modified tetracycline analogues as measured by a novel microtiter assay for inhibitors. *Biochemical pharmacology* **52**, 105-111 (1996).

29. Koritsas, V.M. & Atkinson, H.J. An assay for detecting nanogram levels of proteolytic enzymes. *Anal Biochem* **227**, 22-26 (1995).

30. Ratnikov, B. et al. Determination of matrix metalloproteinase activity using biotinylated gelatin. *Anal Biochem* **286**, 149-155 (2000).

31. Baragi, V.M. et al. A versatile assay for gelatinases using succinylated gelatin. *Matrix Biol* **19**, 267-273 (2000).

32. Makowski, G.S. & Ramsby, M.L. Calibrating gelatin zymograms with human gelatinase standards. *Anal Biochem* **236**, 353-356 (1996).

33. Bergmann, U. et al. Enzyme linked immunosorbent assays (ELISA) for the quantitative determination of human leukocyte collagenase and gelatinase. *J Clin Chem Clin Biochem* **27**, 351-359 (1989).

34. Yoshioka, H., Oyamada, I. & Usuku, G. An assay of collagenase activity using enzyme-linked immunosorbent assay for mammalian collagenase. *Anal Biochem* **166**, 172-177 (1987).

35. Bawadi, H.A., Antunes, T.M., Shih, F. & Losso, J.N. In vitro inhibition of the activation of Pro-matrix Metalloproteinase 1 (Pro-MMP-1) and Pro-matrix metalloproteinase 9 (Pro-MMP-9) by rice and soybean Bowman-Birk inhibitors. *J Agric Food Chem* **52**, 4730-4736 (2004).

36. Hanemaaijer, R., Visser, H., Konttinen, Y.T., Koolwijk, P. & Verheijen, J.H. A novel and simple immunocapture assay for determination of gelatinase-B (MMP-9) activities in biological fluids: saliva from patients with Sjogren's syndrome contain increased latent and active gelatinase-B levels. *Matrix Biol* **17**, 657-665 (1998).

37. Hanemaaijer, R. et al. MMP-9 activity in urine from patients with various tumors, as measured by a novel MMP activity assay using modified urokinase as a substrate. *Ann N Y Acad Sci* **878**, 141-149 (1999).

38. Capper, S.J. et al. Determination of gelatinase-A (MMP-2) activity using a novel immunocapture assay. *Ann N Y Acad Sci* **878**, 487-490 (1999).

39. Zhang, J. et al. A one-step sandwich enzyme immunoassay for human matrix metalloproteinase 1 (interstitial collagenase) using monoclonal antibodies. *Clinica chimica acta; international journal of clinical chemistry* **219**, 1-14 (1993).

40. Fujimoto, N. et al. A one-step sandwich enzyme immunoassay for human matrix metalloproteinase 2 (72-kDa gelatinase/type IV collagenase) using monoclonal antibodies. *Clinica chimica acta; international journal of clinical chemistry* **221**, 91-103 (1993).

41. Ohuchi, E., Azumano, I., Yoshida, S., Iwata, K. & Okada, Y. A one-step sandwich enzyme immunoassay for human matrix metalloproteinase 7 (matrilysin) using

monoclonal antibodies. *Clinica chimica acta; international journal of clinical chemistry* **244**, 181-198 (1996).

42. Matsuki, H. et al. A one-step sandwich enzyme immunoassay for human matrix metalloproteinase 8 (neutrophil collagenase) using monoclonal antibodies. *Clinica chimica acta; international journal of clinical chemistry* **244**, 129-143 (1996).

43. Wang, T. et al. One-step sandwich enzyme immunoassay using monoclonal antibodies for detection of human enamelysin (MMP-20). *Eur J Oral Sci* **108**, 530-537 (2000).

44. Chu, Q. et al. Elevation of a collagenase generated type II collagen neoepitope and proteoglycan epitopes in synovial fluid following induction of joint instability in the dog. *Osteoarthritis Cartilage* **10**, 662-669 (2002).

45. Hao, J.L. et al. Effect of galardin on collagen degradation by Pseudomonas aeruginosa. *Experimental eye research* **69**, 595-601 (1999).

46. Geoghegan, K.F., Emery, M.J., Martin, W.H., McColl, A.S. & Daumy, G.O. Site-directed double fluorescent tagging of human renin and collagenase (MMP-1) substrate peptides using the periodate oxidation of N-terminal serine. An apparently general strategy for provision of energy-transfer substrates for proteases. *Bioconjugate chemistry* **4**, 537-544 (1993).

47. Ryzhakova, O.S. & Solov'eva, N.I. [The assay of tissue collagenase activity using fluorescein isothiocyanate labeled collagen]. *Biomed Khim* **51**, 432-438 (2005).

48. Turk, B.E., Huang, L.L., Piro, E.T. & Cantley, L.C. Determination of protease cleavage site motifs using mixture-based oriented peptide libraries. *Nature biotechnology* **19**, 661-667 (2001).

49. Knight, C.G. Fluorimetric assays of proteolytic enzymes. *Methods Enzymol* **248**, 18-34 (1995).

50. Gershkovich, A.A. & Kholodovych, V.V. Fluorogenic substrates for proteases based on intramolecular fluorescence energy transfer (IFETS). *J Biochem Biophys Methods* **33**, 135-162 (1996).

51. Fields, G.B. Using fluorogenic peptide substrates to assay matrix metalloproteinases. *Methods Mol Biol* **151**, 495-518 (2001).

52. Peppard, J. et al. Development of an assay suitable for high-throughput screening to measure matrix metalloprotease activity. *Assay Drug Dev Technol* **1**, 425-433 (2003).

53. What happened to personalized medicine? *Nature biotechnology* **30**, 1 (2012).

54. Lichtinghagen, R. et al. Different mRNA and protein expression of matrix metalloproteinases 2 and 9 and tissue inhibitor of metalloproteinases 1 in benign and malignant prostate tissue. *European urology* **42**, 398-406 (2002).

55. Pascal, L.E. et al. Correlation of mRNA and protein levels: cell type-specific gene expression of cluster designation antigens in the prostate. *BMC Genomics* **9**, 246 (2008).

56. Bajaj, A. et al. Array-based sensing of normal, cancerous, and metastatic cells using conjugated fluorescent polymers. *J Am Chem Soc* **132**, 1018-1022 (2010).

57. Bunz, U.H. & Rotello, V.M. Gold nanoparticle-fluorophore complexes: sensitive and discerning "noses" for biosystems sensing. *Angew Chem Int Ed Engl* **49**, 3268-3279 (2010).

58. Renner, C., Piehler, J. & Schrader, T. Arginine- and lysine-specific polymers for protein recognition and immobilization. *J Am Chem Soc* **128**, 620-628 (2006).

59. Schrader, T. & Koch, S. Artificial protein sensors. *Mol Biosyst* **3**, 241-248 (2007).

60. Wenck, K., Koch, S., Renner, C., Sun, W. & Schrader, T. A noncovalent switch for lysozyme. *Journal of the American Chemical Society* **129**, 16015-16019 (2007).

61. Tominey, A.F. et al. RAFT polymers for protein recognition. *Beilstein J Org Chem* **6** (2010).

62. Mammen, M., Choi, S.-K. & Whitesides, G.M. Polyvalent Interactions in Biological Systems: Implications for Design and Use of Multivalent Ligands and Inhibitors. *Angew Chem Int Ed Engl* **37**, 2754-2794 (1998).

63. Gradl, S.N., Felix, J.P., Isacoff, E.Y., Garcia, M.L. & Trauner, D. Protein surface recognition by rational design: nanomolar ligands for potassium channels. *Journal of the American Chemical Society* **125**, 12668-12669 (2003).

64. Jain, R.K. & Hamilton, A.D. Protein surface recognition by synthetic receptors based on a tetraphenylporphyrin scaffold. *Org Lett* **2**, 1721-1723 (2000).

CHAPTER 2. FLUORESCENT WATER SOLUBLE POLYMERS FOR ISOZYME-SELECTIVE INTERACTIONS WITH MATRIX METALLOPROTEINASE-9

Abstract

Matrix metalloproteinases (MMPs) are over-expressed in various pathological conditions, including numerous cancers. Although these isozymes have similar active sites, the patterns of exposed amino acids on their surfaces are different. This enables selective interactions with other macromolecules. Herein, the synthesis and molecular interactions of two water-soluble, fluorescent polymers which demonstrate selective interactions with recombinant MMP-9 compared to MMP-7 and -10 was reported.

Introduction

Water soluble, flexible polymers have been used by various groups to selectively bind to different proteins.[65-67] The flexibility of the polymer backbone aids in the formation of multiple and complementary interaction sites between the polymer and the amino acid residues on the protein surface. These polymers have been demonstrated to be useful as affinity membranes, as switches to "turn on" enzyme activity, as selective protein immobilization agents, and as protein sensors, etc.[65-67] However, the proteins used in these selective recognition experiments are structurally very different (e.g., lysozyme, bovine serum albumin, and cytochrome c, etc.). To the best of our knowledge, selective binding of polymers to different isozymes of an enzyme family has not been demonstrated.

Matrix metalloproteinases (MMPs) are a group of metalloenzymes that contain Zn^{2+} in the active site pocket and are capable of hydrolyzing the extracellular matrix.[68, 69] These enzymes are involved in a number of different physiological processes, e.g., cell proliferation,

apoptosis, differentiation, angiogenesis, chemokine/cytokine activation, and the expression levels of these enzymes is strictly regulated at multiple levels.[70-73] Various MMP isozymes (in particular MMP-9) are up regulated in degenerative diseases such as arthritis, multiple sclerosis, and metastatic cancers.[73-75] In healthy individuals, the serum concentration of MMP-9 is about 5 – 10 nM.[76] For lung cancer patients, the concentration of this enzyme can be as high as 100 – 200 nM in the bronchial lavage fluids.[77] The levels of MMP-9 serve as diagnostic and prognostic markers for these diseases.[76, 77]

Since isozymes catalyze the same chemical reaction, their active sites are remarkably similar.[78] However, the pattern of amino acid residues on the surface of the isozymes is not under evolutionary pressure and thus not conserved.[79] We reasoned that this difference can be exploited for selective binding of polymers to one isozyme in preference to the others. Herein, selective binding to recombinant human matrix metalloproteinase-9 (MMP-9) by a water soluble, flexible polymer was reported.

Monomer Synthesis

4-vinylbenzoic acid (**Figure 2**) with a benzene ring incorporated into the structure was used to synthesize a set of monomers. This polymerizable moiety was conjugated to an alcohol (for increased water solubility and hydrogen bonding with amino acid residues on the surface of MMPs) and to the fluorogenic dansyl group and to a non-selective MMP inhibitor. Different amino acids such as lysine (positively charged), aspartic acid (negatively charged), and β-alanine (non-polar) were also linked to the polymerizable group to impart electrostatic and hydrophobic properties to the polymers from their respective functional groups chemical properties.

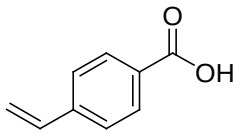

Figure 2. Chemical structure of 4-vinylbenzoic acid.

Aspartic Acid Monomer Synthesis

The protected aspartic acid monomer was synthesized by coupling 4-vinylbenzoic acid ($C_9H_8O_2$; MW = 148.16 g/mol) to L-aspartic acid di-tert-butyl ester hydrochloride [H-Asp(OtBu)-OtBu·HCl; MW = 281.8 g/mol]. To perform this amino acid coupling reaction (**Scheme 1**), the addition of 1.036 g (7 mmol) of $C_9H_8O_2$, 1.453 g (7 mmol) of H-Asp(OtBu)-OtBu·HCl, 0.947 g (7 mmol) of 1-hydroxybenzotriazole (HOBT), 2.676 g (7 mmol) of O-benzotriazole-N,N,N'N'-tetramethyluronium hexafluorophosphate (HBTU) to 25 mL of dichloromethane (CH_2Cl_2). This reaction mixture was stirred under nitrogen at room temperature for 15 minutes before adding 2.37 g (14 mmol) of N-ethyldiisopropylamine (iPr_2NEt).

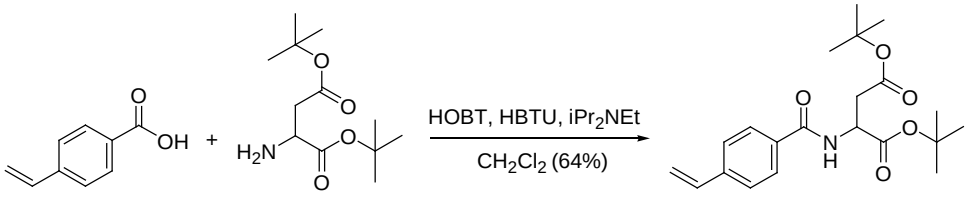

Scheme 1. Synthesis of protected aspartic acid monomer.

This reaction continued to stir under nitrogen at room temperature overnight. The next morning, the reaction was worked up by washing in a separation funnel. It was washed once with 15% brine, twice with distilled water, four times with 20% citric acid solution, and four

times with 7% sodium bicarbonate. The remaining dichloromethane was dried with sodium sulfate and then was removed using a rotary evaporator at 38ºC.

^{1}H NMR spectrum suggested it needed further purification. The crude protected compound was then dissolved in dichloromethane (CH_2Cl_2) and loaded into silica gel. This silica gel was then used to perform an automated flash chromatography using CombiFlash Rf system from Teledyne Isco. A solvent system of dichloromethane and methanol (R_f = 0.9% dichloromethane/10% methanol) was used with the CombiFlash for successful purification (**Figure A1**). The solvent was removed from the system using a rotary evaporator at a temperature not exceeding 38ºC.

Final purified protected aspartic acid monomer had a yield of 1.690 g (64%). ^{1}H NMR (400 MHz, CHLOROFORM-*d*) δ ppm 1.45 (s, 9 H) 1.49 (s, 9 H) 2.86 (dd, *J*=17.1, 4.3 Hz, 1 H) 2.98 (dd, *J*=17.1, 4.0 Hz, 1 H) 4.77 - 4.94 (m, 1 H) 5.36 (d, *J*=11.1 Hz, 1 H) 5.84 (d, *J*=17.6 Hz, 1 H) 6.74 (dd, *J*=17.6, 10.8 Hz, 1 H) 7.20 (d, *J*=7.7 Hz, 1 H) 7.45 (s, 2 H) 7.78 (d, *J*=8.3 Hz, 2 H).

To deprotect, 1.690 g (4.504 mmol) of protected aspartic acid monomer was mixed with 15 mL trifluoroacetic acid (TFA) and 0.5 mL of triisopropylsilane (TIPS) under nitrogen at room temperature for 2 to 3 hours **(Scheme 2)**. The TFA was removed from the round bottom flask using a rotary evaporator at a temperature not exceeding 38ºC.

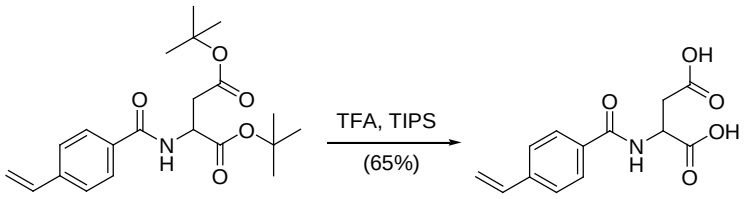

Scheme 2. Synthesis of de-protected aspartic acid monomer.

The remaining mixture was dissolved in methanol (MeOH) and loaded into silica gel. This silica gel was then used to perform automated flash chromatography using CombiFlash Rf system from Teledyne Isco. Using a solvent system of dichloromethane and methanol (R_f = 0.1; 90% dichloromethane/10% methanol), the CombiFlash was successful in removing the TIPS from the reaction mixture and allowed for the purification of the product (**Figure A2**). The solvent was again removed from the system using a rotary evaporator at 38ºC.

Final purified aspartic acid monomer had a product yield of 0.770 g, 65%. This compound will polymerize at temperatures above 160ºC. ^{1}H NMR (400 MHz, METHANOL-d_4) δ ppm 2.85 - 3.04 (m, 2 H) 4.96 (dd, *J*=7.1, 5.5 Hz, 1 H) 5.35 (d, *J*=10.9 Hz, 1 H) 5.90 (d, *J*=17.6 Hz, 1 H) 6.79 (dd, *J*=17.6, 11.1 Hz, 1 H) 7.53 (m, *J*=8.4 Hz, 2 H) 7.81 (m, *J*=8.4 Hz, 2 H). ^{13}C NMR (125 MHz, METHANOL-d_4) δ ppm 36.94 51.03 116.55 127.42 128.94 134.36 137.41 142.61 169.72 174.23 174.32.

Lysine Monomer Synthesis

The protected lysine monomer was synthesized by coupling 4-vinylbenzoic acid ($C_9H_8O_2$; MW = 148.16 g/mol) to N^E-Boc-L-lysine t-butyl ester hydrochloride [H-Lys(Boc)-OtBu·HCl; MW = 338.9 g/mol]. To perform this coupling reaction (**Scheme 3**) we added 1.036 g (7 mmol) of $C_9H_8O_2$, 2.337 g (7 mmol) of H-Lys(Boc)-OtBu·HCl, 0.946 g (7 mmol) of 1-hydroxybenzotriazole (HOBT), 2.658 g (7 mmol) of O-benzotriazole-N,N,N'N'-tetramethyluronium hexafluorophosphate (HBTU) to 20 mL of dichloromethane (CH_2Cl_2). This reaction mixture was stirred under nitrogen at room temperature for 15 minutes before adding 2.38 g (14 mmol) of N-ethyldiisopropylamine (iPr_2NEt).

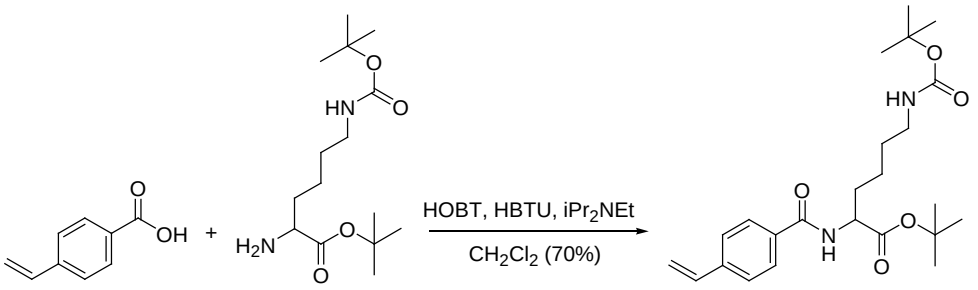

Scheme 3. Synthesis of protected lysine monomer.

This reaction continued to stir under nitrogen at room temperature overnight. The next morning, the reaction was worked up by washing in a separation funnel. It was washed once with 15% brine, twice with distilled water, four times with 20% citric acid solution, and four times with 7% sodium bicarbonate. The remaining dichloromethane was dried over sodium sulfate before being removed using a rotary evaporator at 38ºC.

^{1}H NMR spectrum suggested it needed further purification. The crude protected compound was then dissolved in methanol (MeOH) and loaded into silica gel. This silica gel was then used to perform an automated flash chromatography using CombiFlash Rf system from Teledyne Isco. A solvent system of dichloromethane and methanol (R_f = 0.9% dichloromethane/10% methanol) was used with the CombiFlash for successful purification (**Figure A3**). The solvent was removed using a rotary evaporator at 38ºC.

Final purified protected lysine monomer had a yield of 2.110 g (70%). ^{1}H NMR (500 MHz, CHLOROFORM-*d*) δ ppm 1.22 (br s, 4 H) 1.41 (br s, 9 H) 1.48 - 1.51 (m, 9 H) 1.72 - 1.82 (m, 1 H) 1.90 - 2.00 (m, 1 H) 3.11 (br s, 2 H) 4.64 (br s, 1 H) 4.69 (d, *J*=5.0 Hz, 1 H) 5.36 (d, *J*=10.9 Hz, 1 H) 5.84 (d, *J*=17.7 Hz, 1 H) 6.75 (dd, *J*=17.7, 10.9 Hz, 1 H) 6.78 - 6.84 (m, 1 H) 7.46 (d, *J*=8.1 Hz, 2 H) 7.78 (d, *J*=8.1 Hz, 2 H).

To deprotect, 2.110 g (4.878 mmol) of protected lysine monomer was mixed with 10 mL trifluoroacetic acid (TFA) and 0.5 mL of triisopropylsilane (TIPS) under nitrogen at room temperature for 3 to 4 hours **(Scheme 4)**. The TFA was removed from the round bottom flask using a rotary evaporator at 38ºC.

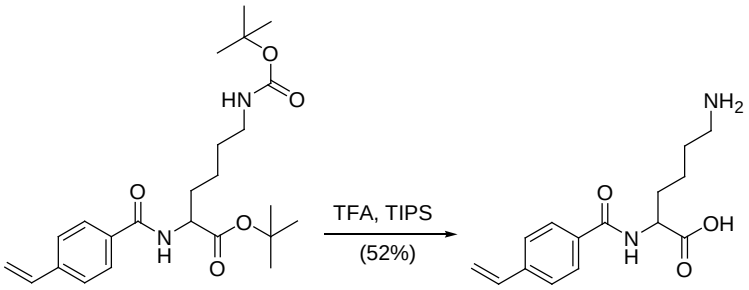

Scheme 4. Synthesis of de-protected lysine monomer.

The remaining mixture was dissolved in methanol (MeOH) and loaded into silica gel. This silica gel was then used to perform automated flash chromatography with the CombiFlash Rf system from Teledyne Isco. A solvent system of dichloromethane and methanol (R_f = 0.1; 90% dichloromethane/10% methanol) was used with the CombiFlash to successfully removed the TIPS from the reaction mixture and allowed for the purification of the product (**Figure A4**). The solvent was removed from the system using a rotary evaporator at 38ºC.

Final purified lysine monomer had a product yield of 0.810 g, 52%. It polymerizes above 185ºC. ^{1}H NMR (400 MHz , METHANOL-d_4) δ ppm 1.29 (br s, 1 H) 1.36 - 1.57 (m, 3 H) 1.57 - 1.77 (m, 3 H) 1.84 (dq, *J*=14.1, 7.1 Hz, 1 H) 1.92 - 2.04 (m, 1 H) 2.91 (t, *J*=7.4 Hz, 2 H) 4.47 (t, *J*=6.0 Hz, 1 H) 5.35 (d, *J*=11.1 Hz, 1 H) 5.89 (d, *J*=17.6 Hz, 1 H) 6.79 (dd, *J*=17.6, 10.9 Hz, 1 H) 7.53 (m, *J*=8.2 Hz, 2 H) 7.83 (m, *J*=8.1 Hz, 2 H). ^{13}C NMR (100 MHz, METHANOL-d_4) δ ppm 23.59 28.38 33.59 40.73 56.31 116.44 127.45 128.71 134.93 137.43 142.41 168.87 178.69.

β-Alanine Monomer Synthesis

The protected β-alanine monomer was synthesized by coupling 4-vinylbenzoic acid ($C_9H_8O_2$; MW = 148.16 g/mol) to β-alanine t-butyl ester hydrochloride [β-Ala-OtBu·HCl; MW = 181.7 g/mol]. To perform this amino acid coupling reaction (**Scheme 5**), 1.041 g (7 mmol) of $C_9H_8O_2$, 1.294 g (7 mmol) of β-Ala-OtBu·HCl, 0.947 g (7 mmol) of HOBT, 2.657 g (7 mmol) of HBTU was added to 25 mL of dichloromethane (CH_2Cl_2). This reaction mixture was stirred under nitrogen at room temperature for 15 minutes before adding 2.34 g (14 mmol) of N-ethyldiisopropylamine (iPr_2NEt).

This reaction continued to stir under nitrogen at room temperature overnight. The next morning, it was worked up by washing in a separation funnel. It was washed once with 15% brine solution, twice with distilled water, four times with 20% citric acid solution, and four times with 7% sodium bicarbonate. The remaining dichloromethane was dried over sodium sulfate before being removed using a rotary evaporator at 38ºC.

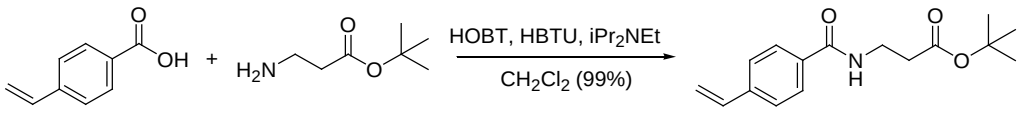

Scheme 5. Synthesis of protected β-alanine monomer.

^{1}H NMR spectrum suggested it needed further purification. The crude protected compound was dissolved in methanol (MeOH) and loaded into silica gel. This silica gel was then used to perform an automated flash chromatography with the CombiFlash Rf system from Teledyne Isco. Using a solvent system of dichloromethane and methanol (R_f = 0.9% dichloromethane/10% methanol), the CombiFlash was successful in the purification. The solvent was again removed from the system using a rotary evaporator at 38ºC.

Final purified protected aspartic acid monomer had a yield of 1.900 g (99%). ^{1}H NMR (500 MHz, CHLOROFORM-d) δ ppm 1.47 (s, 9 H) 2.56 (t, *J*=6.0 Hz, 2 H) 3.69 (q, *J*=6.0 Hz, 2 H) 5.35 (d, *J*=10.9 Hz, 1 H) 5.84 (d, *J*=17.6 Hz, 1 H) 6.74 (dd, *J*=10.9 Hz, 1 H) 6.87 (br s, 1H) 7.42-7.50 (m, *J*= 8.0 Hz, 2H), 7.70-7.76 (m, *J*= 8.3 Hz, 2H).

To deprotect, 1.900 g (6.900 mmol) was mixed with 10 mL trifluoroacetic acid (TFA) and 0.5 mL of triisopropylsilane (TIPS) under nitrogen at room temperature for 3 to 4 hours **(Scheme 6)**. The TFA was removed from the round bottom flask using a rotary evaporator at 38ºC.

The mixture was dissolved in methanol (MeOH) and loaded into silica gel. This silica gel was then used to perform automated flash chromatography with the CombiFlash Rf system from Teledyne Isco. A solvent system of dichloromethane and methanol (R_f = 0.1; 90% dichloromethane/10% methanol) was used with the CombiFlash to successfully removing the TIPS from the reaction mixture and allowed for the purification of the product. The solvent was again removed from the system using a rotary evaporator at 38ºC.

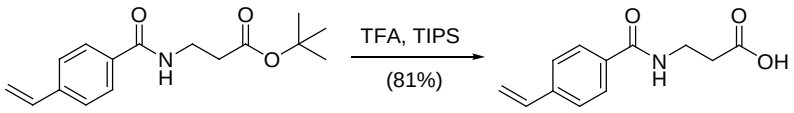

Scheme 6. Synthesis of de-protected β-alanine monomer.

Final purified β-alanine monomer had a product yield of 1.230 g, 81%. This compound polymerizes above 170ºC. ^{1}H NMR (400 MHz, METHANOL-d_4) δ ppm 2.64 (t, *J*=7.0 Hz, 2 H) 3.63 (t, *J*=6.9 Hz, 2 H) 5.34 (d, *J*=11.1 Hz, 1 H) 5.88 (d, *J*=17.6 Hz, 1 H) 6.78 (dd, *J*=17.6, 10.9 Hz, 1 H) 7.51 (m, *J*=8.2 Hz, 2 H) 7.77 (m, *J*=8.2 Hz, 2 H). ^{13}C NMR (100 MHz, METHANOL-d_4) δ ppm 34.79 37.18 116.42 127.38 128.75 134.78 137.42 142.37 170.02 175.52.

3-Amino-1,2-Diol Monomer Synthesis

A solution of 4-vinylbenzoic acid (0.445 g, 3 mmol), 3-amino-1,2-diol (0.271 g, 3 mmol), and EDC·HCl (0.578 g, 3 mmol) in methanol was stirred under nitrogen at room temperature for 3 hours (**Scheme 7**). Solvent was then removed under reduced pressure. The product was purified using automated flash chromotrography over silica gel using dichloromethane/methanol (R_f = 0.5; 90% dichloromethane/10% methanol) as the mobile phase.

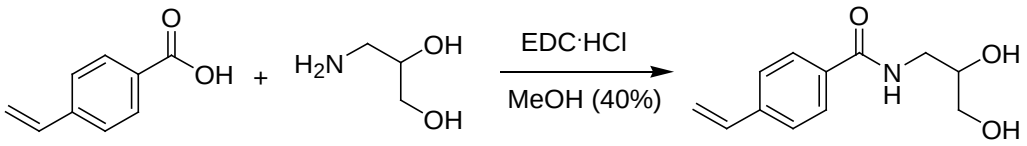

Scheme 7. Synthesis of 3-amino-1,2-diol monomer.

Yield (0.265, 40%); mp: 119-122ºC. ^{1}H NMR (400 MHz, METHANOL-d_4) δ ppm 3.42 (dt, *J*=13.4, 6.4 Hz, 1 H) 3.51 - 3.59 (m, 3 H) 3.80 - 3.87 (m, 1 H) 5.34 (d, *J*=10.8 Hz, 1 H) 5.89 (d, *J*=17.6 Hz, 1 H) 6.79 (dd, *J*=17.6, 10.8 Hz, 1 H) 7.52 (m, *J*=8.3 Hz, 2 H) 7.80 (m, *J*=8.5 Hz, 2 H) 8.40 (br s, 1 H). ^{13}C NMR (100 MHz, METHANOL-d_4) δ ppm 44.19 65.35 72.24 116.45 127.39 128.80 134.71 137.41 142.41 170.48.

2-Amino-1,3-Diol Monomer Synthesis (Alternative Monomer)

A solution of 4-vinylbenzoic acid (2.667 g, 18 mmol), 2-amino-1, 3-diol (1.641 g, 18 mmol), and BOP (7.962 g, 18 mmol) in 75 mL of dichlormethane was stirred under nitrogen at room temperature for 1 hour. N-ethyldiisopropylamine (iPr_2NEt) 7.8 mL (45 mmol) (**Scheme 8**) was then added. Solvent was removed under reduced pressure. The product was purified with automated flash chromotrography (**Figure A5**) over silica gel with dichloromethane/methanol (R_f = 0.5; 90% dichloromethane/10% methanol) as the mobile phase.

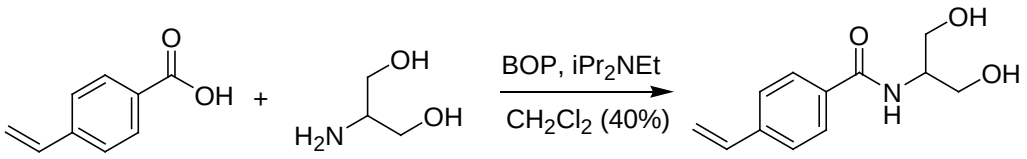

Scheme 8. Synthesis of 2-amino-1,3-diol monomer.

Yield (1.591, 40%), ^{1}H NMR (400 MHz, METHANOL-d_4) δ ppm 3.74 (d, *J*=5.0 Hz, 4 H) 4.17 (t, *J*=5.0 Hz, 1 H) 5.34 (d, *J*=10.9 Hz, 1 H) 5.89 (d, *J*=17.6 Hz, 1 H) 6.79 (dd, *J*=17.5, 11.1 Hz, 1 H) 7.51 (m, *J*=7.7 Hz, 2 H) 7.82 (m, *J*=7.7 Hz, 2 H). ^{13}C NMR (125 MHz, METHANOL-d_4) δ ppm 55.31 62.24 116.39 127.33 128.91 135.00 137.45 142.33 170.22.

Dansyl Monomer Synthesis

Monoboc ethylenediamine (1.280 g, 8 mmol), 4-vinylbenzoic acid (1.184 g, 8 mmol), BOP (3.540 g, 8 mmol), and methylmorpholine (2.634 mL, 24 mmol) were stirred at room temperature under nitrogen in dichloromethane (**Scheme 9**). The solvent was removed under reduced pressure and the product was characterized using NMR. ^{1}H NMR (400 MHz, CHLOROFORM-*d*) δ ppm 1.43 (s, 9H) 3.39-3.41 (m, 2H) 3.51-3.59 (m, 2H) 5.12 (br s, 1H) 5.34 (d, *J*=10.8 Hz, 1H) 5.82 (d, *J*=17.6 Hz, 1H) 6.73 (dd, *J*=17.6, 10.9 Hz, 1H) 7.43 (d, *J*=8.2 Hz, 2H) 7.78 (d, *J*=7.9 Hz, 2H).

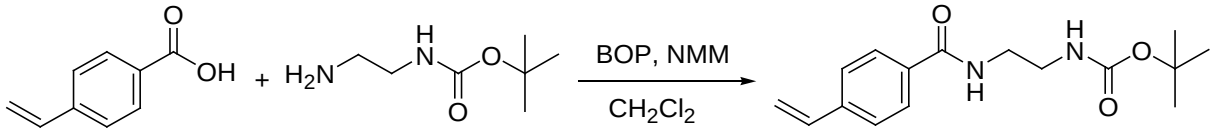

Scheme 9. Synthesis of protected ethylenediamine.

The product was de-protected by using a solution of hydrochloric acid 4 (N) in diethyl ether (**Scheme 10**). This resulting compound was then dried under reduced pressure. ^{1}H NMR

(400 MHz, METHANOL-d_4) δ ppm 3.18 (t, *J*=5.5 Hz, 2H) 3.68 (t, *J*=5.2 Hz, 2H) 5.36 (d, *J*=10.8 Hz, 1H) 5.91 (d, *J*=17.6 Hz, 1H) 6.80 (dd, J=17.4, 10.8 Hz, 1H) 7.54 (d, *J*=8.2 Hz, 2H) 7.86 (d, *J*=8.2 Hz, 2H).

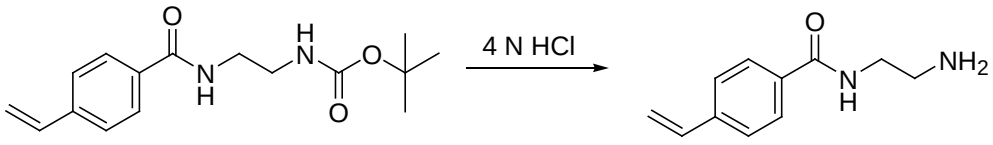

Scheme 10. Synthesis scheme of de-protected ethylenediamine.

This compound (0.625 g, 2.8 mmol), was reacted with dansyl chloride (0.782 g, 2.9 mmol), N-ethyldiisopropylamine (1.16 mL, 8.3 mmol), in dichloromethane and stirred at room temperature under nitrogen (**Scheme 11**). The product was purified using automated flash chromatography over silica gel with dichloromethane/methanol (Rf = 0.5; 90% dichloromethane/10% methanol) as the mobile phase.

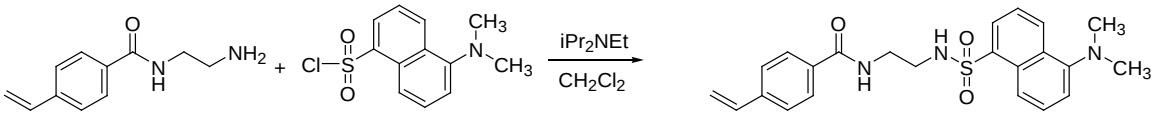

Scheme 11. Synthesis of dansyl chloride monomer.

Yield: (0.474 g, 40%); mp: 136-140ºC. ^{1}H NMR (400 MHz, METHANOL-d_4) δ ppm 2.83 (s, 6H) 3.07 (t, *J*=6.2 Hz, 2H) 3.38 (t, *J*= 6.2 Hz, 2H) 5.34 (d, *J*=11.0 Hz, 1H) 5.88 (d, *J*=17.6 Hz, 1H) 6.77 (dd, *J*=17.6, 10.0 Hz, 1H) 7.18 (d, *J*=7.5 Hz, 1H) 7.44 (m, *J*=8.4 Hz, 2H) 7.50-7.55 (m, 2H) 7.59 (m, *J*=8.2 Hz, 2H) 8.19 (d, *J*=7.3 Hz, 1H) 8.31 (d, *J*=8.7 Hz, 1H) 8.50 (d, *J*=8.5 Hz, 1H). ^{13}C NMR (125 MHz, METHANOL-d_4) δ ppm 41.03 43.43 45.89 116.42 116.48 120.48 124.37 127.29 128.71 129.32 130.42 130.99 131.34 131.42 134.39 136.82 137.43 142.29 153.30 170.05.

Inhibitor Monomer Synthesis

To a stirred solution of 4-vinylbenzoic acid (0.74 mg, 5 mmol) and mono-Boc protected 2,2'- (ethylenedioxy) dis ethyl amine (1.235 g, 5 mmol) was created in dichloromethane (40 mL). To this solution NMM (1.65 mL, 15 mmol) was added. This reaction mixture was stirred for 5 minutes before BOP (2.21 g, 5 mmol) was added (**Scheme 12**). After stirring at room temperature overnight, the reaction was quenched with brine. The reaction mixture was diluted with an additional 60 mL of dichloromethane. This 100 mL of dichloromethane was washed with 10% citric acid, 5% $NaHCO_3$ solution. The organic layer was then dried over sodium sulfate, solvent evaporated off, and the residue obtained was purified with flash chromatography (R_f = 0.5, 5% methanol in CH_2Cl_2). Yield: (1.590 g, 84%) ^{1}H NMR (400 MHz, CHLOROFORM-*d*) δ ppm 1.40 (br s, 9H) 3.28 (br s, 2H) 3.52 (m, 2H) 3.59-3.65 (m, 8H) 4.97 (br s, 1H) 5.27 (s, 1H) 5.32 (d, *J*=10.8 Hz, 1H) 5.80 (d, *J*=17.4 Hz, 1H) 6.68-6.73 (m, 1H) 7.44 (m, 2H) 7.73 (m, 2H).

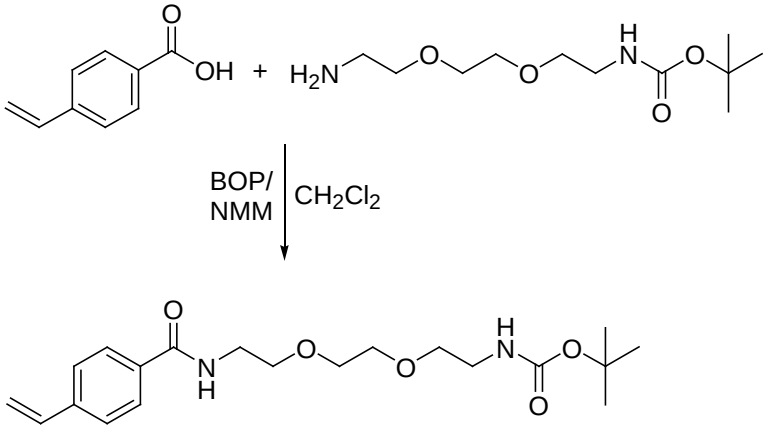

Scheme 12. Synthesis of protected linker.

The obtained product (1.45 g, 3.84 mmol) was stirred with hydrochloric acid 2 N in diethyl ether (10 mL) for 4 hours (**Scheme 13**). The precipitate formed was dissolved with a few

drops of methanol and then 5 mL of hydrochloric acid 2N in diethyl ether was added and stirred for 2 hours. This resulted in 1.203 g (100%) of deprotected product. ^{1}H NMR (400 MHz, METHANOL-d_4) δ ppm 3.09 (br s, 2H) 3.35 (s, 1H) 3.60 (t, *J*=5.2 Hz, 2H) 3.63-3.78 (m, 8H) 5.35 (d, *J*=10.8 Hz, 1H) 5.90 (d, *J*=17.6 Hz, 1H) 6.70-6.86 (m, 1H) 7.53 (d, *J*=7.9 Hz, 2H) 7.82 (d, *J*=8.2 Hz, 2H).

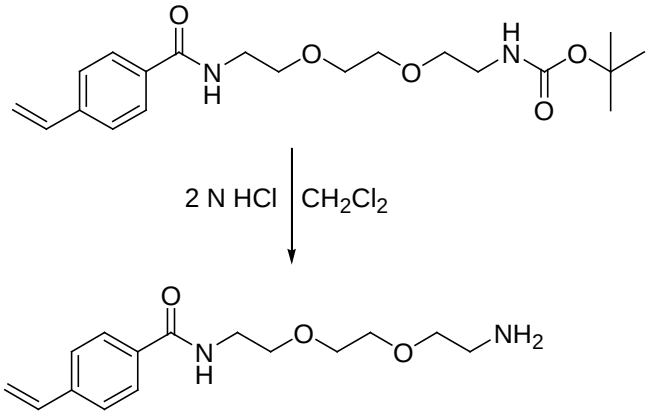

Scheme 13. Synthesis of de-protected linker.

Following a protocol similar to the first step, BOC deported adduct [N-(2-(2-(2-aminoethoxy)ethoxy)ethyl)-4-vinylbenzamide hydrochloride] (0.537 g, 1.70 mmol) was conjugated with 3-(trityloxycarbamoyl)propanoic acid (0.611 g, 1.63 mmol) employing BOP (0.722 g, 1.63 mmol) and NMM (0.71 mL, 6.518 mmol) in dichloromethane (35 mL) (**Scheme 14**). The crude product obtained after usual work up was purified by crystallization (dichloromethane/hexane) affording 0.741 g (72%) of pure product. ^{1}H NMR (500 MHz, CHLOROFORM-*d*) δ ppm 1.69 (s, 1H) 1.85 (br s, 1H) 2.14 (m, 2H) 2.26-2.38 (m, 1H) 3.37 (br s, 2H) 3.51-3.65 (m, 10H) 5.29-5.41 (m, 2H) 5.84 (d, *J*=17.4 Hz, 1H) 6.15-6.31 (m, 1H) 6.68-6.82 (m, 1H) 7.26-7.41 m, 18H) 7.45 (d, *J*=7.9 Hz, 5H) 7.79 (br s, 2H) 8.32 (s, 1H).

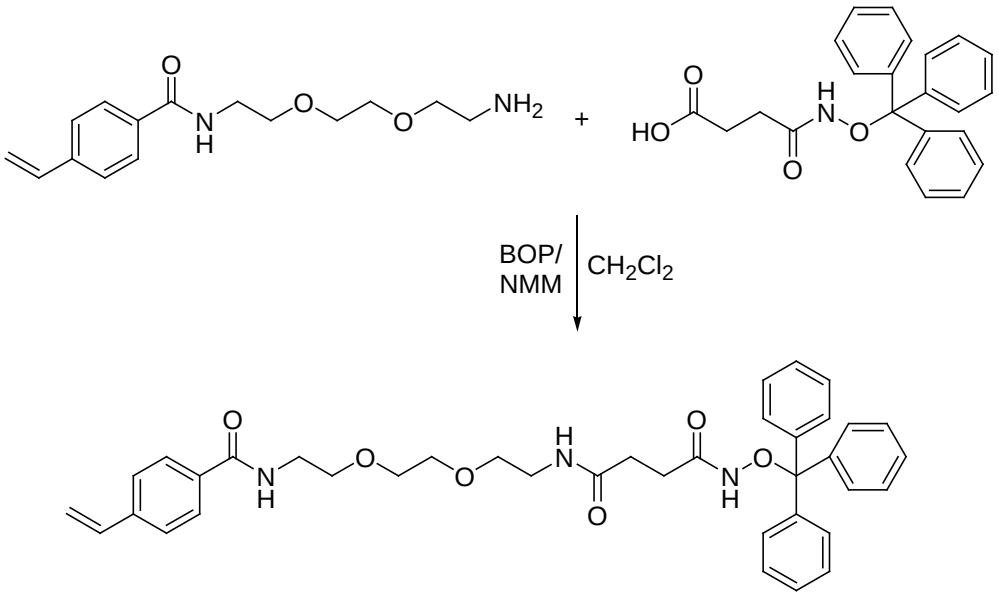

Scheme 14. Synthesis of protected MMP inhibitor

The obtained product (0.635 g, 1 mmol) was treated with 5% TIPS in TFA (3 mL) for 2 hours (**Scheme 15**). Addition of excess ether to the reaction mixture resulted in precipitate formation. The precipitate was centrifuged, washed with ether, and dried under vacuum.

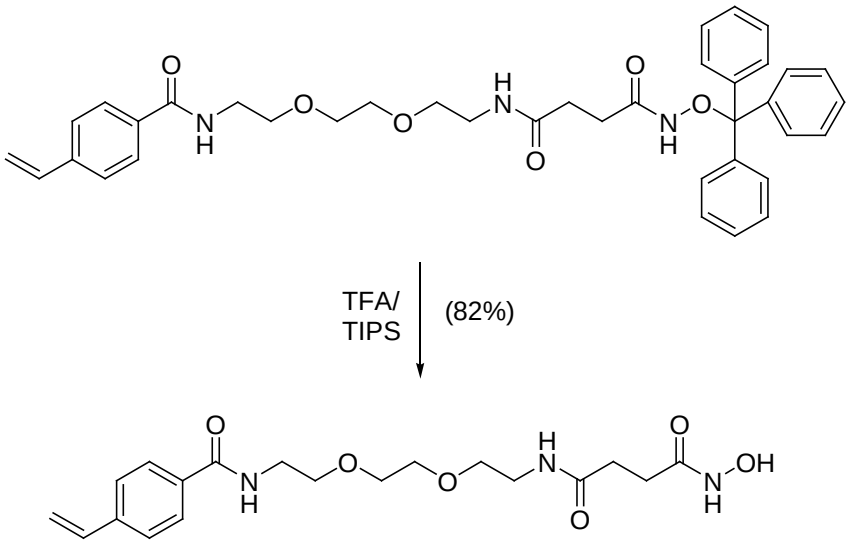

Scheme 15. Synthesis of de-protected MMP inhibitor monomer.

The final product obtained was 0.321 g (82%). mp: 135-138ºC. ^{1}H NMR (400 MHz, METHANOL-d_4) δ ppm 2.35 (t, *J*=7.3 Hz, 2H) 2.48 (t, *J*=7.3 Hz, 2H) 3.29-3.36 (m, 3H) 3.53 (t, *J*=5.4 Hz, 2H) 3.55-3.60 (m, 2H) 3.63 (br s, 2H) 3.64-3.70 (m, 4H) 5.34 (d, *J*=10.8 Hz, 1H) 5.89 (d, *J*=17.6 Hz, 1H) 6.79 (dd, *J*=17.6, 10.1 Hz, 1H) 7.52 (m, *J*=8.3 Hz, 2H) 7.80 (m, *J*=8.0 Hz, 2H). ^{13}C NMR (100 MHz, METHANOL-d_4) δ ppm 29.35 32.13 40.50 41.02 70.69 70.73 71.47 116.45 127.39 128.82 134.83 137.41 142.36 170.07 171.77 174.51.

Polymer Synthesis

Random copolymers were prepared from these synthesized monomers (**Figure 3**) using azoisobutyronitrile (AIBN) as the free-radical initiator following a literature protocol.[2,3] We systemically varied the starting monomer compositions (**Table 4**) and studied the interactions of the resultant polymers with recombinant human MMP-7, -9, and -10. The molecular weights of the polymers were determined by gel permeation chromatography (GPC). The molecular weights were in the range of 83-129 kDa with polydispersities in the range 1.2 – 2.5 (**Table 5**).

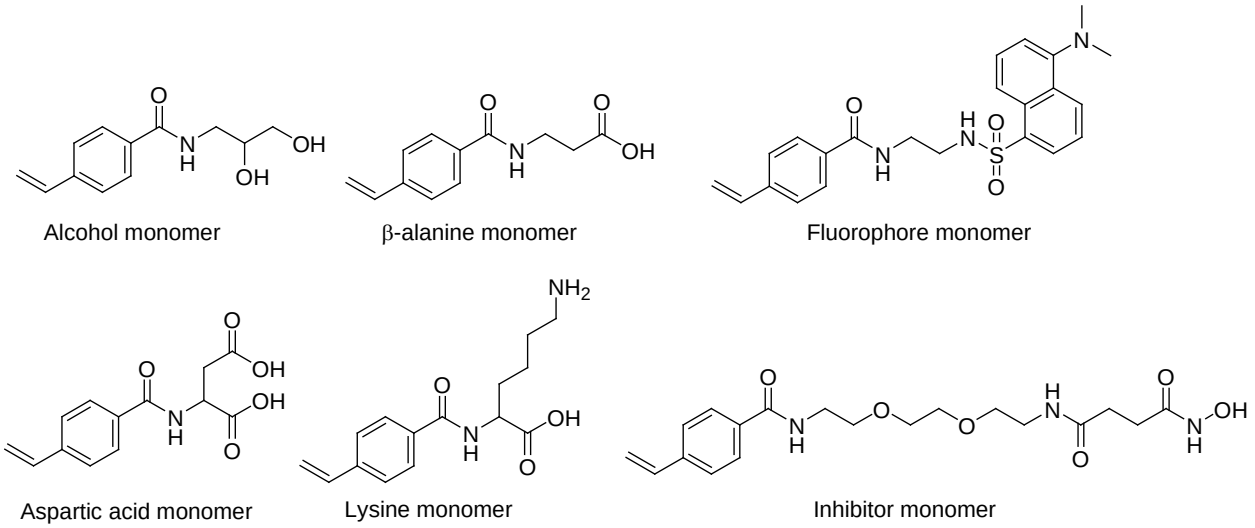

Figure 3. Structures of the monomers used for polymer synthesis.

Table 4. The composition of the monomers for random polymers. Note that **Polymer P8** used the alterative alcohol monomer (2-amino-1,3-diol).

Polymer	Monomers (mol%)					
	Dansyl	**Alcohol**	**Inhibitor**	**Asp**	**Lys**	**β-Ala**
P1	10	80	-	-	10	-
P2	10	70	10	-	10	-
P3	10	80	-	10	-	-
P4	10	70	10	10	-	-
P5	18	45	19	9	9	-
P6	12	64	-	12	12	-
P7	11	78	-	-	-	11
P8	11	78*	-	-	-	11

Table 5. GPC results, with weight average molecular weight (M_w), number average molecular weight (M_n), polydispersities (P.I.) of the polymers and the concentrations used during the experiments with the MMP isozymes.

Polymer	M_w	M_n	P.I.	Concentration Used (nM)
P1	106,622	66,942	1.59	29
P2	128,790	104,510	1.23	24
P3	83,618	40,895	2.04	36
P4	115,498	72,963	1.58	26
P5	114,428	78,161	1.46	27
P6	89,801	37,978	2.36	34
P7	127,656	77,145	1.65	24
P8	101,702	50,044	2.00	30

Interactions of the Polymers with MMP Isozymes

To study the interactions of the synthesized polymers with the MMP isozymes, nanomolar solutions of the polymers (25 – 35 nM in 30 mM phosphate buffer, pH = 7.4, (**Table 5**) were prepared and the MMP isozymes were added to make 200 nM of the final enzyme concentration.

The polymers (2 mg) were weighed and dissolved in 1 mL of the 30 mM phosphate buffer (pH = 7.4). Proper dilutions were performed to achieve the desired concentration in the cuvette. MMP-9 (10 µL of the 4.2 µM) was added to the cuvette and the solution was excited at 325 nm. The emission spectra were recorded between 350 nm and 750 nM (510 nm were the

peak emission intensities for 4-vinylbenzamide polymer). Ratios of (polymer peak vs. polymer-enzyme peak) were calculated at the respective emission spectra for the two series and Binary Logit regression analysis was performed to obtain the statistical significance. The same procedure was followed for MMP-7 and MMP-10.

The change in the emission spectra of the polymer incorporated dansyl group was recorded in the region 350-750 nm (λ_{ex} = 325 nm; **Figure 4**). We observed that the relative decrease in emission intensity (at 510 nm for polyvinylbenzamide polymers **P1** – **P8**) depends on the polymer used and the MMP isozyme tested. The ratios of the fluorescence emission intensities (at 541 nm and 510 nm) in the absence and in the presence of the MMP isozymes was calculated (**Table 6-8**) and subjected to statistical analyses to determine if they are significantly differences.

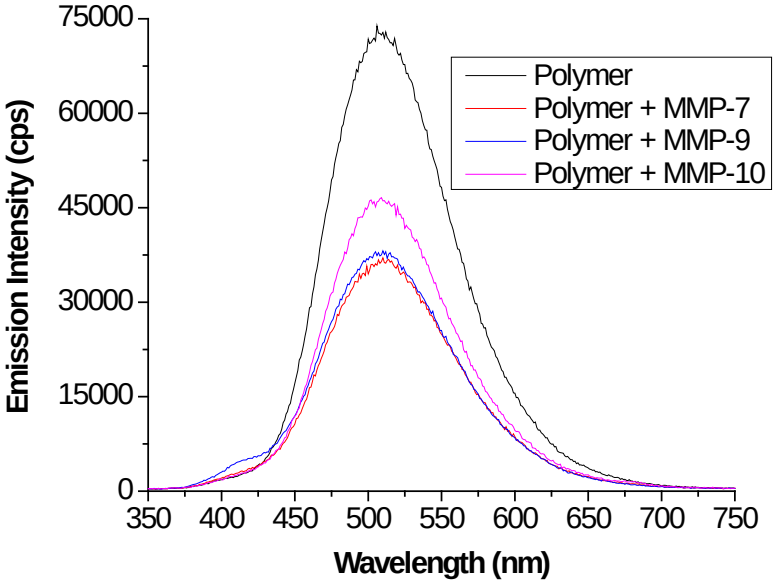

Figure 4. Fluorescence emission spectra of **Polymer P5**, (27 nM in 30 mM phosphate buffer, pH = 7.4; ex = 325 nm, black trace) in presence of 200 nM of recombinant human MMP-7 (red trace), MMP-9 (blue trace), and MMP-10 (purple trace).

Table 6. Fluorescent ratios of MMP-7.

	Run 1	Run 2	Run 3	Run 4	Run 5	Run 6
$P1_{510}$	1.09783	1.08970	1.07176	1.07978	1.07277	1.08885
$P1_{541}$	1.08405	1.09298	1.09321	1.07111	1.07275	1.08148
$P2_{510}$	1.05239	1.05164	1.04327	1.04826	1.05629	1.04406
$P2_{541}$	1.05940	1.05578	1.05952	1.05406	1.04519	1.04951
$P3_{510}$	1.07888	1.08605	1.02746	0.99775	0.99682	0.98468
$P3_{541}$	1.10317	1.05610	1.06255	1.00531	1.00290	0.99485
$P4_{510}$	1.03065	1.03742	1.02874	1.02269	1.01495	1.02749
$P4_{541}$	1.06111	1.05475	1.04369	1.04994	1.04771	1.05224
$P5_{510}$	1.20789	1.20448	1.23337	1.26453	1.25552	1.29332
$P5_{541}$	1.19144	1.21621	1.22159	1.24446	1.26990	1.27098
$P6_{510}$	1.03540	1.05658	1.07026	1.08790	1.07769	1.07476
$P6_{541}$	1.03204	1.07047	1.07672	1.08078	1.08591	1.05451
$P7_{510}$	1.05087	1.07378	1.05462	1.01353	1.02684	1.01151
$P7_{541}$	1.03192	1.07887	1.04068	1.01775	1.03912	1.00646
$P8_{510}$	1.07188	1.03198	1.06037	1.04851	1.08244	1.08398
$P8_{541}$	1.08123	1.06384	1.06747	1.10968	1.09674	1.10670

Table 7. Fluorescent ratios of MMP-9.

	Run 1	Run 2	Run 3	Run 4	Run 5	Run 6
$P1_{510}$	1.14732	1.14285	1.11874	1.11335	1.12647	1.14149
$P1_{541}$	1.17349	1.16273	1.16237	1.13856	1.12754	1.17205
$P2_{510}$	1.19975	1.19227	1.17954	1.16186	1.16541	1.15314
$P2_{541}$	1.18965	1.17300	1.16603	1.15512	1.17812	1.14650
$P3_{510}$	1.06144	1.08530	1.07744	1.06119	1.06869	1.07705
$P3_{541}$	1.04606	1.02972	1.06898	1.07775	1.05101	1.07898
$P4_{510}$	1.09672	1.10802	1.11834	1.09193	1.10704	1.09401
$P4_{541}$	1.11690	1.13318	1.11916	1.13294	1.08714	1.11336
$P5_{510}$	1.15423	1.15773	1.16043	1.15044	1.15356	1.14449
$P5_{541}$	1.16323	1.14936	1.16324	1.15008	1.15288	1.16503
$P6_{510}$	1.13889	1.13282	1.13606	1.12979	1.13404	1.13917
$P6_{541}$	1.12903	1.14651	1.15977	1.13732	1.13134	1.14907
$P7_{510}$	1.01543	1.07006	1.07435	0.99356	1.01356	0.98843
$P7_{541}$	1.04386	1.05369	1.08421	1.01547	1.02578	1.00430
$P8_{510}$	1.13582	1.07807	1.03383	0.97331	0.98958	0.99852
$P8_{541}$	1.09587	1.10469	1.03873	0.97229	0.99426	1.00425

Table 8. Fluorescent ratios of MMP-10.

	Run 1	Run 2	Run 3	Run 4	Run 5	Run 6
$\mathbf{P1_{510}}$	1.12621	1.12921	1.14616	1.13816	1.09163	1.06355
$\mathbf{P1_{541}}$	1.15478	1.15889	1.17158	1.14549	1.13467	1.08726
$\mathbf{P2_{510}}$	0.91725	0.91235	0.90278	0.90973	0.89907	0.90285
$\mathbf{P2_{541}}$	0.93883	0.93366	0.92990	0.92315	0.92081	0.92315
$\mathbf{P3_{510}}$	1.08760	1.07466	1.06813	1.07964	1.07322	1.08252
$\mathbf{P3_{541}}$	1.10781	1.10275	1.10492	1.09497	1.08741	1.09992
$\mathbf{P4_{510}}$	1.05327	1.06246	1.08098	1.05226	1.08082	1.05289
$\mathbf{P4_{541}}$	1.07053	1.08281	1.08254	1.06241	1.06010	1.08197
$\mathbf{P5_{510}}$	1.23600	1.24553	1.23246	1.22913	1.23249	1.24499
$\mathbf{P5_{541}}$	1.25551	1.24516	1.24089	1.21503	1.23581	1.22290
$\mathbf{P6_{510}}$	1.13737	1.16487	1.14267	1.16902	1.15933	1.15735
$\mathbf{P6_{541}}$	1.1651	1.16058	1.16751	1.15883	1.14841	1.16564
$\mathbf{P7_{510}}$	1.04396	0.99985	1.00403	1.01677	1.01285	1.00499
$\mathbf{P7_{541}}$	1.03455	1.02685	1.02844	1.02199	1.02959	1.01064
$\mathbf{P8_{510}}$	0.98939	1.01358	0.96394	0.94997	0.92981	0.91336
$\mathbf{P8_{541}}$	1.00353	1.02859	1.01541	0.98267	0.94960	0.96129

Statistical Data Analysis

The primary objective of the statistical analysis was to determine to what extent the polymer selectively interacts with the MMP-9 isozyme. A common approach to identify these relationships is linear discriminat analysis.[80, 81] However, the large number of polymers (8) relative to the small number of replications (6) for each enzyme-MMP pair made this approach infeasible.[82] A commonly used alternative, employed in this analysis, is (binary) logistic regression.[83] More specifically, each of the 18x1 data matrices containing the fluorescence intensities for a given polymer (6 replications and 3 MMPs per polymer) were "stacked" or "blocked" together to form a larger (144x1) vector of fluorescence intensity readings (8 polymers with 18 observations).[83] Additional columns in the data matrix were appended by creating a series of binary variables that identify each polymer, and these binary indicator variables were subsequently interacted with the fluorescence data to create a fully interacted data matrix (144x16). Lastly, three columns of binary variables were appended, where each new

column identified a particular MMP (-7, -9 or -10). The full data matrix is provided in **Tables 6-8**.

The value of this approach is that it allows for the estimation of a fully interacted logit model of the following form:

$$P(MMP_i^k = 1 \mid D, F) = \sum_{j=1}^{22} D_i^j \left(\beta_j + \gamma_j F_i^j\right)$$

$$P(MMP_i^k = 0 \mid D, F) = 1 - P(MMP_i^k = 1 \mid D, F)$$

where: i indexes each observation; P() denotes the cumulative logistic distribution; D is a binary indicator of each (j = 1,...,J) polymer, k denotes each isozyme (MMP-7, -9, and -10), F is the fluorescence of each isozyme; J denotes the number of polymers (8) and β, γ are parameter estimates. While this is estimated as single maximum likelihood estimation, the stacked data matrix allows separate intercept and slope estimates for each polymer included in the regression. That is, each of the polymer-specific response functions in a given group is "stacked" and estimated together to preserve adequate degrees of freedom to run the regression.

Because the goal of the analysis was to indentify which polymers selectively interacts with MMP-9, the equation above was estimated as a binary logit model, where the dependent variable takes a value of one for a MMP-9 isozyme, and zero if the isozyme is in the remaining categories (MMP-7, -10) (**Table 11-12**). This ensured a parsimonious estimation procedure without being forced to estimate above equation multiple times for each isozyme-copolymer grouping (MMP-9 versus MMP-7 (**Table 9-10**), MMP-9 versus MMP-10 (**Table 13-14**), etc.). Additionally, because each polymer has a separate response function with two parameter estimates (a slope and an intercept), results are presented using an odds ratio (with accompanying 95% profile confidence intervals) capturing the joint effects of these intercept and slope parameters for a given polymer on the MMP-9 isozyme. Values greater than unity (and

whose confidence intervals do not contain a value of one) indicate that the polymer significantly predicts or identifies the given MMP relative to its alternatives.

Table 12 identifies those polymers whose odds ratios are significantly greater than unity. This statistical analysis revealed that it is possible to design polymers that are able to selectively interact with isozymes within the MMP family. In particular, note that **Polymer P5** uniquely and significantly interacts with MMP-9 among the 4-vinylbenzamide copolymer group.

Table 9. Logit analysis of MMP-7 versus MMP-9/MMP-10, using the dependent variable to identify MMP-7.

Variable	Coeff.	Std. Err.	Wald Chi-Square Stat.	P-value	Significant
Binary Variables Identifying the Polymer					
P1	77.750	33.193	5.487	0.019	*
P2	-1.143	5.308	0.046	0.830	
P3	31.533	17.595	3.212	0.073	
P4	197.400	110.700	3.180	0.075	
P5	-27.898	17.859	2.440	0.118	
P6	86.747	36.973	5.505	0.019	*
P7	-9.430	23.668	0.159	0.690	
P8	-35.903	16.608	4.674	0.031	*
Slope Dummy Interaction Term between Fluorescence and Polymer					
P1*Fluorescence	-70.395	30.095	5.471	0.019	*
P2*Fluorescence	0.499	5.026	0.010	0.921	
P3*Fluorescence	-30.342	16.612	3.336	0.068	
P4*Fluorescence	-186.000	104.500	3.171	0.075	
P5*Fluorescence	22.437	14.611	2.358	0.125	
P6*Fluorescence	-78.430	33.243	5.566	0.018	*
P7*Fluorescence	8.515	22.884	0.138	0.710	
P8*Fluorescence	33.531	15.605	4.617	0.032	*
-2*Log-Likelihood Function			152.5460		
-2*Restricted Log-Likelihood Function			226.7210		
Chi-Square TestStatistic Value			74.1746	< 0.0001	*
Degrees of Freedom			16		
Number of Observations			144		

Table 10. Odds ratio estimates evaluated at grand sample mean of fluorescence for MMP-7 versus MMP-9/MMP-10.

Variable	Odds Ratio	95% Profile CI Lower Limit	95% Profile CI Upper Limit	Evaluated at Fluorescence Mean Value	Significant or chance
P1	2.616	0.464	14.764	1.091	
P2	0.549	0.194	1.559	1.091	
P3	0.209	0.045	0.963	1.091	Chance
P4	0.004	< 0.001	2.956	1.091	
P5	0.033	< 0.001	1.600	1.091	
P6	3.298	0.272	39.963	1.091	
P7	0.868	0.057	13.262	1.091	
P8	1.960	0.441	8.719	1.091	

Table 11. Logit analysis of MMP-9 versus MMP-7/MMP-10, using the dependent variable to identify MMP-9.

Variable	Coeff.	Std. Err.	Wald Chi-Square Stat.	P-value	Significant
Binary Variables Identifying the Polymer					
P1	-40.453	21.849	3.428	0.064	
P2	-50.592	22.452	5.078	0.024	*
P3	6.540	14.455	0.205	0.651	
P4	-110.500	50.124	4.856	0.028	*
P5	101.800	45.529	4.996	0.025	*
P6	-16.870	15.386	1.202	0.273	
P7	-14.904	23.818	0.392	0.532	
P8	0.661	9.693	0.005	0.946	
Slope Dummy Interaction Term between Fluorescence and Polymer					
P1*Fluorescence	35.098	19.111	3.373	0.066	
P2*Fluorescence	45.612	20.267	5.065	0.024	*
P3*Fluorescence	-6.737	13.592	0.246	0.620	
P4*Fluorescence	101.000	46.110	4.800	0.029	*
P5*Fluorescence	-85.875	38.488	4.978	0.026	*
P6*Fluorescence	14.423	13.579	1.128	0.288	
P7*Fluorescence	13.801	23.018	0.360	0.549	
P8*Fluorescence	-1.235	9.339	0.018	0.895	
-2*Log-Likelihood Function			156.6180		
-2*Restricted Log-Likelihood Function			226.7210		
Chi-Square TestStatistic Value			70.1024	< 0.0001	*
Degrees of Freedom			16		
Number of Observations			144		

Table 12. Odds ratio estimates evaluated at grand sample mean of fluorescence for MMP-9 versus MMP-7/MMP-10.

Variable	Odds Ratio	95% Profile CI Lower Limit	95% Profile CI Upper Limit	Evaluated at Fluorescence Mean Value	Significant or chance
P1	0.114	0.004	0.637	1.091	Chance
P2	0.433	0.005	3.838	1.091	
P3	0.446	0.120	1.360	1.091	
P4	0.771	0.112	> 999.999	1.091	
P5	> 999.999	15.387	> 999.999	1.091	*
P6	0.321	0.050	1.089	1.091	
P7	1.162	0.087	16.038	1.091	
P8	0.504	0.116	1.781	1.091	

Table 13. Logit analysis of MMP-10 versus MMP-7/MMP-9, using the dependent variable to identify MMP-10.

Variable	Coeff.	Std. Err.	Wald Chi-Square Stat.	P-value	Significant
Binary Variables Identifying the Polymer					
P1	-17.456	16.315	1.145	0.285	
P2	40.105	17.263	5.397	0.020	*
P3	-105.900	52.267	4.108	0.043	*
P4	10.8502	19.034	0.325	0.569	
P5	-28.069	17.901	2.459	0.117	
P6	-157.500	87.793	3.218	0.073	
P7	21.801	27.572	0.625	0.429	
P8	29.070	14.369	4.093	0.043	*
Slope Dummy Interaction Term between Fluorescence and Polymer					
P1*Fluorescence	14.900	14.386	1.073	0.300	
P2*Fluorescence	-40.454	17.352	5.435	0.020	*
P3*Fluorescence	97.359	47.997	4.115	0.043	*
P4*Fluorescence	-10.621	17.655	0.362	0.548	
P5*Fluorescence	22.577	14.645	2.377	0.123	
P6*Fluorescence	136.700	76.081	3.226	0.073	
P7*Fluorescence	-21.726	26.773	0.659	0.417	
P8*Fluorescence	-28.956	14.129	47.200	0.040	*
-2*Log-Likelihood Function			162.3030		
-2*Restricted Log-Likelihood Function			226.7210		
Chi-Square TestStatistic Value			64.4174	< 0.0001	*
Degrees of Freedom			16		
Number of Observations			144		

Table 14. Odds ratio estimates evaluated at grand sample mean of fluorescence for MMP-10 versus MMP-7/MMP-9.

Variable	Odds Ratio	95% Profile CI Lower Limit	95% Profile CI Upper Limit	Evaluated at Fluorescence Mean Value	Significant or chance
P1	0.301	0.049	1.134	1.091	
P2	0.018	< 0.001	0.305	1.091	Chance
P3	1.305	0.301	6.177	1.091	
P4	0.479	0.150	1.249	1.091	
P5	0.032	< 0.001	0.769	1.091	Chance
P6	< 0.001	< 0.001	0.332	1.091	Chance
P7	0.150	0.002	2.159	1.091	
P8	0.081	0.003	0.513	1.091	Chance

Polymer P5 contains the aspartic acid and the lysine monomers (10 mol% each) and 20 mol% of the inhibitor monomer. Decreasing the amount of the inhibitor monomer to 10 mol% (**P2** and **P4**) or omitting this monomer from the polymers (**P6**) led to the loss of selective interactions of the polymers with MMP-9 (**Table 11-12**). When the amount of inhibitor monomer (to 10 mol%) or incorporation of the β-alanine-based monomer in the polymer (**P7** and **P8**) was reduced it also had negative effect on the selective interactions with MMP-9 (**Table 11-12**). We also observed that the **Polymer P5** (100 nM each) is effective in inhibiting the activity of the enzyme MMP-9 (**Figure 5**). These observations indicated that possibly the inhibitor on the polymers is interacting with the active site of MMP-9 and the charged amino acids are forming additional interactions with the amino acid residues on the surface of the enzyme. However, increasing the amount of inhibitor monomer to 30 mol% in the polymers did not improve the selective binding to MMP-9 (data not shown). We do not have an explanation for this observation yet.

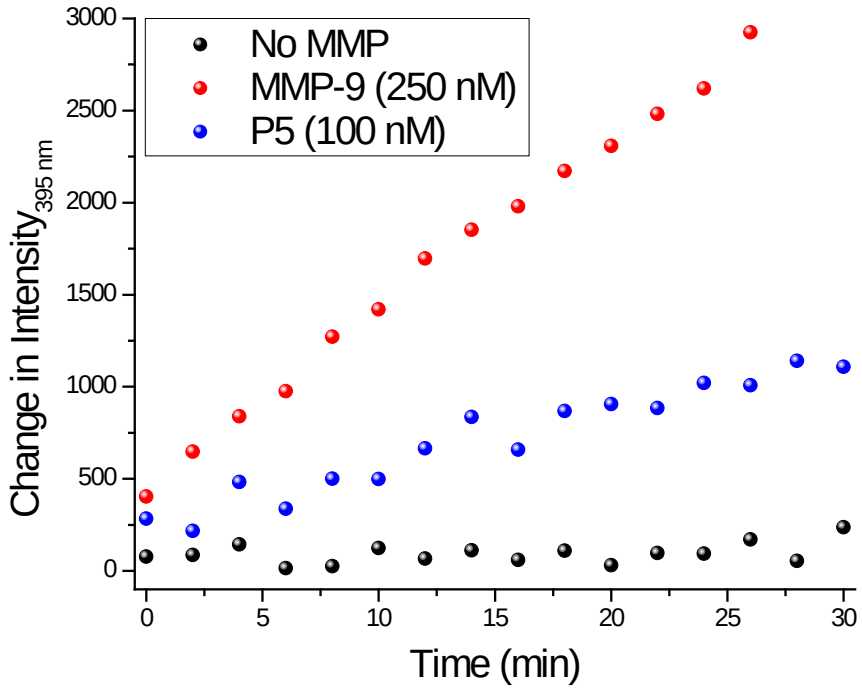

Figure 5. MMP-9 inhibition assay. The changes in fluorescence emission intensity (395 nm) of the MMP-9 fluorogenic substrate are shown with MMP-9 (250 nM, red spheres). The rate of increase of emission intensity was substantially reduced in the presence of 100 nM of polymer P5 (blue spheres). The emission intensity did not increase when the assay mixture was devoid of the enzyme MMP-9 (black spheres).

Conclusion

In conclusion, we have synthesized flexible, water-soluble polymers containing charges and a weak inhibitor for the MMPs. This polymer demonstrated selective interactions to the isozyme MMP-9 compared to MMP-7 and -10, even in a complex mixture of proteins (e.g., dilute human serum). We anticipate that by incorporating more potent and selective MMP inhibitors in the polymer and by optimizing the polymer structures, the selectivity of the interactions with MMP-9 could be further enhanced and maintained in more concentrated human serum samples.

References

65. Wenck, K., Koch, S., Renner, C., Sun, W. & Schrader, T. A noncovalent switch for lysozyme. *Journal of the American Chemical Society* **129**, 16015-16019 (2007).

66. Renner, C., Piehler, J. & Schrader, T. Arginine- and lysine-specific polymers for protein recognition and immobilization. *J Am Chem Soc* **128**, 620-628 (2006).

67. Schrader, T. & Koch, S. Artificial protein sensors. *Mol Biosyst* **3**, 241-248 (2007).

68. Fisher, J.F. & Mobashery, S. Mechanism-based profiling of MMPs. *Methods Mol Biol* **622**, 471-487 (2010).

69. Bellayr, I.H., Mu, X. & Li, Y. Biochemical insights into the role of matrix metalloproteinases in regeneration: challenges and recent developments. *Future Med Chem* **1**, 1095-1111 (2009).

70. Egeblad, M. & Werb, Z. New functions for the matrix metalloproteinases in cancer progression. *Nature reviews. Cancer* **2**, 161-174 (2002).

71. Overall, C.M. & Lopez-Otin, C. Strategies for MMP inhibition in cancer: innovations for the post-trial era. *Nature reviews. Cancer* **2**, 657-672 (2002).

72. Klein, G., Vellenga, E., Fraaije, M.W., Kamps, W.A. & de Bont, E.S. The possible role of matrix metalloproteinase (MMP)-2 and MMP-9 in cancer, e.g. acute leukemia. *Crit Rev Oncol Hematol* **50**, 87-100 (2004).

73. Chang, Y.H. et al. Elevated circulatory MMP-2 and MMP-9 levels and activities in patients with rheumatoid arthritis and systemic lupus erythematosus. *Clin Biochem* **41**, 955-959 (2008).

74. Yong, V.W., Zabad, R.K., Agrawal, S., Goncalves Dasilva, A. & Metz, L.M. Elevation of matrix metalloproteinases (MMPs) in multiple sclerosis and impact of immunomodulators. *J Neurol Sci* **259**, 79-84 (2007).

75. Kessenbrock, K., Plaks, V. & Werb, Z. Matrix metalloproteinases: regulators of the tumor microenvironment. *Cell* **141**, 52-67 (2010).

76. Paczek, L., Michalska, W. & Bartlomiejczyk, I. Trypsin, elastase, plasmin and MMP-9 activity in the serum during the human ageing process. *Age Ageing* **37**, 318-323 (2008).

77. Hurst, N.G. et al. Elevated serum matrix metalloproteinase 9 (MMP-9) concentration predicts the presence of colorectal neoplasia in symptomatic patients. *Br J Cancer* **97**, 971-977 (2007).

78. Verma, R.P. & Hansch, C. Matrix metalloproteinases (MMPs): chemical-biological functions and (Q)SARs. *Bioorg Med Chem* **15**, 2223-2268 (2007).

79. Banerjee, A.L. et al. Inhibition of matrix metalloproteinase-9 by "multi-prong" surface binding groups. *Chem Commun (Camb)*, 2549-2551 (2005).

80. Greene, N.T. & Shimizu, K.D. Colorimetric molecularly imprinted polymer sensor array using dye displacement. *Journal of the American Chemical Society* **127**, 5695-5700 (2005).

81. Nelson, T.L., O'Sullivan, C., Greene, N.T., Maynor, M.S. & Lavigne, J.J. Cross-reactive conjugated polymers: analyte-specific aggregative response for structurally similar diamines. *Journal of the American Chemical Society* **128**, 5640-5641 (2006).

82. Hair, J.F. Multivariate data analysis. (Prentice Hall, Upper Saddle River, N.J.; 1998).

83. Johnson, R.A. & Wichern, D.W. Applied multivariate statistical analysis, Edn. 5th. (Prentice Hall, Upper Saddle River, N.J.; 2002).

CHAPTER 3. FLUORESCENT POLYMER INTERACTIONS WITH CONDITIONED MEDIA FROM PROSTATE CANCER CELLS

Abstract

A novel methodology for identification and differentiation of prostate cancer cells was devised using a water soluble, fluorescent polymer. Step-wise linear discriminant analysis was used to demonstrate that differential modulations of the polymer emission intensities in the presence of conditioned cell culture media could distinguish between prostate cancer subtypes and between cancerous and non-cancer cells. The differences in the compositions of the conditioned cell culture media was likely contributing to different fluorescence spectral patterns of the polymers. This *in vitro* approach may provide a novel platform for the development of an alternative prostate cancer diagnostic and subtyping technique.

Introduction

Fluorescent polymers have been successfully used to distinguish different proteins,[84] isozymes,[85] and for differentiating cancerous, non-cancerous and malignant cell lines.[86] Unfortunately, translation of polymer technology has not yet evolved into any clinical applications. For clinical diagnosis of prostate cancer, analysis of blood, urine, or tumor markers such as prostate-specific antigen (PSA)[87] are used. However, the PSA analysis may provide ambiguous results, leading to over diagnosis of prostate cancer.[88, 89] Fluorescent,[90] luminescent,[91] or other dye-based imaging techniques[92] can also be used to detect different prostate cancer biomarkers. However, these diagnostic techniques do not differentiate the cancer cells into subtypes.

Cellular subtyping technologies come primarily from the field of microbiology. One classical example is the oligonucleotide sequencing employed in DNA microarrays and Southern blots.[93] A more recent development is microRNA sequencing for identification of cancerous biomarkers.[94] However, the employment of both of these techniques is dependent upon phenotypically expressed DNA. The development of epigenetic studies (*e.g.*, histone acetylation and methylation, DNA methylation, *etc.*) demonstrates that phenotype expression can be varied independent of DNA sequences.[95, 96] Thus, to obtain accurate results, we need to monitor at post-translational levels (*i.e.*, expressed proteins) for subtyping cancer cells.

To develop an *in vitro* approach for subtyping prostate cancer cells, the use of water soluble fluorescent polymers was explored. Recently it was demonstrated that a water-soluble, fluorescent polymer can be prepared for selective interactions with the isozyme matrix metalloproteinase-9 (MMP-9) compared to MMP-7 and -10.[85] MMP-9 is a Zn^{2+} containing metalloenzyme overexpressed and secreted at different concentrations by different cancer cells.[97, 98] The enzyme contributes to the growth and metastasis of a large number of cancers.[99] Besides MMP-9, various other extracellular (*e.g.*, MMP-7, urokinase plasminogen activator, *etc.*) and membrane-bound enzymes (a disintegrin and a metalloproteinase, ADAMs) are also overexpressed by metastatic cancer cells, albeit different amounts.[100-102] Thus it is reasoned that differential expression levels of various extracellular enzymes by the cancer cells will lead to differential modulations of fluorescence emission intensity from the water soluble polymers in the presence of conditioned cell culture media. Herein, we demonstrate that this strategy can be used for distinguishing prostate cancer cells from non-cancerous cells and for subtyping different prostate cancer cells. Human prostate and other cancer cells have been detected employing monoclonal antibodies as the recognition elements.[103-105] However, preparation and production

of monoclonal antibodies in large scale (> 1 g) can be really challenging. Proper storage and handling conditions must be followed to ensure that the monoclonal antibodies are not denatured and retain the selective binding properties. In contrast, the polymers reported here are easy to prepare on a large scale, and no special storage and handling procedures are needed.

Monomers **1** – **5** (**Figure 6**) were used to prepare the water-soluble, random **Polymer P5** employing AIBN as the free-radical initiator. It was previously observed (Chapter 2) that this polymer was able to distinguish recombinant human MMP-9 from MMP-7 and -10.[85] **Polymer P5** was prepared with the monomers containing 4-vinylbenzamide as the polymerizable group (starting with 45 mol% of monomer **1**, 9 mol% of monomer **2**, 9 mol% of monomer **3**, 18 mol% of monomer **4**, and 19 mol% of monomer **5**). Polymerization was performed in degassed DMF at 80°C. The polymers were purified using drop-wise addition of ethyl acetate. These polymers were then characterized by gel permeation chromatography (**Table 15**), using a Waters-2690 with a refractive index detector and N,N-dimethylformamide as the solvent.

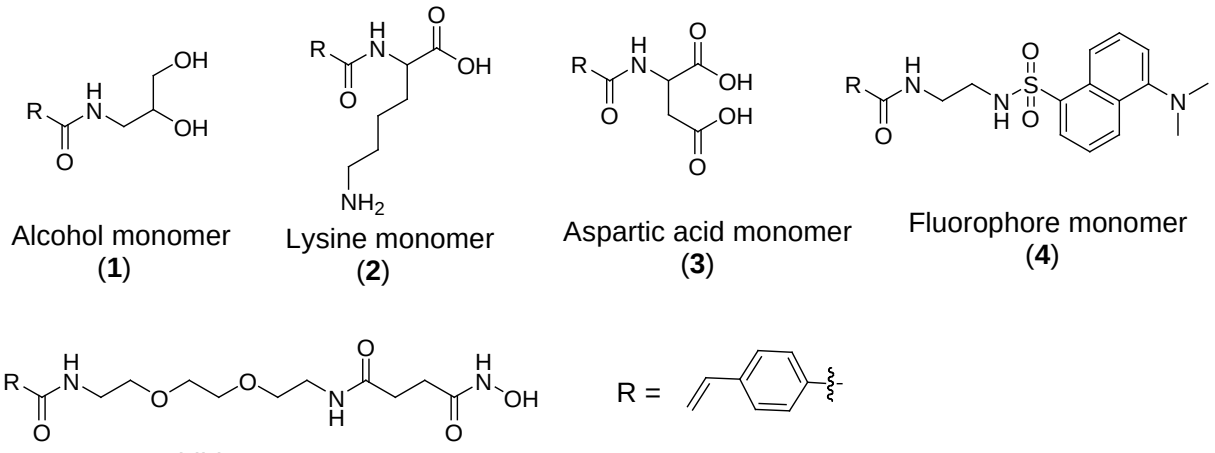

Figure 6. Structures of monomers for water-soluble, fluorescent polymer (**Polymer P5**).

Polymer P5 was expected to interact with MMP-9 using a variety of non-covalent interactions. In contrast to the reported polymers for differential interactions with cells,[86] this

polymer contains an attached MMP inhibitor (from the inhibitor monomer **5**). The hydroxamic acid moiety will interact with the Zn^{2+} ion in the active site pocket.[106] This interaction could serve as the initial anchoring site for the enzymes to the polymer and facilitate the formation of the additional surface binding interactions to the MMP-9 enzyme. For example, the polyamide backbone of the polymer can form hydrogen bonds with the enzyme surface. **Polymer P5** contains the benzamide groups and has the potential to interact with surface amino acids that contain conjugation.[107] Lysine (positive charge) and aspartic acid (negative charge) groups on the polymers can interact with complementary charges on the enzyme's surface. Hydrogen bonding interactions with the enzyme are also possible from the polymerized alcohol monomer **1**.

Table 15. Molecular weights of the **Polymer P5** determined by gel permeation chromatography.

	Polymer P5
M_w	114,428
M_n	78,161
P.I.	1.46
Concentration used	27 nM

For the fluorescence experiments, a phenol-free conditioned cell culture media from the prostate cancer cell lines (22Rv1 and PC-3), pancreatic cancer (PANC1), and non-cancerous cell line (HEK-293) was used. The experiments were conducted in 30 mM phosphate buffer (pH = 7.4). These cells were grown with a dye-free media in a humidified atmosphere of 5% CO_2 at 37ºC to a state of confluence. Upon reaching a confluent state, the cell's conditioned media was then harvested for fluorescence experiments.

Amongst the selected prostate cancer cells, 22Rv1 is androgen-dependent and PC-3 is androgen-independent.[108, 109] 22Rv1 is a prostate cancer cell line derived from a human prostatic

carcinoma xenograft, CWR22R.[108] This cell line represents both primary and relapsed cancer and is androgen-dependent.[108] Although this cell line is an androgen presenting cell line, it does not respond well to hormonal treatment.[110] However, it has been reported that it can be inhibited by using glycogen synthase kinase-3 (GSK-3) inhibitors. For example, SB216763 was reported by Kypta group, to inhibit growth and proliferation of 22Rv1 cells.[109] However, due to the potential side effects such of GSK-3 inhibitors, they should only be used in special cases were they are likely to be effective. The 22Rv1 cell line was grown in RPMI media (10% FBS and 1% antibiotics) and taken through three splitting cycles. Subsequently, the media was replaced with a dye-free RPMI. After two splittings, the cells were grown until confluent before culturing the media for fluorescence experiments.

PC-3 is an aggressive prostate cancer cell line. Due to the lack of androgen presenting cells, they do not respond to hormonal treatments. It is unlikely they would respond to GSK-3 inhibitors, which act by phosphorylation of the androgen presenting cells.[109] Differentiation between 22Rv1 and PC-3 cells would allow for the development of a low-cost, effectively strategic therapeutic plan. The PC-3 cell line was grown in RPMI media (10% FBS and 1% antibiotics) and taken through three splitting cycles. Subsequently, the media was replaced with a dye-free RPMI. After two splitting, the cells were grown until confluent before culturing the media for fluorescence experiments.

PANC-1 is a human pancreatic cancer isolated from a 56 year old male.[111] This cancerous cell line was used as a control to demonstrate that our polymer system could differentiate between prostate cancers cells from non-prostate cancer cells. The cell line was grown in DMEM media (10% FBS and 1% antibiotics) and taken through three splitting cycles.

Subsequently, the media was replacing with a dye-free DMEM. After two splittings, the cells were grown until confluent before culturing the media for fluorescence experiments.

HEK-293 is a human embryonic kidney cell line. This non-cancer cell line has been reported to secrete some amounts of MMP-9.[112, 113] This cell line will show that it is possible for our system to differentiate between non-cancerous cells and cancerous cells. This cell line was grown in MEM media (10% FBS and 1% antibiotics) and taken through three splitting cycles. Subsequently, the media was replaced with a dye-free MEM. After two splitting, the cells were grown until confluent before culturing the media for fluorescence experiments.

Upon the cells reaching a confluent state in their respective dye-free media, they were then aseptically transferred into a sterile centrifuge tube and centrifuged for 8 minutes at 226 g. Supernatant was then removed and used for the fluorescence and ELISA experiments. Additionally, the RPMI, DMEM, and MEM media before cell culture were used as the controls for fluorescence experiments.

The experiments revealed variations in emission spectra of the **Polymer P5** when exposed to the conditioned cell culture media from different cells. The emission spectra of the polymers in the presence of media before cell culture were used as the controls for these experiments. The control emission spectra of the polymer were subtracted from the emission spectra in presence of the conditioned media to generate the corresponding difference spectra (**Figure 7**).

To determine if the intensity changes correlated with the levels of MMP-9 secreted by these cells, the total concentration (*i.e.*, active and inactive) of MMP-9 in the conditioned cell culture media was determined by employing a commercially available ELISA kit. We observed that the PANC1 cells secreted the highest amount of MMP-9 in the conditioned media (2 ng/mL)

and the amounts of MMP-9 secreted by the other cells were similar (740 – 780 pg/mL). Clearly, the changes in the emission intensity of the polymers do not correlate with the concentration of secreted MMP-9. Other proteins in the conditioned media are interacting with the polymers, causing the observed intensity changes in the emission spectra.

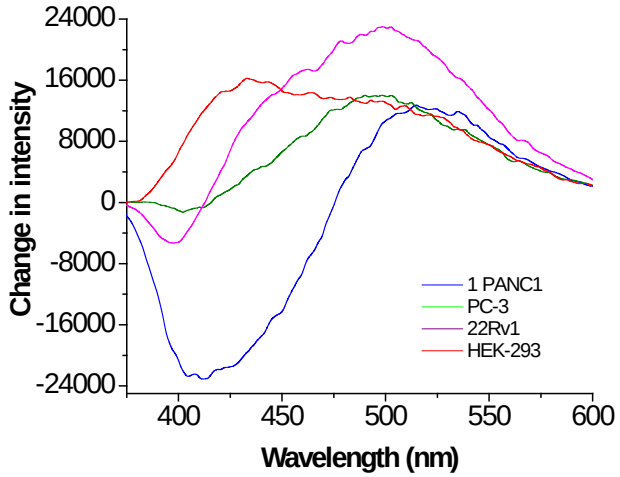

Figure 7. The difference emission spectra for **Polymer P5** in the presence of conditioned cell culture media from prostate cancer. The cancer cells PANC-1 (blue trace), PC-3 (green trace), 22Rv1 (pink trace) and HEK-293 (red trace). The emission spectra in the presence of unconditioned media were subtracted from the emission spectra in the presence of conditioned media to generate this plot.

While no explanation is available for the observed pattern of emission intensity changes, it is reasoned that these differential modulations can be used to distinguish the cancer cells. Toward this endeavor, ratios of emission intensity (410, 520 and 541 nm) in the presence of conditioned and unconditioned culture media (**Table 16**) were calculated. These ratios were subsequently subjected to linear discriminant analysis (LDA).

An issue which potentially confounds the empirical analysis is the fact that the polymer exhibits multiple peak emission intensity ratios. Without first identifying a true peak value, any results are potentially confounded, since a given polymer is found to be inferior maybe because it

does not adequately discriminate between the different cell lines, or because the emission intensities recorded for the polymer-cell line pair in question were not evaluated at their maximum values. To account for this possibility, LDA was applied in a stepwise fashion. First LDA was applied to the polymer, where we evaluated each potential peak value (410 nm, 510 nm and 541 nm) based on its ability to discriminate among (or predict) the four cell lines. Consistent with **Table 16**, each of these analyses was conducted using 32 observations (4 cell lines x 8 replications) and 4 variables (the cell line indicator and the three emission intensity wavelength variables). Once the optimal wavelengths/emission intensity ratios was established the analysis to evaluate the polymer, could proceed.

Table 16. Ratio table for the fluorescence spectral measurements from conditioned cell culture media from prostate cancer. Ratios were generated by taking condition cell culture media responses and dividing it by the corresponding unconditioned media responses.

Media	Run 1	Run 2	Run 3	Run 4	Run 5	Run 6	Run 7	Run 8
$PANC1_{410\ nm}$	0.847175	0.79479	0.820133	0.873235	0.963781	1.166412	1.072606	1.046227
$PC\text{-}3_{410\ nm}$	0.980398	1.146483	1.134677	1.10082	0.845879	0.870458	0.851185	0.871067
$22Rv1_{410\ nm}$	0.957827	1.199962	1.683281	1.747369	0.976151	1.011236	1.012318	1.04488
$HEK\text{-}293_{410\ nm}$	1.35795	1.462229	1.533244	1.616637	1.229342	1.432922	1.467823	1.454648
$PANC1_{510\ nm}$	1.157132	1.192934	1.136687	1.128721	1.110368	1.133213	1.133845	1.080713
$PC\text{-}3_{510\ nm}$	1.205312	1.168119	1.118452	1.078845	1.020244	0.971663	0.977633	0.933846
$22Rv1_{510\ nm}$	1.360548	1.312755	1.408855	1.373154	1.199632	1.068929	1.017879	1.017785
$HEK\text{-}293_{510\ nm}$	1.205637	1.153849	1.148267	1.147307	1.13584	1.118666	1.100398	1.080768
$PANC1_{541\ nm}$	1.214931	1.226186	1.20726	1.162033	1.178908	1.171664	1.148778	1.113138
$PC\text{-}3_{541\ nm}$	1.20055	1.147366	1.080755	1.037216	1.036532	1.022657	0.987939	0.956024
$22Rv1_{541\ nm}$	1.320663	1.295402	1.38728	1.306137	1.200993	1.056485	0.995993	0.974746
$HEK\text{-}293_{541\ nm}$	1.170907	1.153743	1.135018	1.130831	1.11153	1.10938	1.083695	1.069458

In a given application of LDA, the researcher has the option of using prior information to specify the predictor variables in the analysis, or using stepwise, exploratory techniques (using Wilks' Lambda and F-tests as exclusion/inclusion criteria) to identify a smaller subset set of predictor variables. In this paper, prior information exists on the possible emission peaks. In the final LDA analysis, we also expect the polymer (**Polymer P5**), when evaluated with LDA at their optimal wavelengths, to be included in the final LDA analysis, regardless of the use of such

exclusion/inclusion criteria. As such, stepwise predictor selection criteria will not be used in the final stage of the analysis, as expected the use of these methods is moot (*i.e.* all predictor variables will pass the inclusion criteria). To ensure consistency across all LDA analysis, all candidate wavelength ratios in each of the LDA analyses was included and used to identify the optimal emission intensity ratios. In passing it was noted that replacement of our analysis with stepwise exclusion/inclusion criteria obtained quantitatively, but not qualitatively, similar results. More specifically, the same optima emission intensity ratio was identified in both instances.

The use of LDA is well-established in the literature, and the reader is referred to those sources to familiarize oneself with the detailed mechanics underlying the technique.[84, 86, 114, 115] In summary, we used standard F-tests and Wilks' Lambda values to examine mean differences across the predictor variables, and to access the fitness of the predictor variables (*i.e.* the emission intensity ratios in the first two applications of LDA or the two polymers in the final LDA) to discriminate across cell lines. Chi-square tests are used to assess the significance of any eigenvalues (and the canonical correlations and canonical discriminate functions characterized using these metrics) extracted by LDA. The overall contribution of each predictor variable to a given canonical function can be assessed using the discriminant function coefficients and the resulting structure matrix. The contribution of each predictor to the overall LDA can be assessed using "potency indices," where larger values indicated a greater contribution to the overall model. The global fit of the LDA model can be examined using plots of the canonical discriminant functions. A useful LDA model will produce plots that clearly distinguish between the cell lines as separate groups. Lastly, internal validity is assessed by examining the percentage of cell line observations that were correctly predicted by the model. Computed predicted values using both traditional and (leave one out) cross-validation techniques were used.

Models that correctly predicted a high percentage of observations, and display consistency in predicted values across both techniques, are interpreted as having greater internal validity.

Table 17 provides means, F-statistics and Wilks' Lambda values for each of the P2 polymer emission intensities, and for each cell line type. Note that smaller Wilks' Lambda values are preferred to larger values, since they indicate a greater potential for the given emission intensity to discriminate across cell lines. All F-statistics have significant p-values (less than 0.05), indicating that significant (joint) differences exist across group means for each cell line. For the HEK-293 cell line, the 410 nm emission intensity appeared to be the highest value. The 541 nm intensity was the highest for the PANC1 cell line. For the other cell lines, the highest mean emission intensities appeared at 510 nm. Wilks' Lambda values are lowest for 410 nm, followed by 510 nm and 541 nm.

Table 17. Tests of equality of group means.

Cell Line	410 nm[a, b]	510 nm[a, b]	541 nm[a,b]
PANC1	0.948	1.134	1.178
PC-3	0.975	1.059	1.059
22Rv1	1.204	1.220	1.192
HEK-293	1.444	1.136	1.121
Wilks' Lambda	0.457	0.729	0.735
F-Statistic	11.089	3.465	3.368
P-Value	< 0.001	0.029	0.032

[a] first panel provides group-specific means [b] second panel provides statistics and p-values

Table 18 identifies the number of significant canonical correlations and canonical functions. At the 5% level, all three canonical functions are significant. The first canonical explains 63.3% of the variation across cell lines. The remaining functions explain 25.9% and 10.8%, respectively. Based on these results, we focus primarily on the first discriminant function.

Figure 8 contains a canonical function plot of the first two canonical functions which explains 89.2% of the variation in the cell lines. The HEK-293 is clearly distinguished as a group in the plot, but PANC-1, PC-3 and 22Rv1 overlap slightly. Traditional and cross-validated discriminant functions each correctly predicted 62.5% and 56.3% of the cell lines, respectively. This indicated a moderate degree of interval validity.

Table 18. Canonical function summary[a]

Fct.	Eigen-Value	Pct. of Variance Explained	Canonical Correl.	Wilks' Lambda[a]	Chi-Square Statistic	P-Value
1	2.021	63.3	0.818	0.135[b]	55.144	< 0.001
2	0.826	25.9	0.673	0.407[c]	24.739	< 0.001
3	0.346	10.8	0.507	0.743[d]	8.181	0.004

[a] Lower values for Wilks' Lambda indicate greater discrimination. Wilks' Lambda and chi-squae tests apply sequentially. [b] tests functions 1-3 cumulatively. [c] test functions 2-3 cumulatively [d] tests function 3.

Table 19 contains the standardized discriminant function coefficients, which measure the relative contributions from each of the emission intensity to a specific discriminant function. For function 1, the 540 nm wavelength exhibits the highest coefficient in absolute value, although and 510 nm emission intensity is only slightly smaller in absolute magnitude. The 510 nm exhibited the highest value for the second function, while 540 nm had the largest coefficient for the third canonical function.

Table 20 contains the structure matrix and the cumulative potency indices. This was used to access the overall contribution of each emission intensity to the discriminatory power of the LDA. The potency indices suggest that 410 nm emission intensity provided the largest overall contribution to the model's ability to distinguish between the cell lines.

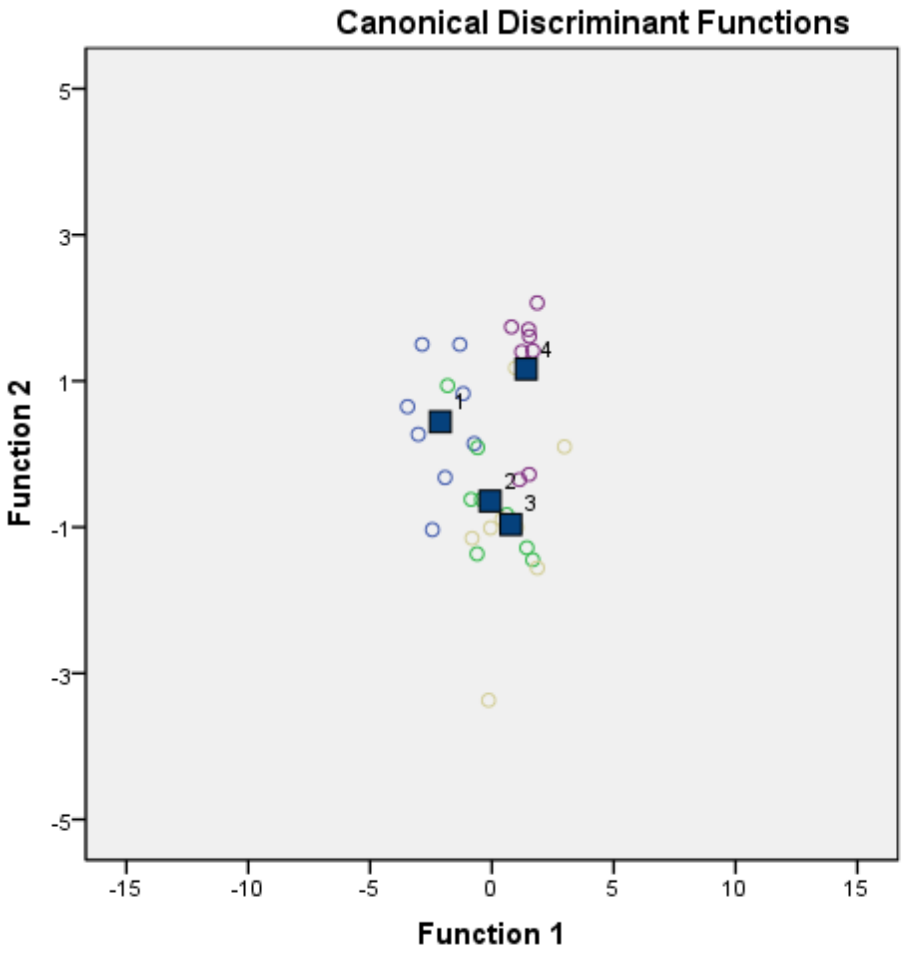

Figure 8. The canonical discriminant functions plots of **Polymer P5** with prostate cancer cell lines. This clearly shows the separation between the cell lines PANC1 (blue #1), PC-3 (green #2), 22Rv1 (yellow #3), and HEK-293 (purple #4). The boxes represent the four group's centroids.

Table 19. Standardized canonical discriminant function coefficients.

Predictor	Canonical Function 1	Canonical Function 2	Canonical Function 3
410 nm	0.544	1.113	0.066
510 nm	3.191	-3.906	0.235
541 nm	-3.416	3.285	0.736

Table 20. Structure matrix and potency index.

Predictor	Canonical Function 1	Canonical Function 2	Canonical Function 3	Potency Index
410 nm	0.645	0.552	0.529	0.372
510 nm	-0.092	-0.014	0.996	0.113
540 nm	0.106	-0.111	0.988	0.116

Conclusions

In conclusion, a water-soluble, fluorescent polymer that incorporated an inhibitor for the Zn^{2+}-containing metalloenzyme MMP-9 was prepared. This polymer showed differential modulations in emission spectra in the presence of conditioned cell culture media from cancer cells. It is likely that besides MMP-9, other proteins in the conditioned media are non-specifically interacting with the polymer. Despite these non-specific interactions, we can distinguish between the two prostate cancer cell lines using this *in vitro* polymer-based approach. We noted that the **Polymer P5** does not have good ability to discriminate the PC-3 cells from the PANC1 cells. Due to the complex nature of the conditioned cell culture media, an explanation yet for this lack of discrimination between these two cell lines is illusive.

References

84. Miranda, O.R., Creran, B. & Rotello, V.M. Array-based sensing with nanoparticles: 'chemical noses' for sensing biomolecules and cell surfaces. *Curr Opin Chem Biol* **14**, 728-736 (2010).

85. Dutta, R. et al. Fluorescent water soluble polymers for isozyme-selective interactions with matrix metalloproteinase-9. *Bioorg Med Chem Lett* **21**, 2007-2010 (2011).

86. Bajaj, A. et al. Array-based sensing of normal, cancerous, and metastatic cells using conjugated fluorescent polymers. *J Am Chem Soc* **132**, 1018-1022 (2010).

87. Oesterling, J.E. Prostate specific antigen: a critical assessment of the most useful tumor marker for adenocarcinoma of the prostate. *J Urol* **145**, 907-923 (1991).

88. Mokete, M., Shackley, D.C., Betts, C.D., O'Flynn, K.J. & Clarke, N.W. The increased rate of prostate specific antigen testing has not affected prostate cancer presentation in an inner city population in the UK. *BJU Int* **97**, 266-269 (2006).

89. Cooperberg, M.R., Lubeck, D.P., Meng, M.V., Mehta, S.S. & Carroll, P.R. The changing face of low-risk prostate cancer: trends in clinical presentation and primary management. *J Clin Oncol* **22**, 2141-2149 (2004).

90. Zhang, H., Uselman, R.R. & Yee, D. Exogenous near-infrared fluorophores and their applications in cancer diagnosis: biological and clinical perspectives. *Expert Opin Med Diagn* **5**, 241-251 (2011).

91. Maldiney, T. et al. Synthesis and functionalization of persistent luminescence nanoparticles with small molecules and evaluation of their targeting ability. *Int J Pharm* (2011).

92. Gao, X., Cui, Y., Levenson, R.M., Chung, L.W. & Nie, S. In vivo cancer targeting and imaging with semiconductor quantum dots. *Nat Biotechnol* **22**, 969-976 (2004).

93. Hsing, A.W. et al. Polymorphic CAG and GGN repeat lengths in the androgen receptor gene and prostate cancer risk: a population-based case-control study in China. *Cancer Res* **60**, 5111-5116 (2000).

94. Porkka, K.P. et al. MicroRNA expression profiling in prostate cancer. *Cancer Res* **67**, 6130-6135 (2007).

95. Minucci, S. & Pelicci, P.G. Histone deacetylase inhibitors and the promise of epigenetic (and more) treatments for cancer. *Nat Rev Cancer* **6**, 38-51 (2006).

96. Howitz, K.T. et al. Small molecule activators of sirtuins extend Saccharomyces cerevisiae lifespan. *Nature* **425**, 191-196 (2003).

97. Banerjee, J. et al. Release of liposomal contents by cell-secreted matrix metalloproteinase-9. *Bioconjug Chem* **20**, 1332-1339 (2009).

98. Banerjee, J. et al. Liposome-mediated amplified detection of cell-secreted matrix metalloproteinase-9. *Chem Commun (Camb)* **46**, 3209-3211 (2010).

99. Roy, R., Yang, J. & Moses, M.A. Matrix metalloproteinases as novel biomarkers and potential therapeutic targets in human cancer. *J Clin Oncol* **27**, 5287-5297 (2009).

100. Koskensalo, S. et al. MMP-7 overexpression is an independent prognostic marker in gastric cancer. *Tumour Biol* **31**, 149-155 (2010).

101. Duffy, M.J., McKiernan, E., O'Donovan, N. & McGowan, P.M. The role of ADAMs in disease pathophysiology. *Clin Chim Acta* **403**, 31-36 (2009).

102. Almasi, C.E. et al. Prognostic and predictive value of intact and cleaved forms of the urokinase plasminogen activator receptor in metastatic prostate cancer. *Prostate* (2010).

103. Taylor, R.M. et al. Multifunctional iron platinum stealth immunomicelles: targeted detection of human prostate cancer cells using both fluorescence and magnetic resonance imaging. *J Nanopart Res* **13**, 4717-4729 (2011).

104. Li, Q. et al. Detection of micrometastases in peripheral blood of non-small cell lung cancer with a refined immunomagnetic nanoparticle enrichment assay. *Int J Nanomedicine* **6**, 2175-2181 (2011).

105. Ziegler, V.G., Knaup, J., Stahl, D., Krammer, B. & Plaetzer, K. Fluorescence detection and depletion of T47D breast cancer cells from human mononuclear cell-enriched blood preparations by photodynamic treatment: Basic in vitro experiments towards the removal of circulating tumor cells. *Lasers Surg Med* **43**, 548-556 (2011).

106. Zucker, S. & Cao, J. Selective matrix metalloproteinase (MMP) inhibitors in cancer therapy: ready for prime time? *Cancer Biol Ther* **8**, 2371-2373 (2009).

107. Samanta, U., Pal, D. & Chakrabarti, P. Packing of aromatic rings against tryptophan residues in proteins. *Acta Crystallogr D Biol Crystallogr* **55**, 1421-1427 (1999).

108. Sramkoski, R.M. et al. A new human prostate carcinoma cell line, 22Rv1. *In Vitro Cell Dev Biol Anim* **35**, 403-409 (1999).

109. Mazor, M., Kawano, Y., Zhu, H., Waxman, J. & Kypta, R.M. Inhibition of glycogen synthase kinase-3 represses androgen receptor activity and prostate cancer cell growth. *Oncogene* **23**, 7882-7892 (2004).

110. Kim, H.J., Park, Y.I. & Dong, M.S. Comparison of prostate cancer cell lines for androgen receptor-mediated reporter gene assays. *Toxicol In Vitro* **20**, 1159-1167 (2006).

111. Lieber, M., Mazzetta, J., Nelson-Rees, W., Kaplan, M. & Todaro, G. Establishment of a continuous tumor-cell line (panc-1) from a human carcinoma of the exocrine pancreas. *Int J Cancer* **15**, 741-747 (1975).

112. Liu, H., Chen, B. & Lilly, B. Fibroblasts potentiate blood vessel formation partially through secreted factor TIMP-1. *Angiogenesis* **11**, 223-234 (2008).

113. Harris, J.E. & Friedland, J.S. l-Glutamate in Middlebrook 7H9 culture medium upregulates matrix metalloproteinase-2 secretion from human astrocytoma cells. *J Neurosci Methods* **173**, 291-294 (2008).

114. Johnson, R.A. & Wichern, D.W. Applied multivariate statistical analysis, Edn. 5th. (Prentice Hall, Upper Saddle River, N.J.; 2002).

115. Hair, J.F. Multivariate data analysis. (Prentice Hall, Upper Saddle River, N.J.; 1998).

CHAPTER 4. FLUORESCENT POLYMER-BASED POST-TRANSLATIONAL DIFFERENTIATION AND SUBTYPING OF BREAST CANCER CELLS

Abstract

Herein, we report the application of a synthesized fluorescent, water soluble polymer for post-translational subtyping and differentiation of breast cancer cells *in vitro*. The fluorescence emission spectra from this polymer was differently modulated in the presence of conditioned cell culture media from various breast cancer cells. This polymer differentiates at a post-translational level possibly due to their ability to interact with extracellular enzymes that are over-expressed in cancerous conditions.

Introduction

Sub-typing of breast cancer cells is highly important for the development of molecular medicine. However, current technologies (*i.e.* microarray, polymerase chain reaction, etc.) accomplish this objective at the pre-translational level.[116] These technologies are complex, time consuming, and expensive.[117, 118] Additionally, they do not account for important post-translational modifications (*i.e.*, pre-enzyme vs. active enzyme,[119] histone acetylation,[120, 121] methylation,[122] methionine removal,[123] *etc.*) that should be considered when grouping the breast cancer sub-types.[124] This study explored the application of fluorescent polymers to interact with extracellular proteins to allow for the differentiation and sub-typing of breast cancer cells at a post-translational level.

Fluorescent polymers have been used to distinguishing between enzymes,[125] isozymes,[119] and evaluate the effectiveness of antibiotics.[126] Our group has recently demonstrated the application of polymers towards sub-typing prostate cancer cells.[127] However, they have not

been investigated for their ability to distinguish between and sub-type different breast cancer cells. These breast cancer cell subtypes developed using different molecular mechanisms, and thus required different treatment options.

This system was designed from combinatorial screening of a small library which identified a polymer for selective interactions with metalloenzymes.[119] Metalloenzymes are expressed at different levels in different cancers and cell lines.[128]

It was expected that the selected polymer (**Figure 9**) will interact with extracellular metalloenzymes (such as MMP-7, MMP-9, ADAM-10, ADAM-12, etc.) through several mechanisms. The polymerizable moiety of 4-vinylbenzoic acid (**Polymer P5**, **Figure 9**) was used to create this polymer. **Polymer P5** was characterized using gel permeation chromatography (**Table 21**).

A known Zn^{2+} metalloenzyme inhibitor was conjugated to this polymerizable moiety.[119] It is expected that this inhibitor interacts with various metalloenzymes active site pocket by chelating the Zn^{2+} ion.[119] This anchor was facilitated by the formation of additional interactions between the polymer and the solvent-exposed surface amino acid residues. For example, aspartic acid (negatively charged at pH = 7.4) and lysine (positively charged at pH = 7.4) on the polymer form complementary interactions with opposite changes on the enzyme surface. Hydrogen bonding interactions between the polymer and the proteins from 3-amino-1,2-propanediol monomer; additional hydroxyl groups increased the polymer's water solubility. The diaminonaphthlenesulfonyl (dansyl)-containing monomer was incorporated to render the polymer fluorescent.

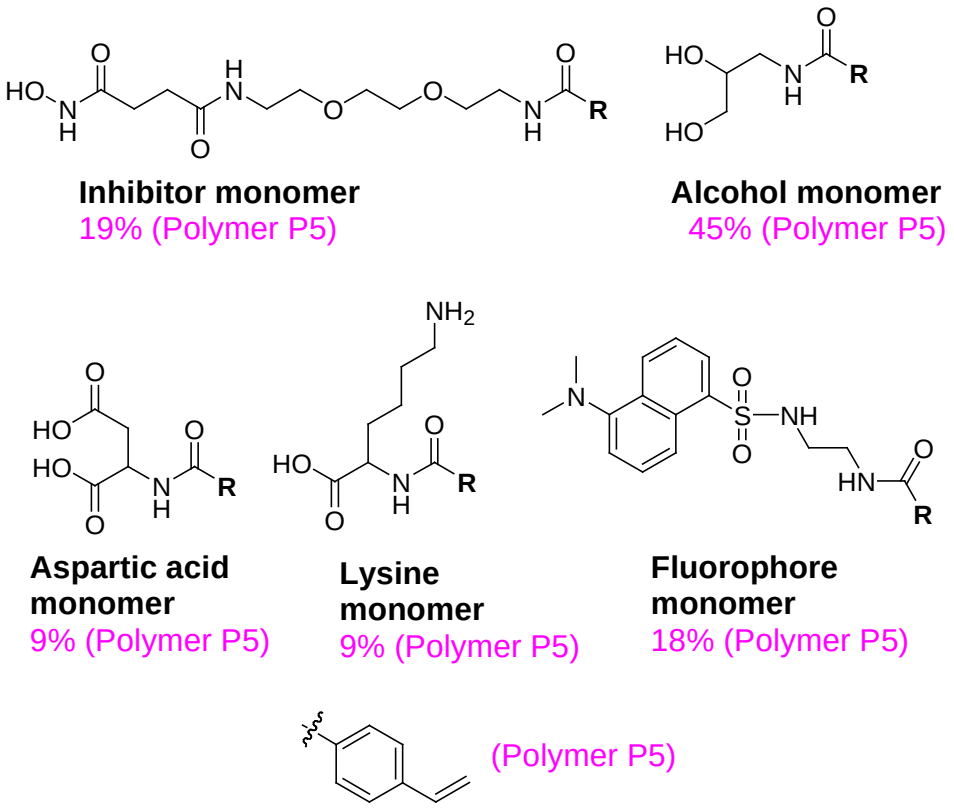

Figure 9. The monomers used for the synthesis of **Polymer P5**. Monomers were polymerized with AIBN as an activator at 80°C using DMF, and the resultant polymer was precipitated using drop-wise addition of ethyl acetate.

Table 21. Results of the GPC of **Polymer P5**.

Polymer	M_w	M_n	P.I.	Concentration (nM)
Polymer P5	114,428	78,161	1.46	27

The polymer's ability to distinguish between multi-drug resistant (MDA-MB-231) and non-resistant (MCF-7) breast cancer cells was examined. These cell lines were selected due to the difference in treatment options.[129] Thus, by distinguishing between these cells it will allow researchers and clinical providers the necessary information to develop and select the most effective breast cancer drug. Additionally, the polymers' ability to distinguish breast cancer from non-breast cancer and non-cancerous cells was also examined. In this endeavor, a cervical cancer cell line (HeLa) and a non-cancerous cell line (HEK-293) were tested in this analysis. All

cells were grown as instructed in their respective phenol red free media and upon reaching confluency, the dye-free conditioned culture media was then harvested for the fluorescence spectroscopic studies.

Cell Culture Studies

MCF-7 is a classical human breast cancer cell line obtained from a 69 year old female.[130] This cell line was established by the Michigan Cancer Foundation in 1973.[130] It was commonly used breast cancer model and should respond to several traditional drug therapies.[130]

MDA-MB-231 is another human breast cancer cell line that was obtained from a 51 year old female.[131] It distinguishes itself from MCF-7 in that it has a mutant p53 gene.[132] It also differs in that it is a multiple drug resistant breast cancer cell line.[133] Thus, being diagnosed with a breast cancer that is similar to this one means administration of many drugs will not successfully control the cancer. The patient will then suffer through the medications painful side-effects and the financial burden of therapy. Thus strategies for more aggressive means of detection coupled with the ability to distinguish between cancer sub-types, needed to be explored.

To demonstrate the polymers ability to distinguish breast cancer from non-breast cancer, the polymer's response to HeLa cells was explored. This cervical cancer cell line was taken from a female.[134] This is one of the most commonly used and oldest cancer cell lines.[135]

HEK-293 is a human embryonic kidney cell line.[136] This is a non-cancerous cell line, but has been reported to secrete MMP-9.[137] This cell line was used to demonstrate our polymers ability to distinguish between cancerous and non-cancerous cells, which secrete MMP-9.

All cell lines were cultured as instructed and maintained at 37°C in an atmosphere of 5% CO_2 in humidified air. HEK-293, MCF-7, and HeLa cells were all grown in MEM media with 10% FBS and 1% antibiotics. MDA-MB-231 was grown in DMEM media with 10% FBS and 1% antibiotics. They were all sub-cultured (each 3-5 days) for a total of three splits in their respected phenol red media. They were then split twice (each 3-5 days) in their respected phenol-free media. During the cell splitting process, HBSS and Trypsin-Versene were used as needed. Upon reaching a confluent state, the conditioned media was then aseptically transferred from the cultured flask into centrifuge tube. Before being allocated for their fluorescent studies, the conditioned media was then centrifuged at 226 g for 8 minutes to pellet and remove any remaining cells or debris.

Fluorescence Spectroscopy

Fluorescence spectroscopic experiments were performed by adding 50 µL of the respective harvested phenol-free conditioned cell culture media to a 200 µL solution of **Polymer P5** (27 nM) in phosphate buffer (30 mM, pH = 7.4). The solution was excited at 325 nm and collected the emission spectra (375 – 600 nm), repeated for eight total runs. For control, 50 µL of the corresponding phenol-free culture media (before cell growth) was added to the polymer solutions (200 µL) and the emission spectra was recorded.

The difference spectra (**Figure 10**) indicated each polymer responds differently to the conditioned cell culture media tested. In the presence of most of the conditioned media (except from the MDA-MB-231 cells), the emission from the polymer-incorporated dansyl groups increased in intensity and the emission maxima was blue-shifted. These results indicate that the polymer-bound dansyl groups experienced a more hydrophobic micro-environment in the

presence of conditioned media.[119] An explanation for the different spectral pattern observed in the presence of the conditioned media from the multi-drug resistant MDA-MB-231 cells is unclear. For analysis, the ratios of the emission intensities of the polymers in the presence of conditioned cell culture media over the corresponding unconditioned media were calculated at three different wavelengths (410, 510, and 541 nm). These ratios (**Table 22**) were submitted for statistical analysis to determine which wavelengths the polymer had the highest discrimination ability for the cells.

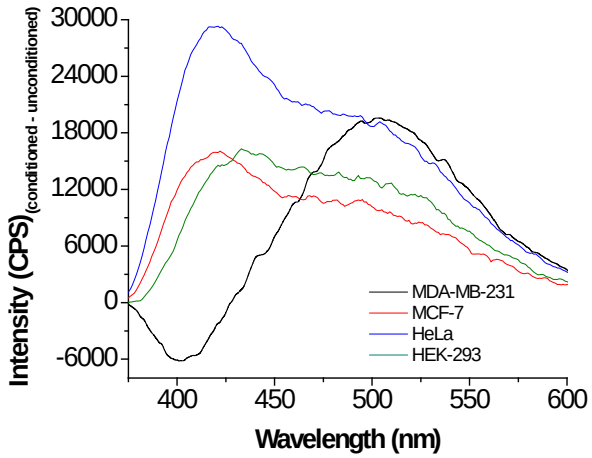

Figure 10. The difference emission spectra for **Polymer P5** in the presence of conditioned cell culture media from breast cancer. MCF-7 (red), MDA-MB-231 (black), HeLa (blue), and HEK-293 (green). The plots were generated by subtracting unconditioned media from conditioned media to remove any fluorescence signal variation caused by the media.

Table 22. Table of ratios generated from fluorescent experiments.

Cell Line	Run 1	Run 2	Run 3	Run 4	Run 5	Run 6	Run 7	Run 8
MDA-MB-231$_{410\ nm}$	0.95345	0.925732	0.911819	0.909788	0.854827	0.747671	0.807543	0.897796
MCF-7$_{410\ nm}$	1.430649	1.595537	1.542606	1.541282	1.581215	1.683029	1.721094	1.819321
HeLa$_{410\ nm}$	1.859018	1.863717	1.991359	1.974274	1.688984	1.777685	1.824472	1.897512
HEK-293$_{410\ nm}$	1.35795	1.462229	1.533244	1.616637	1.229342	1.432922	1.467823	1.454648
MDA-MB-231$_{510\ nm}$	1.288346	1.222454	1.185932	1.143421	1.064746	1.037664	1.025797	1.012537
MCF-7$_{510\ nm}$	1.158239	1.119843	1.044218	1.020922	1.153711	1.152986	1.116271	1.112301
HeLa$_{510\ nm}$	1.443343	1.308815	1.279059	1.280228	1.27433	1.195992	1.216297	1.194899
HEK-293$_{510\ nm}$	1.205637	1.153849	1.148267	1.147307	1.13584	1.118666	1.100398	1.080768
MDA-MB-231$_{541\ nm}$	1.283912	1.232823	1.157046	1.141286	1.053587	1.047762	1.007657	1.019795
MCF-7$_{541\ nm}$	1.171913	1.094961	1.041461	0.989715	1.149254	1.138179	1.113694	1.123459
HeLa$_{541\ nm}$	1.411381	1.262355	1.277228	1.217731	1.218143	1.192556	1.18488	1.142353
HEK-293$_{541\ nm}$	1.170907	1.153743	1.135018	1.130831	1.11153	1.10938	1.083695	1.069458

LDA Analysis

Table 23 contains means, F-statistics and Wilks' Lambda values for **Polymer P5**'s emission intensity, disaggregated by cell line type. In passing it is noted that smaller values for the Wilks' Lambda indicated a greater potential for the given emission intensity to discriminate across cell lines. All F-statistics have associated p-values less than 0.05 indicated significant differences exist across group means for each cell lines. For the MDA-MD-231 cell line, the 510 nm emission intensity appears to be the highest value. For all other cell lines, the highest mean emission intensities appear at 410 nm. Wilks' Lambda values are lowest for 410 nm, followed by 510 nm, and 541 nm.

Table 23. Tests of equality of group means for **Polymer P5**.

Cell Line	410 nm[a, b]	510 nm[a, b]	541 nm[a, b]
MDA-MB-231	0.876	1.123	1.118
MCF-7	1.614	1.110	1.103
HeLa	1.860	1.274	1.238
HEK-293	1.444	1.136	1.121
Wilks' Lamdba	0.066	0.514	0.620
F-Statistic [3, 28]	131.264	8.821	5.722
P-Value	< 0.001	< 0.001	0.003

[a] first panel provides group-specific means [b] second panel provides statistics and p-values.

Table 24 identifies the number of significant canonical correlations and canonical functions. At the 5% level, two of three canonical functions significantly explained the four cell lines. Of these, the first canonical function is most important, as it explained 94.8% of the variation across cell lines. The remaining functions explain 5.1% and 0.1%, respectively. Based on these results, we focus primarily on the first discriminant function.

Figure 11 contains a canonical function plot of the first two canonical functions (explaining 99.9% of the variation in the cell lines). Note that cell lines 1 (MDA-MB-231) and 4 (HEK-293) are clearly distinguished as a group in the plot, while groups 2 (MCF-7) and 3

(HeLa) overlap slightly. Traditional and cross-validated discriminant functions each correctly predicted 90.6% of the cell lines, respectively, indicating a reasonable (but not perfect) degree of interval validity.

Table 24. Canonical function summary[a] for **Polymer P5**.

Fct.	Eigenvalue	Pct. Of Variance Explained	Canonical Correl.	Wilk's Lambda[a]	Chi-Square Statistic	P-Value
1	15.309	94.8	0.969	0.033[b]	93.686	< 0.001
2	0.823	5.1	0.672	0.541[c]	16.914	0.002
3	0.015	0.1	0.120	0.986[d]	0.396	0.529

[a] Lower values for Wilks' Lambda indicate greater discrimination. Wilks' Lambda and chi-square tests apply sequentially. [b] tests functions 1-3 cumulatively. [c] tests functions 2-3 cumulatively [d] test function 3.

Table 25 contains the standardized discriminant function coefficients, which measure the relative contributions of each emission intensity to a specific discriminant function. For function 1, the 540 nm wavelength exhibited the highest coefficient in absolute value. However, the 410 nm and 510 nm emission intensities carry values which (in absolute magnitude) are only slightly smaller in absolute magnitude than for 540 nm. Concomitantly, the 510 nm exhibits the highest value for the second function, while 540 nm has the largest coefficient for the third (insignificant) canonical function. In both the second and third canonical functions, the coefficient values for the 410 nm variable suggest that the 410 intensities have very little contribution to the second and third canonical discriminant functions. On the other hand, the 510 nm and 540 nm coefficient values for the second and third functions are large in absolute value, implying that these predictors contribute substantially to these functions.

To assess the overall contribution of each emission intensity to the discriminatory power of the LDA, we present **Table 26**, which contains the structure matrix and the cumulative potency indices. The potency indices suggest that 410 nm emission intensity provides the largest overall contribution to the model's ability to distinguish between the cell lines.

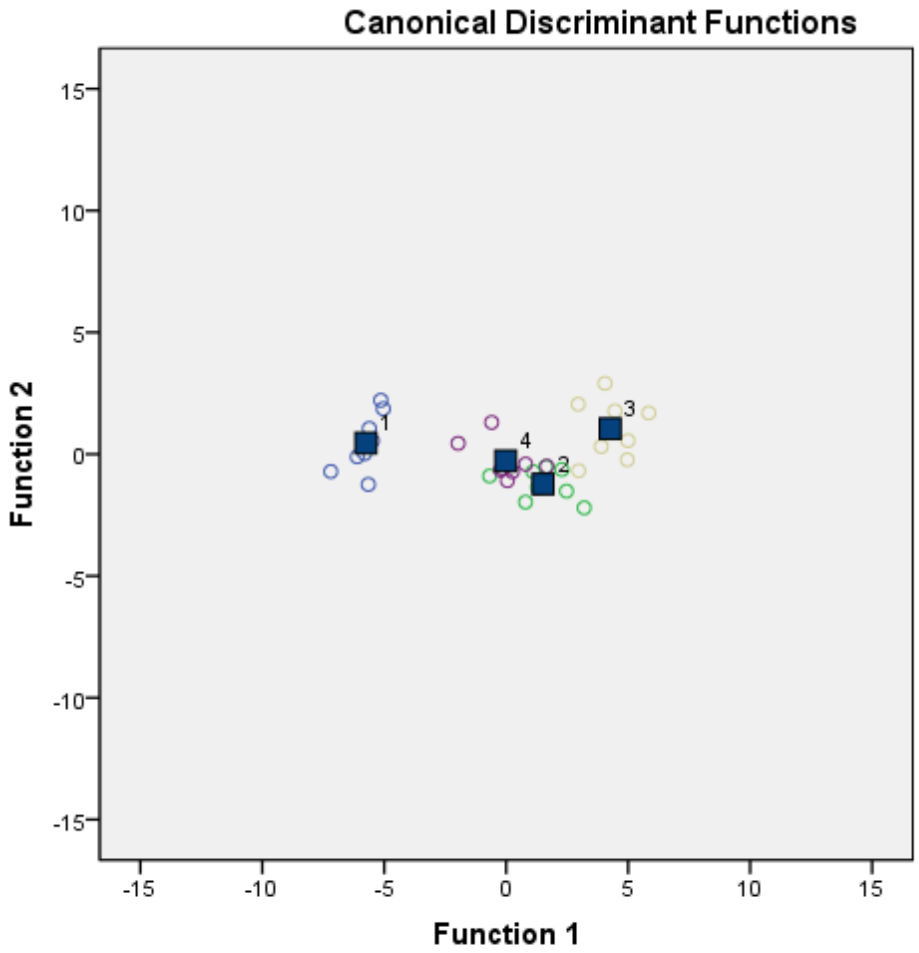

Figure 11. Polymer P5's canonical correlation plot for breast cancer cells. Between two largest canonical correlations and each of the four cell lines: MDA-MB-231 (group 1), MCF-7 (group 2), HeLa (group 3), and HEK-293 (group 4).

Table 25. Standardized canonical discriminant function coefficients for **Polymer P5**.

Predictor	Canonical Function 1	Canonical Function 2	Canonical Function 3
410 nm	1.008	-0.224	0.036
510 nm	1.193	3.087	-3.048
540 nm	-1.1280	-2.284	3.692

Overall, the LDA has a clear and intuitive interpretation. The results in **Table 24** suggest that the first canonical function is, by far, the most important discriminant function. **Table 25** and **Table 26** jointly suggested that while all three emission intensity variables contributed to the

first canonical function, the 510 nm and 540 nm variable contribute relatively more to the second and third canonical discriminant functions, while the 410 nm variable contributes very little to these latter functions. This implies that the 410 nm emission intensity is the "best" determinant of the cell lines for **Polymer P5**. The Wilks' Lambda and F-statistics in **Table 23** supports this assertion, as the 410 nm variable exhibits the highest mean values for 3 of the 4 cell lines.

Table 26. Structure matrix and potency index for **Polymer P5**.

Predictor	Canonical Function 1	Canonical Function 2	Canonical Function 3	Potency Index
410 nm	0.958	-0.109	0.265	0.871
510 nm	0.161	0.814	0.559	0.059
540 nm	0.123	0.673	0.730	0.038

It is possible that the conditioned media may contain globular proteins whose folding patterns are dependent upon hydrophobic interactions.[138] Thus **Polymer P5's** ability to participate in hydrophobic and π-π interactions maybe neutralized.[139] Thus utilization of a more hydrophilic polymer is likely more advantageous towards increasing the interactions and differentiation of globular proteins. However, other contributing factors included a reduction in flexibility and increased steric hindrance that lead to such results. These results are consistent with the previous report on polymer-based prostate cancer cell differentiation.[127]

Due to the complex nature of the conditioned media, it will be difficult to investigate which proteins or biomolecules contributed to the overall differentiation between the cancer cell subtypes. This was consistent with predictions regarding technological advancements within the field of proteomics and secretomics. It has been predicted that technologies will get faster, better discrimination ability, and offer increased potential for clinical application, while lacking a full understanding of the mechanism.[140] Although the mechanism of differentiation requires further investigation, our polymers clearly identify a simple, inexpensive methodology to subtype breast

cancer cells at a post-translational level, and does so at a greater level than for prostate cancer cell lines.

Conclusions

In conclusion, we synthesized water soluble fluorescent polymers that effectively differentiate breast cancer cell subtypes. Since this methodology works at a post-translational level, it offers a desirable alternative over the standard molecular biological techniques (*i.e.*, DNA sequencing). This is due to our method being affected only by phenotypically expressed genetic variations within the breast cancer cells.

References

116. Marchionni, L. et al. Systematic review: gene expression profiling assays in early-stage breast cancer. *Ann Intern Med* **148**, 358-369 (2008).

117. Zhang, D., Carr, D.J. & Alocilja, E.C. Fluorescent bio-barcode DNA assay for the detection of Salmonella enterica serovar Enteritidis. *Biosens Bioelectron* **24**, 1377-1381 (2009).

118. Shendure, J. & Ji, H. Next-generation DNA sequencing. *Nat Biotechnol* **26**, 1135-1145 (2008).

119. Dutta, R. et al. Fluorescent water soluble polymers for isozyme-selective interactions with matrix metalloproteinase-9. *Bioorg Med Chem Lett* **21**, 2007-2010 (2011).

120. Scott, M.D., Haldar, M.K. & Mallik, S. in Bioactive Natural Products: Opportunities and Challenges in Medicinal Chemistry. (ed. G. Brahmachari) (World Scientific Publishing, 2011).

121. Choudhary, C. et al. Lysine acetylation targets protein complexes and co-regulates major cellular functions. *Science* **325**, 834-840 (2009).

122. Heo, I. & Kim, V.N. Regulating the regulators: posttranslational modifications of RNA silencing factors. *Cell* **139**, 28-31 (2009).

123. Haldar, M.K., Scott, M.D., Sule, N., Srivastava, D.K. & Mallik, S. Synthesis of barbiturate-based methionine aminopeptidase-1 inhibitors. *Bioorganic & medicinal chemistry letters* **18**, 2373-2376 (2008).

124. Lim, Y.P. Mining the tumor phosphoproteome for cancer markers. *Clinical cancer research : an official journal of the American Association for Cancer Research* **11**, 3163-3169 (2005).

125. Renner, C., Piehler, J. & Schrader, T. Arginine- and lysine-specific polymers for protein recognition and immobilization. *J Am Chem Soc* **128**, 620-628 (2006).

126. Zhu, C., Yang, Q., Liu, L. & Wang, S. Rapid, Simple, and High-Throughput Antimicrobial Susceptibility Testing and Antibiotics Screening. *Angew Chem Int Ed Engl* (2011).

127. Scott, M.D. et al. Differentiation of Prostate Cancer Cells by Using Flexible Fluorescent Polymers. *Analytical chemistry* **84**, 17-20 (2012).

128. Park, S.Y. et al. Histone deacetylases 1, 6 and 8 are critical for invasion in breast cancer. *Oncol Rep* **25**, 1677-1681 (2011).

129. Roomi, M.W., Monterrey, J.C., Kalinovsky, T., Rath, M. & Niedzwiecki, A. Patterns of MMP-2 and MMP-9 expression in human cancer cell lines. *Oncol Rep* **21**, 1323-1333 (2009).

130. Soule, H.D., Vazguez, J., Long, A., Albert, S. & Brennan, M. A human cell line from a pleural effusion derived from a breast carcinoma. *J Natl Cancer Inst* **51**, 1409-1416 (1973).

131. Aspinall, S.R., Stamp, S., Davison, A., Shenton, B.K. & Lennard, T.W. The proliferative effects of 5-androstene-3 beta,17 beta-diol and 5 alpha-dihydrotestosterone on cell cycle analysis and cell proliferation in MCF7, T47D and MDAMB231 breast cancer cell lines. *J Steroid Biochem Mol Biol* **88**, 37-51 (2004).

132. Hui, L., Zheng, Y., Yan, Y., Bargonetti, J. & Foster, D.A. Mutant p53 in MDA-MB-231 breast cancer cells is stabilized by elevated phospholipase D activity and contributes to survival signals generated by phospholipase D. *Oncogene* **25**, 7305-7310 (2006).

133. Chen, J. et al. PKD2 mediates multi-drug resistance in breast cancer cells through modulation of P-glycoprotein expression. *Cancer Lett* **300**, 48-56 (2011).

134. Masters, J.R. HeLa cells 50 years on: the good, the bad and the ugly. *Nat Rev Cancer* **2**, 315-319 (2002).

135. Rahbari, R. et al. A novel L1 retrotransposon marker for HeLa cell line identification. *Biotechniques* **46**, 277-284 (2009).

136. Graham, F.L., Smiley, J., Russell, W.C. & Nairn, R. Characteristics of a human cell line transformed by DNA from human adenovirus type 5. *J Gen Virol* **36**, 59-74 (1977).

137. Malik, M.T. & Kakar, S.S. Regulation of angiogenesis and invasion by human Pituitary tumor transforming gene (PTTG) through increased expression and secretion of matrix metalloproteinase-2 (MMP-2). *Mol Cancer* **5**, 61 (2006).

138. Voet, D. & Voet, J.G. Biochemistry, Edn. 3rd. (J. Wiley & Sons, New York; 2004).

139. Salonen, L.M., Ellermann, M. & Diederich, F. Aromatic rings in chemical and biological recognition: energetics and structures. *Angewandte Chemie* **50**, 4808-4842 (2011).

140. Woodcock, J. The prospects for "personalized medicine" in drug development and drug therapy. *Clin Pharmacol Ther* **81**, 164-169 (2007).

CHAPTER 5. PYRANINE POLYMER FOR ENHANCED DIFFERENTATION OF BREAST AND PROSTATE CANCER CELL LINES

Abstract

Herein the foundation of the next generation of personalized medicine technology is reported. Using an accelerated form of detection, differentiation, and "sub-typing" between cancer cell types, a knowledge based mechanism is provided for highly effective therapeutics. This was accomplished utilizing not a genomics based approach but via secretomics. Secretomics is a subset of proteomics that measures proteins/enzymes secreted from the cell at a post-translational level. At this level, a nano-diagnostic (*i.e. in vitro* fluorescent polymers) based platform was utilized to rapidly discriminate between breast, prostate, and control cancer cell lines at a post-translational level. Thus this nano-diagnostic system successfully address limitations of pre-translational technologies such as active vs. inactive proteins/enzymes as well as the most debilitating technical issues confronting personalized medicine's practical utilization in therapeutic trails, timing.

Introduction

Traditional cancer therapy is dependent upon a "trial-and-error" methodology.[141, 142] Thus, the patient must suffer through the consequences of receiving improper treatment.[141] To eliminate this problem, a new model of "targeted" therapy has been proposed.[143] This therapeutic option uses molecular biology of disease development to design specific clinical agents that combat the particular cancer subset.[144] It is proposed that improper medical treatments that result from "trail-and error" and its consequences can be eliminated using "targeted therapy".[142] When health care providers identify cancer, as well as the molecular

mechanism of disease development (or subtype), and use this knowledge to prescript agents,[144] it would eliminate improper medical treatments that result from "trial-and-error" and its consequences.[142] This medical model of "targeted therapy" has been named "personalized medicine" by individuals in the field of genetics.[142, 144] The development of trastuzumab (Herceptin) and imatinib (Gleevec) in cancer therapy are two targeted therapy success stories.[144]

Despite these successes a large amount of work needs to be done to further develop this field. For example, technologies that subtype cancer cells are limited primarily to pre-translational methodologies and only measure disease development at the DNA or mRNA level.[142] Unfortunately, post-translational modifications are important factors in the cancer development and need to be considered when subtyping cancer.[145] For example, matrix metalloproteinase-9 (MMP-9) is translated as an inactive pro-MMP-9.[146] It only becomes active and thus physiologically relevant upon activation at a post-translational level.[146] MMP-9 has long been documented as an important contributor to cancerous development and is an important chemotherapeutic target.[147-149] Other potentially important post-translational modifications include: acetylation,[150, 151] methionine removal,[152, 153] methylation,[154] phosphorylation,[151, 155] ubiquitination,[155] etc. Additionally, pre-translational technologies are technically limited in the exorbitant amount of time necessary to develop clinically applicable analytical results.[144]

To address both of these issues, here it is reported the application of a nano-diagnostic platform that used fluorescent polymers to subtype breast and prostate cancer cells at a post-translational level. Fluorescent polymers offer the advantage of being cost-effective[156] and a very fast[157] detection system. They have been used by various groups to identify proteins[158] and stage of cancer.[159] In chapter 3 and 4, it was reported the initial success of utilizing a rationally-designed polymer for subtyping the cancerous cells.[145]

Using a similar formulation, a rationally-designed fluorescent polymer platform was constructed with an enhanced capacity to post-translational differentiation and subtyping of cancerous cells. This was accomplished by altering our fluorophore from a hydrophobic dansyl (**Figure 12**) group to a more hydrophilic pyranine (**Figure 13**), which contains three charged sulfonic acid functional groups. This alteration in fluorophores dramatically enhances our hydrophobic polymer's ability to distinguish and subtype the various cancerous cells.

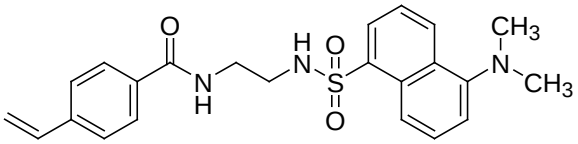

Figure 12. Dansyl chloride monomer.

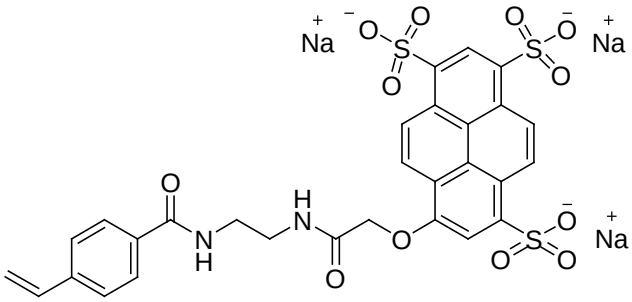

Figure 13. Pyranine monomer.

Methods

Pyranine Monomer Synthesis and Characterization

Polymer P9's pyranine monomer was prepared by synthesizing the first step (**Scheme 16**) according to a reported procedure.[160]

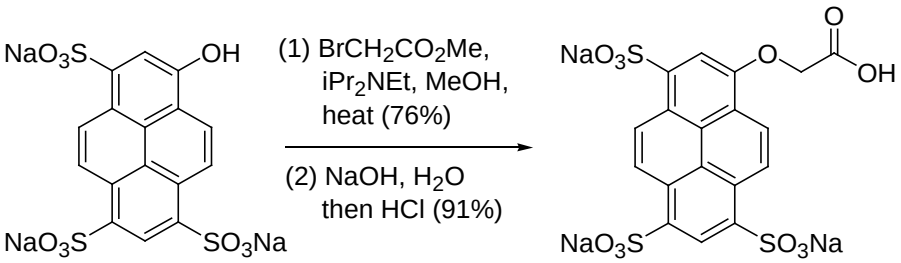

Scheme 16. First step to the pyranine monomer synthesis.

Mono BOC protected amine (832 mg, 5.2 mmol) (**Scheme 17**) was added to a stirred solution of cascade blue (2.329 g, 4 mmol) in 25 mL of DMF followed by HOBT (682 mg, 5.2 mmol). EDC (997 mg, 5.2 mmol) was then added and reaction mixture was stirred overnight at room temperature. Addition of excess isopropyl alcohol to the reaction mixture effected precipitation. The precipitate was centrifuged and then washed with isopropyl alcohol. The residue obtained was again dissolved in little water and precipitated with isopropyl alcohol. Centrifugation and successive wash of the residue with isopropyl alcohol and acetone followed by vacuum drying afforded yellowish green product. Yield: 2.25 g (78%). ^{1}H NMR 400 MHz; δ ppm 1.39 (s, 9 H) 3.22 - 3.28 (m, 2 H) 3.42 – 3.47 (m, 2 H) 4.96 (s, 2 H) 8.36 (s, 1 H) 8.85 (d, J=10 Hz, 1H) 9.14 (d, J=9.6 , 1 H) 9.22-9.28 (m, 2H) 9.4 (s, 1H).

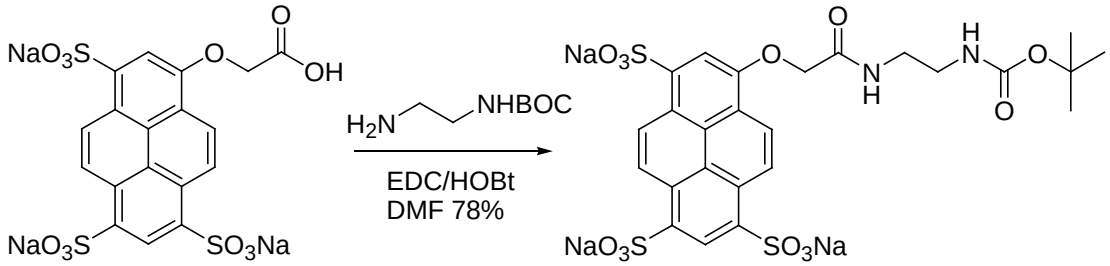

Scheme 17. Attachment of mono BOC protected amine.

This residue was treated with hydrochloric acid 4 (N) in dioxane (15 mL) (**Scheme 18**) for four hours. Solvent was removed under reduced pressure. This afforded BOC de-protected amine hydrochloride derivative of cascasde blue in quantitative yield. This was used without further purification to the next step. ^{1}H NMR (400 MHz, METHANOL-*d4*); δ ppm 2.9 – 3.0 (m, 2 H) 3.4 - 3.5 (m, 2 H) 4.91 (s, 2 H) 7.83 (br s, 3 H) 8.15 (s, 1 H) 8.52 – 8.57 (m, 2H) 8.95 – 9.04 (m, 2 H) 9.18 (d, J=9.6 Hz , 1H).

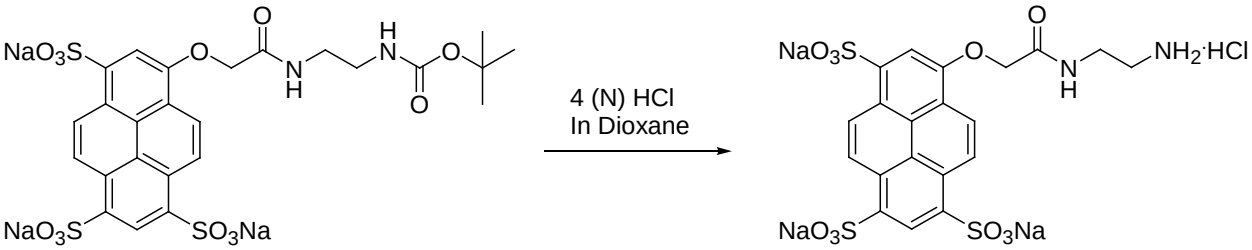

Scheme 18. The de-protection of the amine

A stirred solution of above (0.500 g, 0.75 mmol) in 20 mL of DMF had vinyl benzoic acid (0.560 g, 3.70 mmol) added (**Scheme 19**). This was followed by N-methyl morpholine (831 µL, 7.5 mmol). When the reaction mixture became clear, BOP (1.339 g, 3.03 mmol) was slowly added. This solution was stirred for 14 hours at room temperature under an inert atmosphere. Reaction mixture was precipitated by the addition of excess isopropyl alcohol (IPA), centrifuged, and washed with IPA. This residue was dissolved in water and precipitated with IPA. After centrifugation and successive wash with IPA/acetone, the residue was dried under vacuum.

Yield: 0.490 g (87%) of greenish yellow solid; mp: degrades above 257°C. ^{1}H NMR (500 MHz, CD_3OD, 25°C, TMS); δ ppm 2.9 – 3.0 (m, 2 H) 3.57 - 3.62 (m, 2 H) 4.82 (d, *J*=10.5 Hz, 1 H) 4.9 (s, 2 H) 5.07 (d, *J*=17.5 Hz , 1 H) 5.76 – 5.84 (m, 1 H) 6.2 (d, *J*=8 Hz , 2 H) 6.5 (d, *J*=8 Hz, 2 H) 7.9 (s, 1 H) 8.54 (d, 1 H) 8.75 – 8.82 (m, 2 H) 8.88 (d, 1 H) 9.0 (s, 1 H). ^{13}C NMR

(125 MHz, DEUTERIUM OXIDE) δ ppm 44.66 54.62 69.04 110.49 117.17 122.50 122.65 124.89 125.09 126.29 126.45 126.53 126.86 126.90 127.45 128.53 130.80 131.37 131.83 136.05 136.88 136.92 140.49 141.18 152.71 166.21 170.81 172.41.

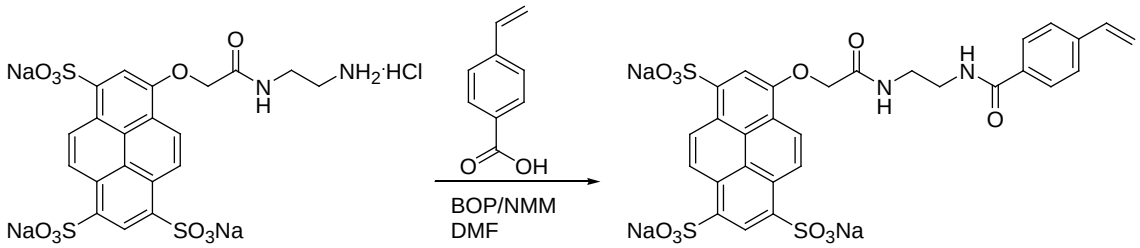

Scheme 19. The final step in the synthesis of the pyranine monomer.

Polymer Synthesis and Characterization

Polymers were fabricated such that they would have a variety of potentially available non-covalent interactions to interact with surface amino acids of secreted proteins/enzymes in the conditioned cell culture media. For example, hydrogen bonding interactions will be formed between the polymer and the proteins/enzymes via hydroxyl functional groups of the incorporated alcohol (**Figure 14**, Monomer 5). Additionally, ionic interactions will be formed using positively charged lysine (**Figure 14**, Monomer 1) and negatively charged aspartic acid (**Figure 14**, Monomer 3) residues. Additionally, a hydroxamic acid moiety (**Figure 14**, Monomer 4) will interact with active site Zn^{2+} ions from various secreted enzymes. These interactions will help facilitate the differentiation between the various cancer subtypes.

We prepared our water soluble **Polymers P9** from monomers 1-5 (**Figure 14**), using 1,1'-azobis(cyclohexane-carbonitrile) as a free-radical initiator in dimethylformamide. Polymers were purified using dialysis cassettes (MWCO 10,000) from Thermo Scientific in distilled water. After dialysis, sample liquid was removed from the cassette and water was removed using freeze-dry to obtain a dry product. Molecular weights of 65,276 was determined using GPC

using an RI detector, an ultrahydrogel 250, 7.8 x 300 mm column, distilled water as the mobile phase at a flow rate of 0.6 mL/min. Polymer size was determined using a 200 kV TEM (**Figure 15**) and AFM (**Figure 16-18**). These polymers were then tested against conditioned cell culture media from both breast and prostate cancers.

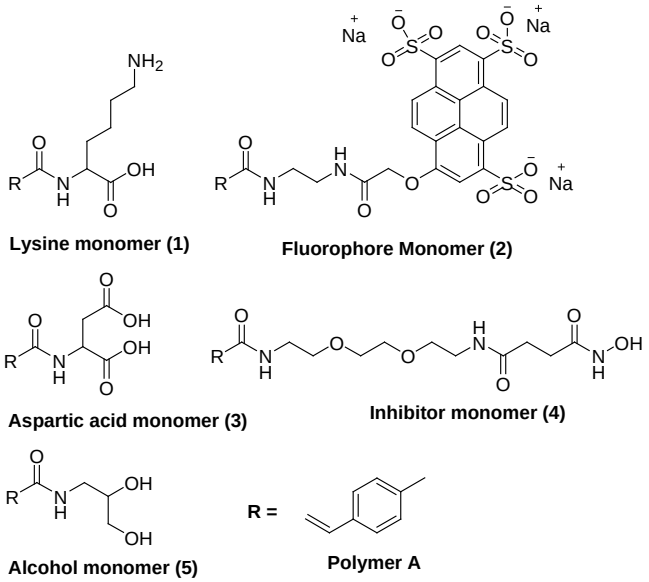

Figure 14. The structures of the monomers used to create **Polymer P9**.

Cell Conditioned Media Harvesting

The synthesized polymer will subtype different cancer cell lines at a secretomics level. Secretomics is a subset of proteomics and is focused on the study of proteins which are secreted out of the cell. This field of study is beneficial in identification of cancer biomarkers.[161]

For the breast cancer cell experiments, we examined MCF-7 (a common breast cancer cell line)[162] and MDA-MB-231 (a multiple drug resistant breast cancer cell line).[163, 164] By distinguishing between them, we can assist in providing proper medical treatment. Additionally, a cervical cancer cell line (HeLa) was used as a non-breast cancer control.[165, 166]

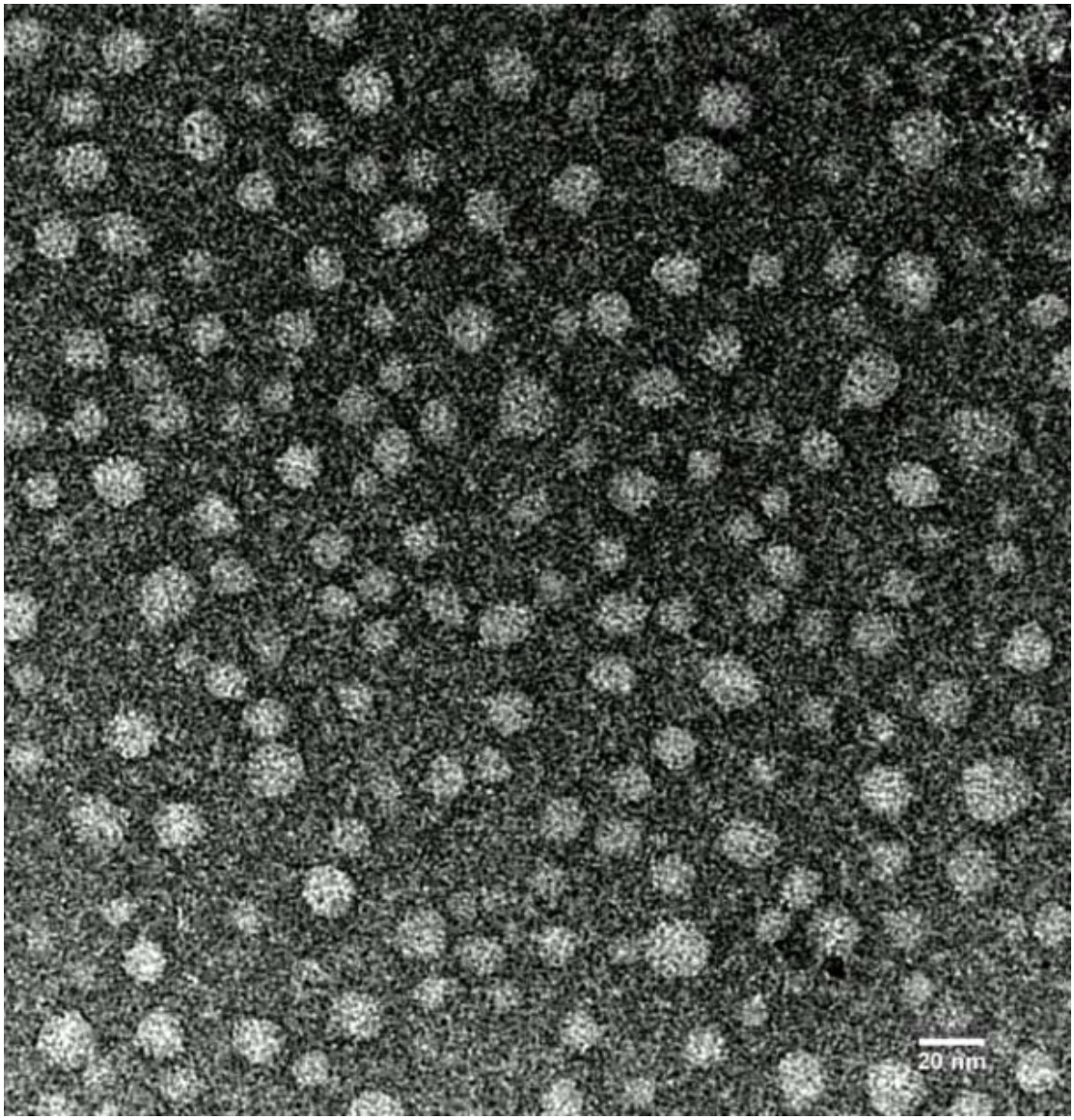

Figure 15. Transmission electron microscopy (TEM) of **Polymer P9**.

For the prostate cancer cell experiments, 22Rv1 (a prostate cancer cell line that represents both primary and relapsed cancer) was examined.[167] It is androgen-dependent, but does not respond well to hormonal treatment.[168] However, it has been reported that it does respond to glycogen synthase kinase-3 (GSK-3) inhibitors. For example the Kypta group reported, SB216763 (a GSK-3 inhibitor) inhibits the growth and proliferation of 22Rv1 cells.[169] GSK-3

inhibitors (including lithium[170]) effect many biological pathways causing several side-effects and should only be utilized in special cases where they can be effective.[171] Hence a PC-3 prostate cancer cell line that is a poor responder to hormonal treatment was examined because it is androgen independent it does not respond to GSK-3 inhibitors.[169]

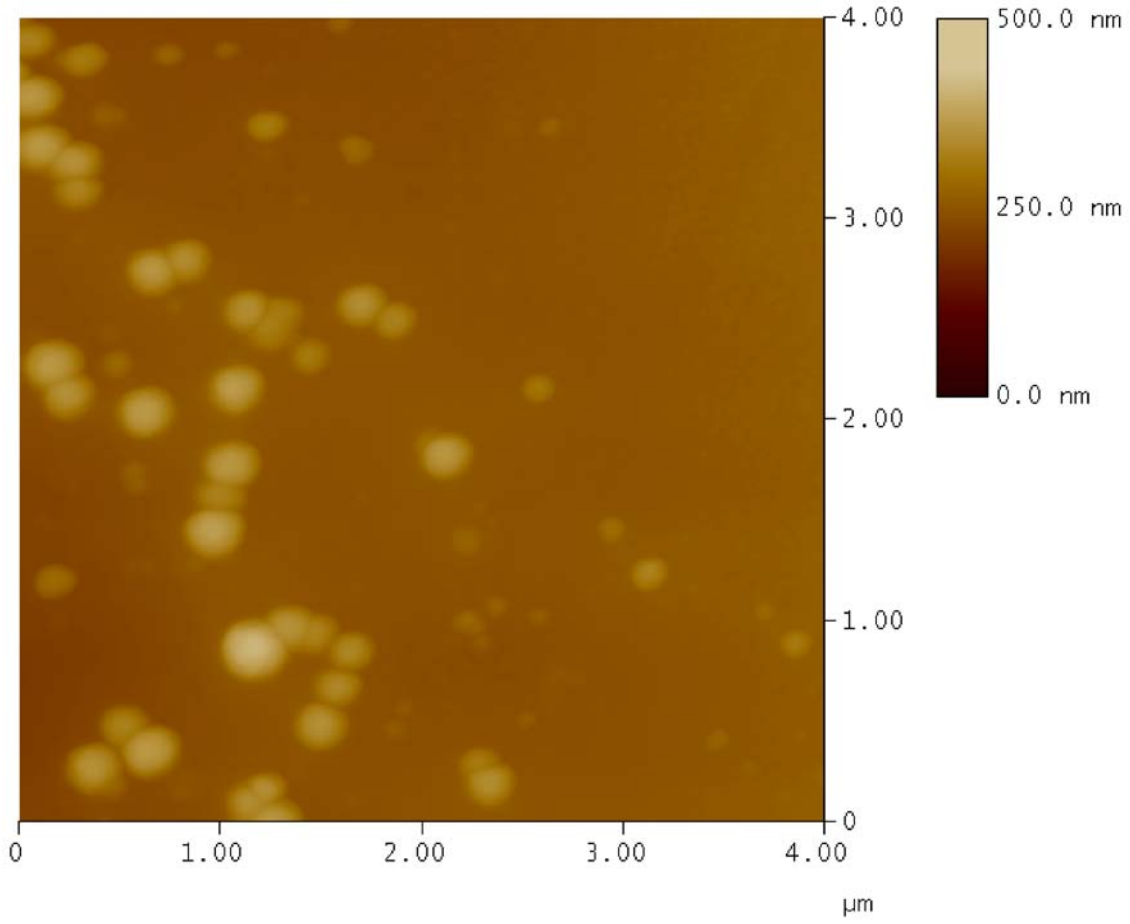

Figure 16. Atomic force microscopy (AFM) image (height) of **Polymer P9**.

Cells were grown in their respective dye-free media in a humidified atmosphere with 5% CO_2 at 37°C to a confluent state. Upon reaching this state, the conditioned media was removed, placed in a sterile centrifuge tube, and centrifuged at 226 g for 8 minutes. The pellet was discarded and supernatant was then used for fluorescence studies.

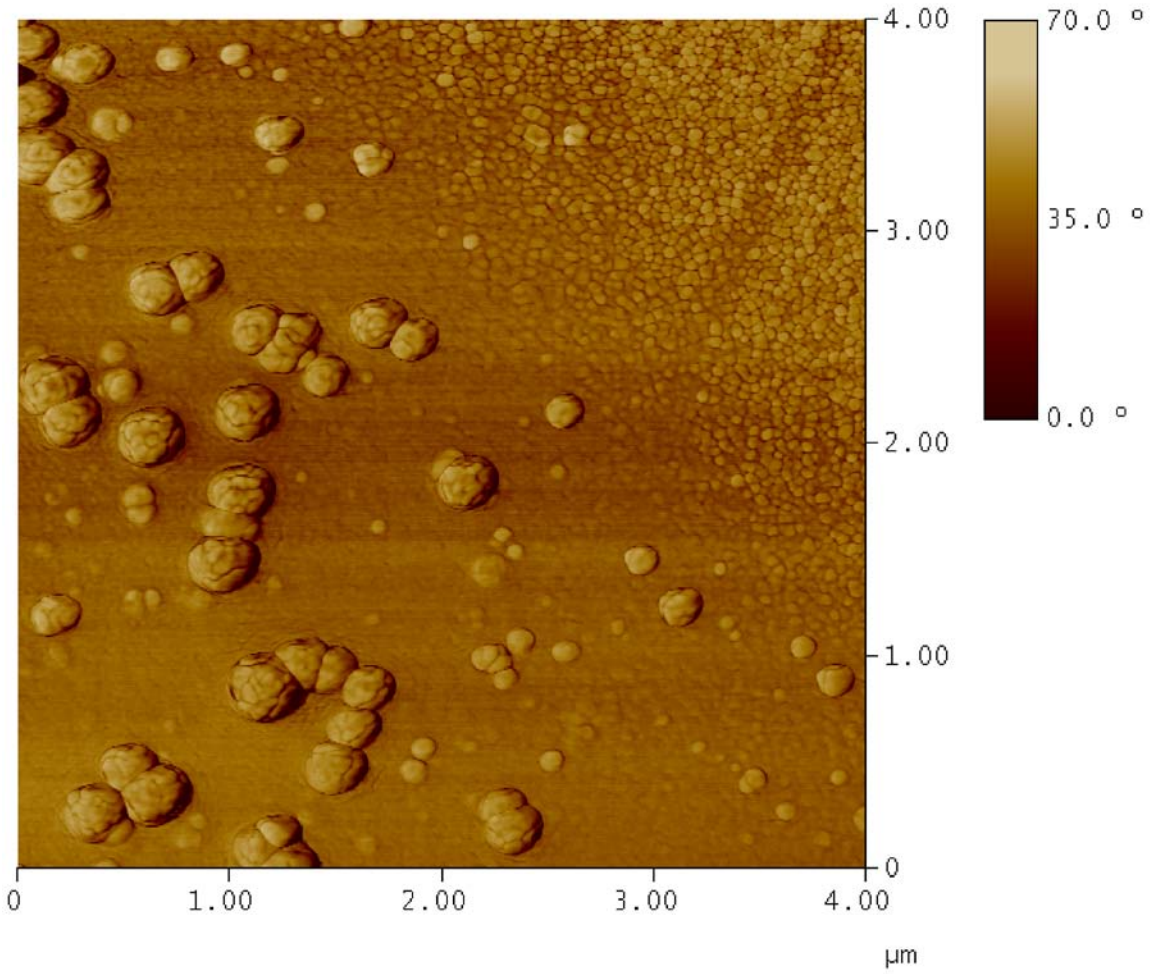

Figure 17. Atomic force microscopy (AFM) image (phase) of **Polymer P9**.

Results and Discussion

Fluorescent Studies Synopsis

Polymer solutions at 50 nM were prepared using 30 mM phosphate buffer (pH = 7.4). 400 µL of this polymer solution was added to 40 µL of respective harvested cell culture conditioned media. The polymer solution was excited at 375 nm and fluorescence emission spectra were collected (**Figure 19** and **20**) and repeated for a total of 10-runs. This experimental procedure was then repeated using the respective unconditioned media. Ratios (**Table 27** and

28) were determined by dividing unconditioned media from conditioned media. All fluorescence experiments were conducted on a Fluoromax-4 spectrofluorometer by HoribaJobin Yvon.

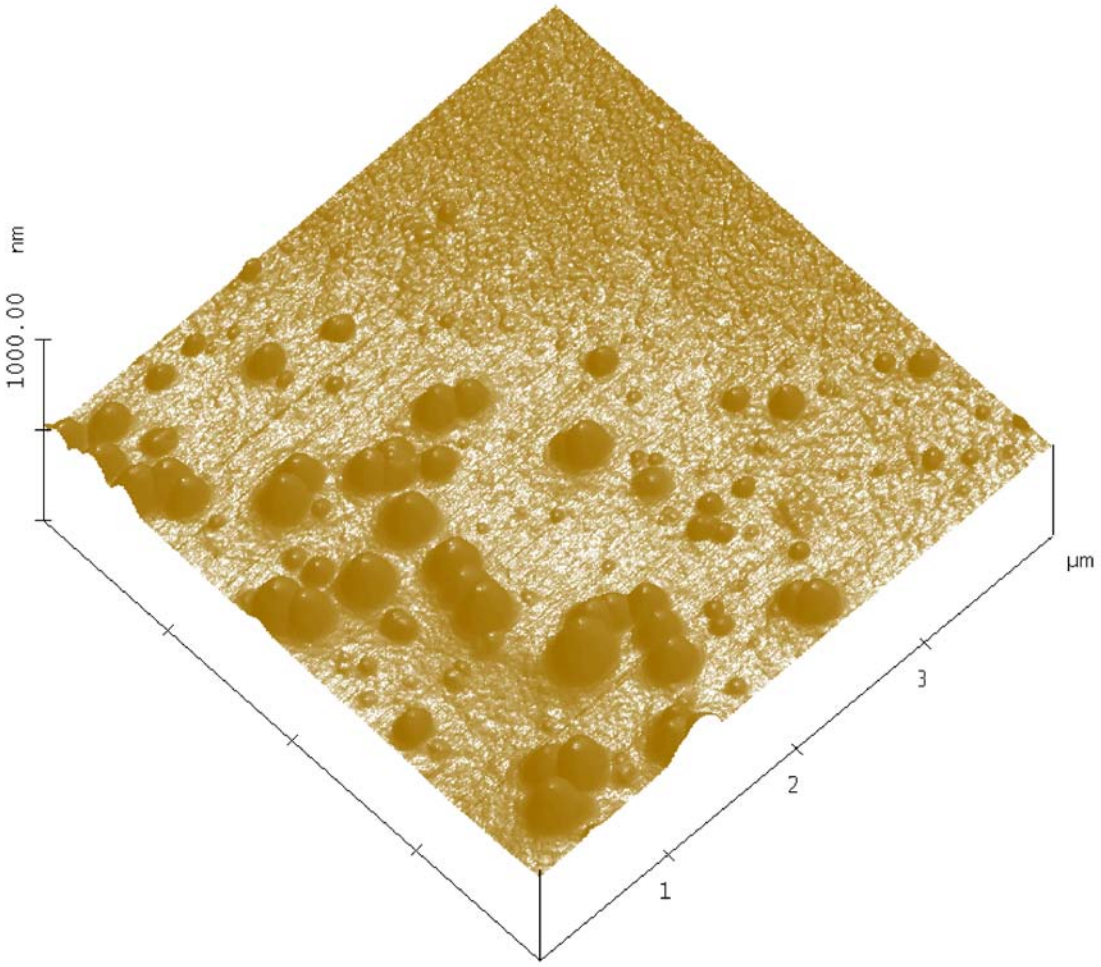

Figure 18. Atomic force microscopy (AFM) image (height image-surface plot) of **Polymer P9**.

Statistical Methods

In order to determine the ability of the polymer to predict (or distinguish between) the different sets of cell lines, linear discriminant analysis (LDA) was applied to the data.[5,19,31] More specifically, LDA was applied to each set of cell lines (breast cancer and prostate cancer)

separately, using a stepwise process. Within a given set of cancer cell lines, there were two emission intensity ratios (416 and 430 nm) at which to evaluate **Polymer P9**. The polymer was analyzed to determine the emission intensity ratio that best discriminated across the cell lines for a specific type of cancer (breast or prostate). For example, in the breast cancer cell lines, LDA evaluating only the two emission intensity ratios for **Polymer P9** to determine whether the 416 nm or the 430 nm was the most preferred intensity ratio and then repeated for the prostate cancer cell lines. Each analysis utilized 4 cell lines and 10 replications, this resulted in 2 variables (or the two intensities), and 40 observations for a given application of LDA.

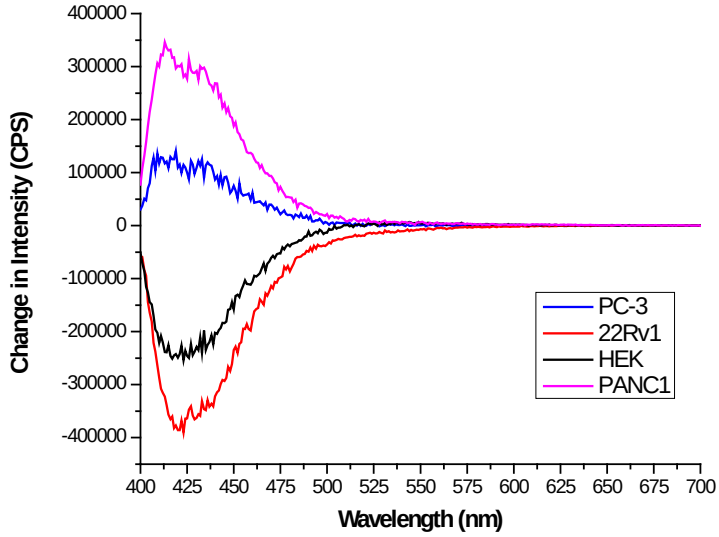

Figure 19. The prostate cancer fluorescence emission spectra for **Polymer P9** in the presence of conditioned cell culture media from prostate cancer. PC-3 (blue), 22Rv1 (Red), HEK-293 (black), and PANC1 (purple). The plots were generated by subtracting unconditioned media from conditioned media to remove any fluorescence signal variation caused by the media.

Statistical Methodology

Linear discriminant analysis (LDA) was used extensively within the literature to determine whether specific nano-particles can be used to identify various types of cancer

cells.[5,19,31] Typical applications of LDA focus on a series of standard statistical metrics. First, F-tests and Wilks' Lambda values are used to assess whether significant (joint) mean differences exist in the cell line emission intensities for **Polymer P9**. If the F-test statistics indicate rejection of the null hypothesis (no difference in mean intensity levels across cell lines), and if the Wilks' Lambda values is relatively small in magnitude, LDA can be pursued in a meaningful fashion. Otherwise, LDA is abandoned in favor of other data analysis techniques.

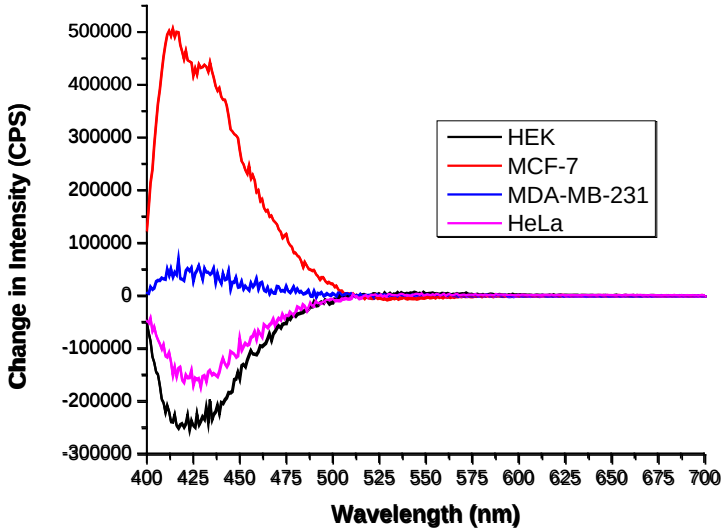

Figure 20. The breast cancer fluorescence emission spectra for **Polymer P9** in the presence of conditioned cell culture media from breast cancer. HEK-293 (black), MCF-7 (red), MDA-MB-231 (blue), and HeLa (purple). The plots were generated by subtracting unconditioned media from conditioned media to remove any fluorescence signal variation caused by the media.

If LDA is pursued, the next step is to extract the eigenvalues from the data matrix and assess them for size (*i.e.*, the percent of variation in the data that they explain) and statistical significance. Only those eigenvalues that are statistically significant are retained, and in most applications of LDA, the number is limited to 2-3 eigenvalues.

Table 27. Prostate cancer's ratios at 416 nm and 430 nm for **Polymer P9**.

#	PC-3 416	22Rv1 416	PANC1 416	HEK-293 416	PC-3 430	22Rv1 430	PANC1 430	HEK-293 430
1	0.972553	1.074614	0.927808	1.053289	0.974671	1.081731	0.930102	1.054472
2	0.964403	1.070701	0.917867	1.043670	0.972627	1.073064	0.922859	1.041582
3	0.967406	1.075200	0.926910	1.047653	0.966067	1.080317	0.925976	1.049853
4	0.977564	1.079791	0.922884	1.046996	0.973462	1.082305	0.926701	1.046969
5	1.002139	1.074994	0.922243	1.045210	0.998983	1.085495	0.925434	1.051576
6	0.999500	1.081874	0.919486	1.048232	0.999728	1.080064	0.924287	1.053205
7	1.007372	1.076411	0.920776	1.051556	1.009028	1.076685	0.926404	1.048884
8	1.008748	1.077440	0.920515	1.050729	1.013368	1.084230	0.924834	1.056728
9	1.008265	1.077146	0.921509	1.053878	1.014944	1.079206	0.919901	1.049850
10	1.011714	1.072966	0.918959	1.055805	1.010347	1.078735	0.925631	1.049264

Table 28. Breast cancer's ratios at 416 nm and 430 nm for **Polymer P9**.

#	HeLa 416	MCF-7 416	MDA-MB-231 416	HEK-293 416	HeLa 430	MCF-7 430	MDA-MB-231 430	HEK-293 430
1	1.032064	0.887919	0.991166	1.053289	1.035298	0.893057	0.992547	1.054472
2	1.027868	0.888404	0.980507	1.043670	1.030100	0.887636	0.985916	1.041582
3	1.028683	0.887457	0.978331	1.047653	1.033300	0.897208	0.985214	1.049853
4	1.029050	0.890266	0.978451	1.046996	1.029434	0.895952	0.981984	1.046969
5	1.030000	0.897444	0.984291	1.045210	1.032261	0.896624	0.984902	1.051576
6	1.027565	0.886477	0.986967	1.048232	1.027444	0.893553	0.983931	1.053205
7	1.029242	0.886714	0.986537	1.051556	1.027523	0.891436	0.986877	1.048884
8	1.027843	0.884036	0.985897	1.050729	1.031314	0.886882	0.987013	1.056728
9	1.026556	0.891131	0.985074	1.053878	1.029974	0.892314	0.985236	1.049850
10	1.026506	0.888726	0.983881	1.055805	1.029545	0.889930	0.987825	1.049264

Third, the eigenvalues are used to create canonical discriminant functions, which use the polymer data to predict which cancer cell line a given observation belongs. These functions can be described as equations (using a series of canonical discriminant function coefficients) or as a plot expressing the groupings of the observations across the two primary canonical functions. Discriminant functions which successfully predict cancer cell lines group the data into distinct, tightly clustered regions in the graph. Poorly fit LDA models fail to show distinct groups by cell line. LDA model fit is also assessed by using cross-validation techniques to identify the percentage observations which LDA assigned to the correct cell line. Models with greater internal validity correctly predict a larger percentage of observations.

Lastly, if a model is shown to accurately predict cell line membership, it is also useful to identify which polymer is primarily responsible for the model's predictions. To address this issue, the eigenvalues, along with the coefficients of the canonical functions, can be used to create potency indices. Higher values for each index indicate a polymer that plays a larger role in the ability of the model to discriminate across cell lines.

In this study, two sets of cell lines (breast cancer and prostate cancer) were analyzed. Since these cell lines are fundamentally different in nature, these sets of cell lines are treated as fundamentally distinct in the data analyses. That is, there will be one series of results dealing only with the breast cancer cell lines, and another series of results dealing only with prostate cancer cell lines.

One complicating feature of the analysis is that, within a given cell line, there are two emission intensity ratios (416 and 430 nm) at which to evaluate **Polymer P9**. This is problematic, considering 4 cell lines and 10 replications, will result in as many as 4 variables and 40 observations for each application of LDA. Since LDA provides more accurate and precise results when the ratio of observations exceeds 15 to 20, a stepwise approach was used to analyze the data. First, and within a given type of cancer cell lines (breast or prostate), each polymer was analyzed separately to determine the emission intensity ratio that best discriminates across the cell lines. For example, in the breast cancer cell lines, LDA was conducted to evaluate only the two emission intensity ratios for **Polymer P9** in order to determine whether the 416 nm or the 430 nm was the most preferred intensity ratio. This process was subsequently repeated with the remaining set of cell lines. In this way, each analysis utilized exactly 2 variables and 40 observations for each application of LDA. Cumulatively, LDA was conducted a total of six different times.

LDA Analysis of Breast Cancer Cell Lines

Table 29 contains the F-statistics, Wilks' Lambda values and basic descriptive statistics for each cell line. Note that both emission intensity ratios exhibit significant joint mean differences across cell lines and very small Wilks' Lambda values. As such, the data appear to be amenable to LDA.

Table 29. Breast cancer's tests of equality of group means for **Polymer P9**.

		Emission Intensity Ratio	
Group	**Cell Line**	**416 nm**	**430 nm**
1	**HeLa**	1.029	1.031
2	**MCF-7**	0.889	0.892
3	**MDA-MB-231**	0.984	0.986
4	**HEK**	1.050	1.050
Wilks' Lambda		0.003	0.003
F-Statistic [3, 36]		4253.495	4435.674
P-Value		<0.001	<0.001

Table 30 contains the eigenvalues and canonical correlations for the two emission intensity ratios. The first eigenvalue explains in excess of 99.9% of the variation in the data, and is statistically significant. The second eigenvalue explains less than 0.1% of the variation in the data and is not statistically significant. This implies that the first eigenvalue and its results canonical discriminant function will play the dominant role in predicting cell line membership.

Table 30. Breast cancer's canonical function summary for **Polymer P9**.

	Function 1	**Function 2**
Eigenvalue	474.569	0.019
Pct. Variance Explained	<99.9	> 0.1
Canonical Correlation	0.999	0.137
Wilks' Lambda	0.002	0.981
Chi-Square Statistic	222.609	0.686
P-Value	<0.001	0.710

Table 31 contains the discriminant function coefficient estimates. **Figure 21** uses these coefficient estimates to construct canonical functions for each eigenvalue and plots cell line group membership based on the two canonical functions. As noted earlier, internally valid LDA models should group the cell lines into distinct, tightly clustered groups, and also correct predict (via cross-validation techniques) the cell line into which the observation falls. Examining **Figure 21**, it should be noted that each group of cell lines is distinct. Moreover, LDA correctly predicts the cell lines for 100% of the observations. Thus, LDA appears to provide reasonable and internally valid results.

Table 31. Breast cancer's standardized discriminant function coefficients for **Polymer P9**.

Emission Intensity	Function 1	Function 2
416 nm	0.553	1.038
430 nm	0.592	-1.016

Table 32 creates potency indices for each of the emission intensities. The 430 nm emission intensity ratio exhibits the highest potency index value, and thus is the "preferred" emission intensity ratio for **Polymer P9**. It should be noted, however, that the 416 nm ratio's potency value is only slightly smaller than that for 430 nm. This implies that the 430 nm ratio is only slightly more preferred than 416 nm, and would also be acceptable for use in subsequent LDA. While we used the 430 nm ratio, we note in passing that we replicated all subsequent breast cancer cell line analyses using the 416 nm ratio and obtained very similar results.

Table 32. Breast cancer's structure matrix and potency index for **Polymer P9**.

Emission Intensity	Function 1	Function 2	Potency Index
416 nm	0.864	0.503	0.746
430 nm	0.883	-0.470	0.780

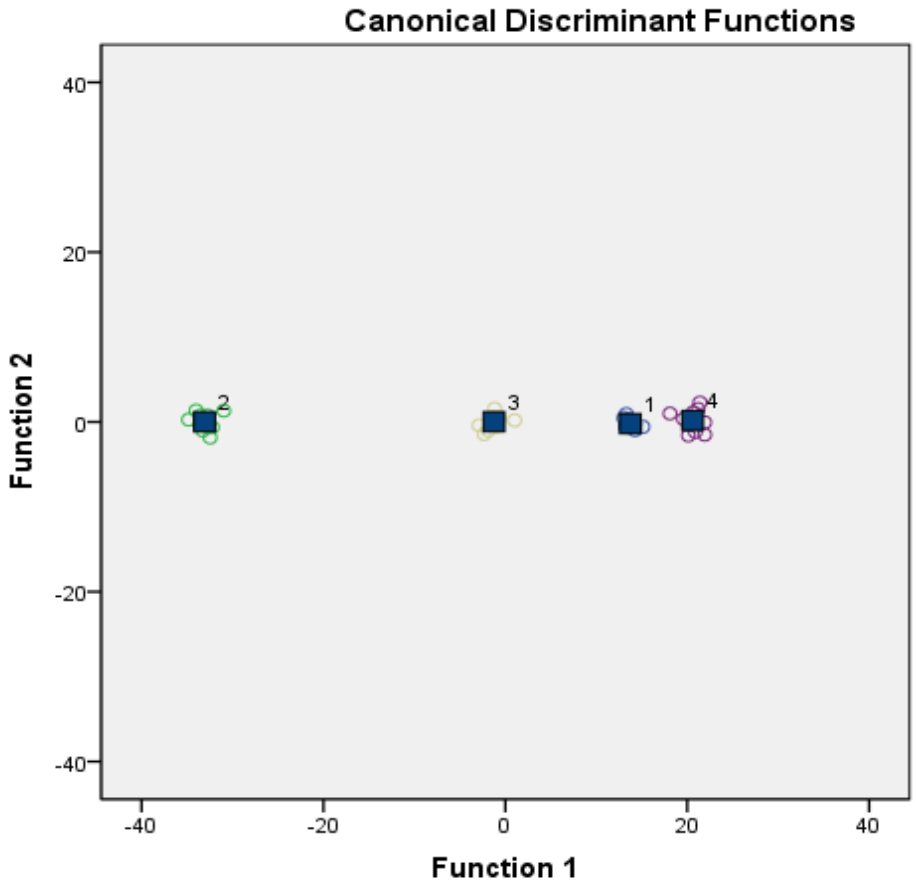

Figure 21. The result of **Polymer P9's** breast cancer cell subtyping. Group #1 is HeLa, Group #2 is MCF-7, Group #3 is MDA-MB-231, and Group #4 is HEK-293. The boxes represent the four group centroids.

LDA Analysis of Prostate Cancer Cell Lines

Table 33 contains the F-statistics, Wilks' Lambda values and basic descriptive statistics for each cell line. Note that both emission intensity ratios exhibit significant joint mean differences across cell lines and very small Wilks' Lambda values. As such, the data appear to be amenable to LDA.

Table 34 contains the eigenvalues and canonical correlations for the two emission intensity ratios. The first eigenvalue explains in excess of 99.6% of the variation in the data, and is statistically significant. The second eigenvalue explains 0.4% of the variation in the data and

is not statistically significant. This implies that the first eigenvalue and its results canonical discriminant function will play the dominant role in predicting cell line membership.

Table 33. Prostate cancer's tests of equality of group means for **Polymer P9**.

		Emission Intensity Ratio	
Group	**Cell Line**	**416 nm**	**430 nm**
1	**PC-3**	0.992	0.993
2	**22Rv1**	1.076	1.080
3	**PANC1**	0.922	0.920
4	**HEK-293**	1.050	1.050
Wilks' Lambda		0.025	0.026
F-Statistic [3, 36]		466.188	449.860
P-Value		<0.001	<0.001

Table 34. Prostate cancer's canonical function summary for **Polymer P9**.

	Function 1	**Function 2**
Eigenvalue	39.63	0.158
Pct. Variance Explained	99.6	0.4
Canonical Correlation	0.988	0.369
Wilks' Lambda	0.021	0.864
Chi-Square Statistic	138.642	5.279
P-Value	<0.001	0.071

Table 35 contains the discriminant function coefficient estimates. **Figure 22** uses these coefficient estimates to construct canonical functions for each eigenvalue and plots cell line group membership based on the two canonical functions. As noted earlier, internally valid LDA models should group the cell lines into distinct, tightly clustered groups, and also correctly predict (via cross-validation techniques) the cell line into which the observation falls. Examining this figure, it should be noted that each group of cell lines is distinct. Moreover, LDA correctly predicts the cell lines for 100% of the observations. Thus, LDA appears to provide reasonable and internally valid results.

Table 35. Prostate cancer's standardized discriminant function coefficients for **Polymer P9**.

Emission Intensity	Function 1	Function 2
416 nm	0.634	-2.647
430 nm	0.383	2.695

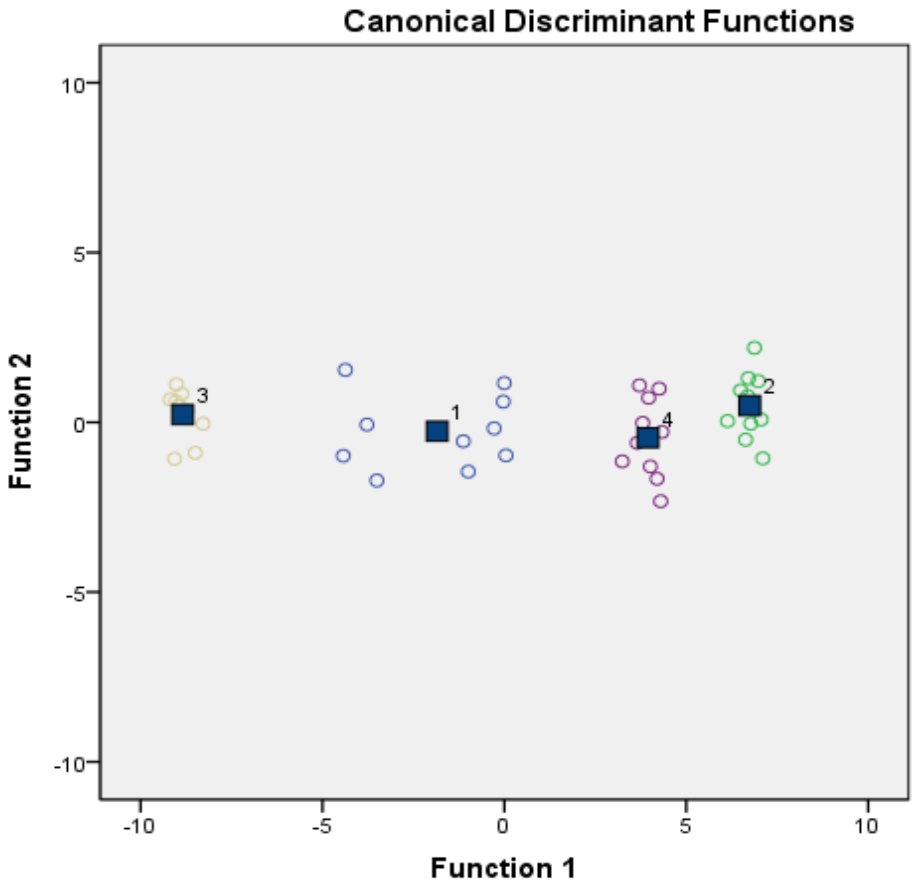

Figure 27. The result of **Polymer P9's** prostate cancer cell subtyping. Group #1 is PC-3, Group #2 is 22Rv1, Group #3 is PANC1, and Group #4 is HEK-293. The boxes represent the four groups centroids.

Table 36 creates potency indices for each of the emission intensities. The 416 nm emission intensity ratio exhibits the highest potency index value, and thus is the "preferred" emission intensity ratio for **Polymer P9**. It should be noted, however, that the 430 nm ratio's potency value is only slightly smaller than that for 416 nm. This implies that the 416 nm ratio is

only slightly more preferred than 430 nm, and would also be acceptable for use in subsequent LDA. While 416 nm ratio was used it should be noted that it replicated all subsequent prostate cancer cell line analyses using the 416 nm ratio.

Table 36. Prostate cancer's structure matrix and potency index for **Polymer P9**.

Emission Intensity	Function 1	Function 2	Potency Index
416 nm	0.990	-0.141	0.976
430 nm	0.972	0.233	0.941

General Discussion

The use of an *in vitro* secretomics-based approach required (for experimental purposes) time to allow the cells to grow such that they will secrete proteins and enzymes. However, the experimental time (to collect data) utilizing fluorescent polymers is significantly faster than other potential secretomics based approaches. For example, the utilization of ELISA would take several hours to overnight, before experimental data would become available and that data may not provide enough information (*i.e.* active vs. pro-enzyme) to successfully subtype the cancerous cells. However, this polymer will produce experimental information that will successfully differentiate and subtype prostate and breast cancer cells within as little as five minutes, thus a substantial reduction in experimental data acquisition time is observed.

Conclusions

The pyranine (versus dansyl) fluorophore has allowed for a dramatic enhancement in the polymer's ability to differentiate and subtype. This does not support our original hypothesis that the natural folding pattern of amino acids are influencing hydrophobic amino acids to lie away from the protein/enzyme's surface and thus preventing the benzene ring of the polymer's

backbone from developing π-π interactions. The mechanism of this polymer's ability to differentiate among cell lines, currently eludes us and any explanation would be pure speculation.

With this in mind, it is possible that the change of a more hydrophilic fluorophore, generated a polymer with greater utility in using its backbone's to apply π-π interactions with protein/enzyme surface hydrophobic amino acids, that would be flanked by a high number of hydrophilic amino acids. If this is indeed the case, the 4-vinylbenzoic acid, likely provided an important element that was absent from our previous reports. Because hydrophobic forces are the driving force behind the formation of tertiary and quaternary protein structures the opportunity to π-π bond with a limited number of hydrophobic surface amino acids is a unique distinguishing characteristic between different proteins, assuming that the polymer's formulation allows for such interactions to occur.

The utilization of nano-sized, fluorescent polymers created a successful nano-diagnostic platform for differentiation, and subtyping of breast and prostate cancer cell-conditioned media. Here subtyping occurs via secretomics at a post-translational level, which accounted for important post-translational modifications. With further refinement, nano-polymers will provide a translational tool for the clinical development of personalized medicine.

References

141. Relling, M.V. & Dervieux, T. Pharmacogenetics and cancer therapy. *Nature reviews. Cancer* **1**, 99-108 (2001).

142. Duffy, M.J. & Crown, J. A personalized approach to cancer treatment: how biomarkers can help. *Clin Chem* **54**, 1770-1779 (2008).

143. Sawyers, C. Targeted cancer therapy. *Nature* **432**, 294-297 (2004).

144. Woodcock, J. The prospects for "personalized medicine" in drug development and drug therapy. *Clin Pharmacol Ther* **81**, 164-169 (2007).

145. Scott, M.D. et al. Differentiation of Prostate Cancer Cells by Using Flexible Fluorescent Polymers. *Analytical chemistry* **84**, 17-20 (2012).

146. Demestre, M., Parkin-Smith, G., Petzold, A. & Pullen, A.H. The pro and the active form of matrix metalloproteinase-9 is increased in serum of patients with amyotrophic lateral sclerosis. *J Neuroimmunol* **159**, 146-154 (2005).

147. Paczek, L., Michalska, W. & Bartlomiejczyk, I. Trypsin, elastase, plasmin and MMP-9 activity in the serum during the human ageing process. *Age Ageing* **37**, 318-323 (2008).

148. Hurst, N.G. et al. Elevated serum matrix metalloproteinase 9 (MMP-9) concentration predicts the presence of colorectal neoplasia in symptomatic patients. *Br J Cancer* **97**, 971-977 (2007).

149. Subramaniam, R. et al. Novel bis-(arylsulfonamide) hydroxamate-based selective MMP inhibitors. *Bioorg Med Chem Lett* **18**, 3333-3337 (2008).

150. Choudhary, C. et al. Lysine acetylation targets protein complexes and co-regulates major cellular functions. *Science* **325**, 834-840 (2009).

151. Appella, E. & Anderson, C.W. Post-translational modifications and activation of p53 by genotoxic stresses. *Eur J Biochem* **268**, 2764-2772 (2001).

152. Haldar, M.K., Scott, M.D., Sule, N., Srivastava, D.K. & Mallik, S. Synthesis of barbiturate-based methionine aminopeptidase-1 inhibitors. *Bioorganic & medicinal chemistry letters* **18**, 2373-2376 (2008).

153. Cooper, A.C. et al. A novel methionine aminopeptidase-2 inhibitor, PPI-2458, inhibits non-Hodgkin's lymphoma cell proliferation in vitro and in vivo. *Clinical cancer research : an official journal of the American Association for Cancer Research* **12**, 2583-2590 (2006).

154. Heo, I. & Kim, V.N. Regulating the regulators: posttranslational modifications of RNA silencing factors. *Cell* **139**, 28-31 (2009).

155. Carpenter, S. & O'Neill, L.A. Recent insights into the structure of Toll-like receptors and post-translational modifications of their associated signalling proteins. *The Biochemical journal* **422**, 1-10 (2009).

156. Dore, K. et al. Fluorescent polymeric transducer for the rapid, simple, and specific detection of nucleic acids at the zeptomole level. *Journal of the American Chemical Society* **126**, 4240-4244 (2004).

157. Kumaraswamy, S. et al. Fluorescent-conjugated polymer superquenching facilitates highly sensitive detection of proteases. *Proceedings of the National Academy of Sciences of the United States of America* **101**, 7511-7515 (2004).

158. Dutta, R. et al. Fluorescent water soluble polymers for isozyme-selective interactions with matrix metalloproteinase-9. *Bioorg Med Chem Lett* **21**, 2007-2010 (2011).

159. Bajaj, A. et al. Array-based sensing of normal, cancerous, and metastatic cells using conjugated fluorescent polymers. *J Am Chem Soc* **132**, 1018-1022 (2010).

160. Nyren-Erickson, E.K. et al. Fluorescent liposomes for differential interactions with glycosaminoglycans. *Anal Chem* **83**, 5989-5995 (2011).

161. Karagiannis, G.S., Pavlou, M.P. & Diamandis, E.P. Cancer secretomics reveal pathophysiological pathways in cancer molecular oncology. *Mol Oncol* **4**, 496-510 (2010).

162. Soule, H.D., Vazguez, J., Long, A., Albert, S. & Brennan, M. A human cell line from a pleural effusion derived from a breast carcinoma. *J Natl Cancer Inst* **51**, 1409-1416 (1973).

163. Chen, J. et al. PKD2 mediates multi-drug resistance in breast cancer cells through modulation of P-glycoprotein expression. *Cancer Lett* **300**, 48-56 (2011).

164. Aspinall, S.R., Stamp, S., Davison, A., Shenton, B.K. & Lennard, T.W. The proliferative effects of 5-androstene-3 beta,17 beta-diol and 5 alpha-dihydrotestosterone on cell cycle analysis and cell proliferation in MCF7, T47D and MDAMB231 breast cancer cell lines. *J Steroid Biochem Mol Biol* **88**, 37-51 (2004).

165. Masters, J.R. HeLa cells 50 years on: the good, the bad and the ugly. *Nat Rev Cancer* **2**, 315-319 (2002).

166. Rahbari, R. et al. A novel L1 retrotransposon marker for HeLa cell line identification. *Biotechniques* **46**, 277-284 (2009).

167. Sramkoski, R.M. et al. A new human prostate carcinoma cell line, 22Rv1. *In Vitro Cell Dev Biol Anim* **35**, 403-409 (1999).

168. Kim, H.J., Park, Y.I. & Dong, M.S. Comparison of prostate cancer cell lines for androgen receptor-mediated reporter gene assays. *Toxicol In Vitro* **20**, 1159-1167 (2006).

169. Mazor, M., Kawano, Y., Zhu, H., Waxman, J. & Kypta, R.M. Inhibition of glycogen synthase kinase-3 represses androgen receptor activity and prostate cancer cell growth. *Oncogene* **23**, 7882-7892 (2004).

170. Marmol, F. Lithium: bipolar disorder and neurodegenerative diseases Possible cellular mechanisms of the therapeutic effects of lithium. *Prog Neuropsychopharmacol Biol Psychiatry* **32**, 1761-1771 (2008).

171. Ibrahim, N., Mouawad, L. & Legraverend, M. Novel 8-arylated purines as inhibitors of glycogen synthase kinase. *Eur J Med Chem* **45**, 3389-3393 (2010).

CHAPTER 6. CONCLUSIONS/FUTURE STUDIES

Matrix metalloproteinases are good examples of the importance of post-translational detection based upon their inactive pro-enzyme versus active enzymatic states. Only by developing a post-translational detection, differentiation, and subtyping technique can these modifications be accounted for. Utilizing a fluorescent water soluble polymer based system that takes advantage of the inaccessible pro-MMP pocket and the accessible active MMP pocket through the use of a Zn^{2+} chelating inhibitor. This assay system addresses the limitations of current fluorimetric assays that include time, high background, and poor solubility. These polymers were constructed from monomers that contain a variety of amino acid, alcohol, fluorophore, and an MMP inhibitor. Alteration of the amount of each monomer allowed for the development of a small library of eight chemically unique polymers. These polymers were screened against recombinant human MMP-7, -9, and -10. Using logit regression analysis, we found that one of the eight polymers selectively interacts with MMP-9 over that of MMP-7 and MMP-10.

Subsequently, it was demonstrated that this polymer formulation was capable of subtyping both prostate and breast cancer cells at a post-translational level. Subtyping is further categorized the type of cancer based upon its molecular biology of disease development along with potential effective therapeutic options. Subtyping is currently preformed at pre-translational levels utilizing genomics. However, as “target medicine” moves forward it has become increasingly apparent that post-translational modifications are important factors that need to be considered for cancer classification.

An enhanced differentiation ability was demonstrated by alteration of the fluorophore. This alteration to a more hydrophilic pyranine fluorophore made unquestionable progress in the ability to separate between the various breast and prostate cancer cell lines at a secretomics level.

In future studies, this project can be further studied by exploring the alteration of the inhibitor to a more isozyme specific for MMP-9. This alteration would lead to a more specific interaction with the active MMP-9. Due to MMP-9's importance in cancer progression and metastasis this would be a favourable result.

Additional modifications can be made to enhance differentiation ability. For example, statistical methodologies maybe altered and/or developed into a computer program. Also, the alteration of the polymeric formulation and or the incorporation of a second fluorophore may provide for greater separation between the cancerous subgroups.

Use of a multi-welled fluorescent plate will shorten experimental time and allow for a greater diversification of sampling population. Finally it will be possible to expand this into the area of antibiotic susceptibility assays by exploring a time dependant fluorescence signal change that can be rapidly quantified to provide a new land of possibilities towards antibiotic development.

APPENDIX A. PURIFICATION OF MONOMERS

SampleName: mds-08-48

Wednesday 01 September 2010 07:36AM

RediSep Column: 40g Silica
Flow Rate: 40 ml/min
Equilibration Volume: 240.0 ml
Initial Waste: 0.0 ml
Air Purge: 1.0 min
Solvent A: A2 dichloromethane
Solvent B: B2 methanol

Peak Tube Volume: Max.
Non-Peak Tube Volume: Max.
Loading Type: Solid
Wavelength 1 (red): 254nm
Peak Width: 2 min
Threshold: 0.20 AU

Run Notes:

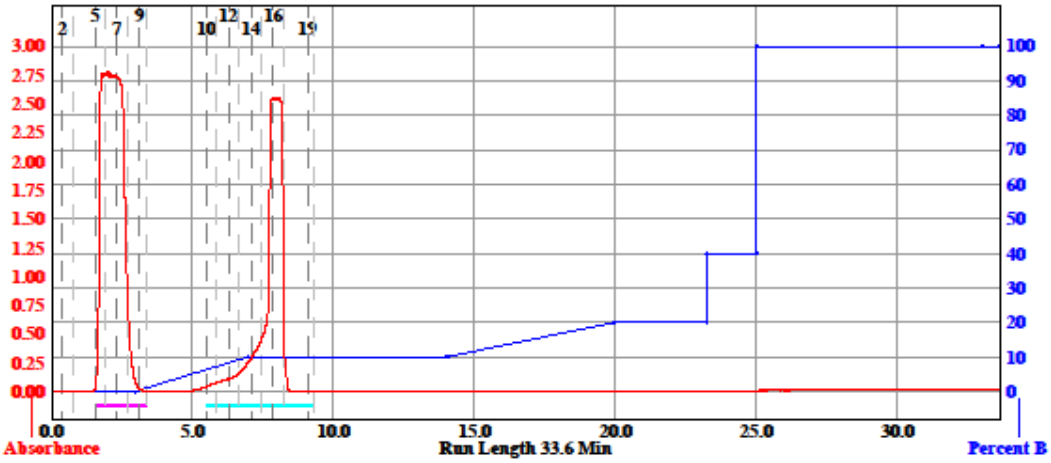

Rack A

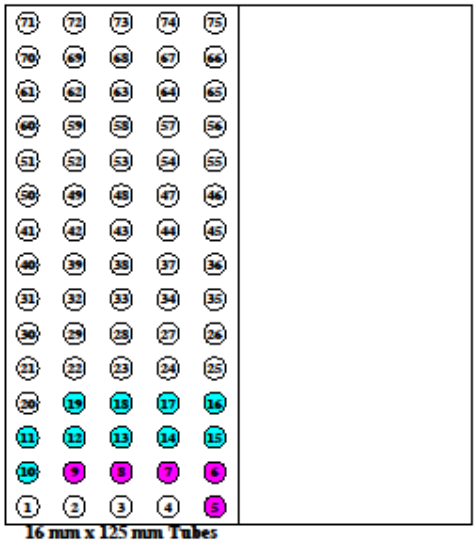

16 mm x 125 mm Tubes

Peak #	Start Tube	End Tube
1	A:5	A:9
2	A:10	A:19

Duration	%B	Solvent A	Solvent B
0.0	0.0	A2 dichlorometha	B2 methanol
3.0	0.0	A2 dichlorometha	B2 methanol
4.0	10.0	A2 dichlorometha	B2 methanol
7.1	10.0	A2 dichlorometha	B2 methanol
5.9	20.0	A2 dichlorometha	B2 methanol
3.3	20.2	A2 dichlorometha	B2 methanol
0.0	39.9	A2 dichlorometha	B2 methanol
1.8	39.9	A2 dichlorometha	B2 methanol
0.0	100.0	A2 dichlorometha	B2 methanol
8.0	100.0	A2 dichlorometha	B2 methanol
8.0	100.0	A2 dichlorometha	B2 methanol

Page 1 of 1

Figure A1. Purification of protected aspartic acid. Purified monomer were found in test tubes 5 to 7 upon removal of the solvent using a rotary evaporator and drying under vacuum.

SampleName: mds-asp-dep

Tuesday 25 August 2009 05:16PM

RediSep Column: 40g Silica
Flow Rate: 40 ml/min
Equilibration Volume: 240.0 ml
Initial Waste: 0.0 ml
Air Purge: 1.0 min
Solvent A: A2 dichloromethane
Solvent B: B2 methanol

Peak Tube Volume: Max.
Non-Peak Tube Volume: Max.
Loading Type: Solid
Wavelength 1 (red): 254nm
Peak Width: 2 min
Threshold: 0.20 AU

Run Notes:

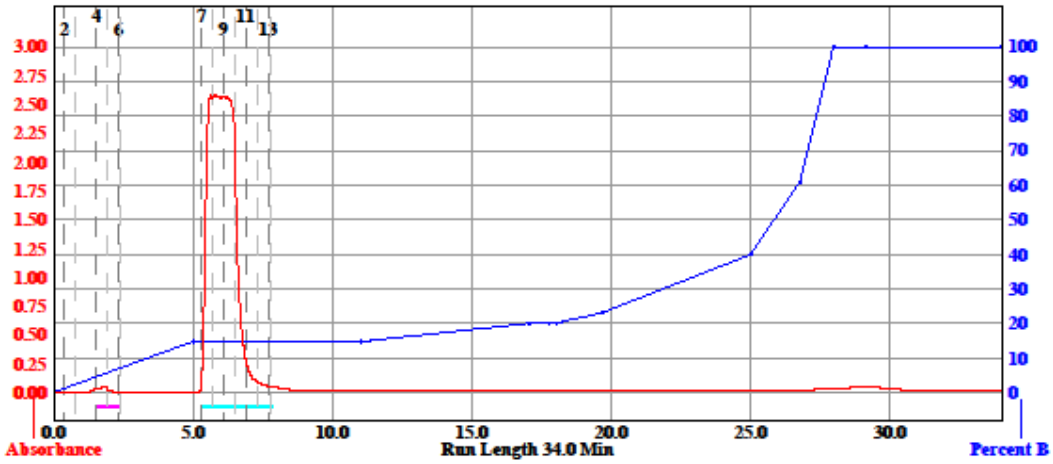

Rack A

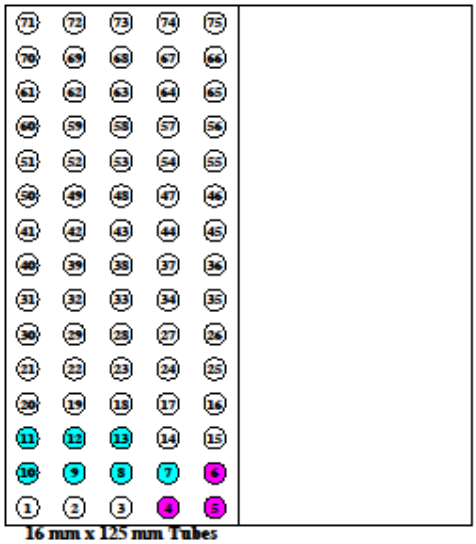

16 mm x 125 mm Tubes

Peak #	Start Tube	End Tube
1	A:4	A:6
2	A:7	A:13

Duration	%B	Solvent A	Solvent B
0.0	0.0	A2 dichlorometha	B2 methanol
0.0	0.0	A2 dichlorometha	B2 methanol
5.0	14.8	A2 dichlorometha	B2 methanol
6.0	14.8	A2 dichlorometha	B2 methanol
6.0	20.0	A2 dichlorometha	B2 methanol
0.8	20.2	A2 dichlorometha	B2 methanol
0.2	20.2	A2 dichlorometha	B2 methanol
1.6	23.0	A2 dichlorometha	B2 methanol
5.3	39.9	A2 dichlorometha	B2 methanol
1.8	60.9	A2 dichlorometha	B2 methanol
---	---	---	---

Page 1 of 1

Figure A2. Purification of de-protected aspartic acid. Purified monomer could be found in test tubes 8 to 10 upon removal of the solvent using rotary evaporator and drying under vacuum.

SampleName: mds-08-45

Wednesday 23 June 2010 01:03PM

RediSep Column: 40g Silica
Flow Rate: 40 ml/min
Equilibration Volume: 240.0 ml
Initial Waste: 0.0 ml
Air Purge: 1.0 min
Solvent A: A2 dichloromethane
Solvent B: B2 methanol

Peak Tube Volume: Max.
Non-Peak Tube Volume: Max.
Loading Type: Solid
Wavelength 1 (red): 254nm
Peak Width: 2 min
Threshold: 0.20 AU

Run Notes:

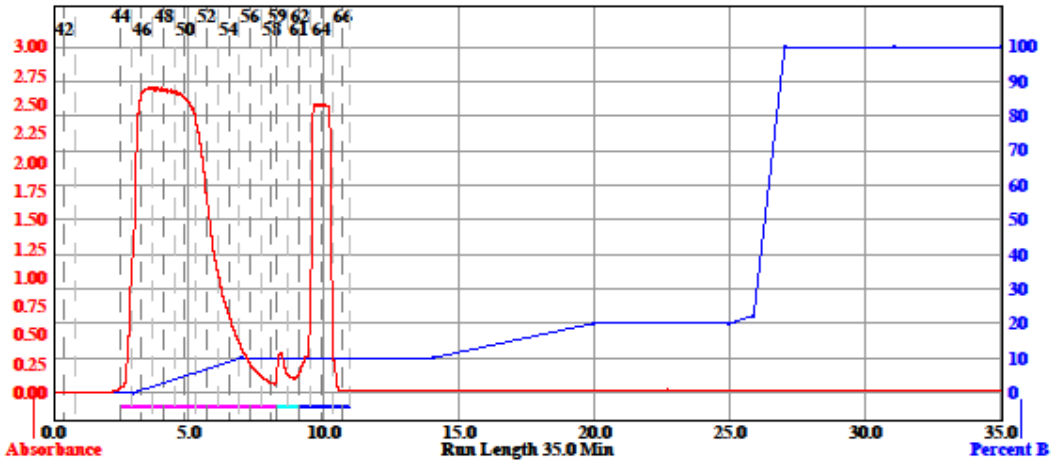

Rack A

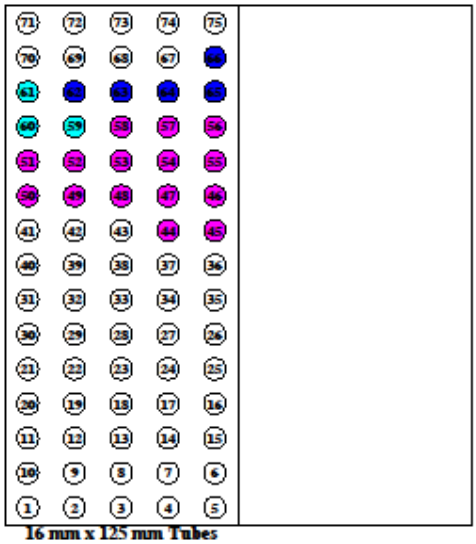

16 mm x 125 mm Tubes

Peak #	Start Tube	End Tube
1	A:44	A:58
2	A:59	A:61
3	A:62	A:66

Duration	%B	Solvent A	Solvent B
0.0	0.0	A2 dichlorometha	B2 methanol
3.0	0.0	A2 dichlorometha	B2 methanol
4.0	10.0	A2 dichlorometha	B2 methanol
7.1	10.0	A2 dichlorometha	B2 methanol
5.9	20.0	A2 dichlorometha	B2 methanol
5.0	20.0	A2 dichlorometha	B2 methanol
0.9	22.2	A2 dichlorometha	B2 methanol
1.1	100.0	A2 dichlorometha	B2 methanol
4.0	100.0	A2 dichlorometha	B2 methanol
0.0	100.0	A2 dichlorometha	B2 methanol
0.0	100.0	A2 dichlorometha	B2 methanol

Page 1 of 1

Figure A3. Purification of protected lysine. Purified monomer were found in test tubes 46 to 49 upon removal of the solvent using a rotary evaporator and drying under vacuum.

SampleName: mds-08-45deprotected

Friday 01 October 2010 08:59AM

RediSep Column: 40g Silica
Flow Rate: 40 ml/min
Equilibration Volume: 240.0 ml
Initial Waste: 0.0 ml
Air Purge: 1.0 min
Solvent A: A2 dichloromethane
Solvent B: B2 methanol

Peak Tube Volume: Max.
Non-Peak Tube Volume: Max.
Loading Type: Solid
Wavelength 1 (red): 254nm
Peak Width: 2 min
Threshold: 0.20 AU

Run Notes:

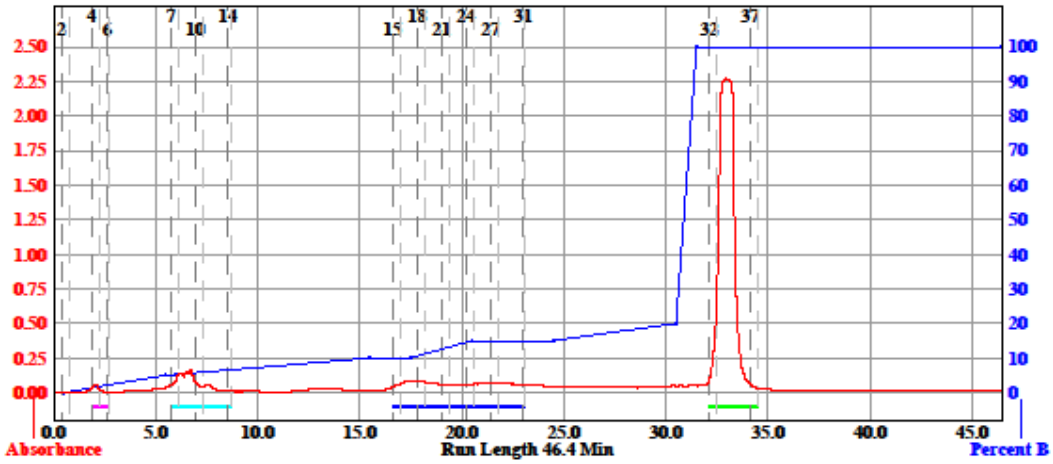

Rack A

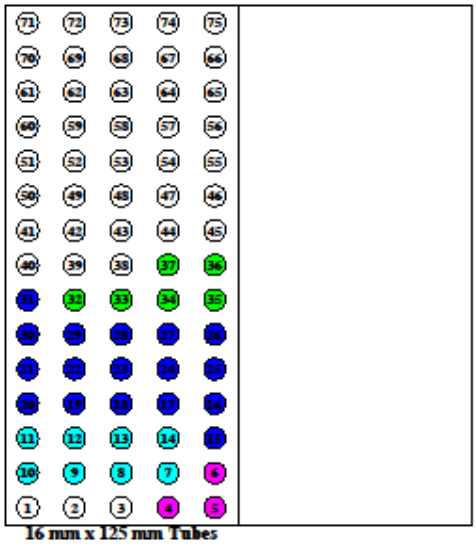

16 mm x 125 mm Tubes

Peak #	Start Tube	End Tube
1	A:4	A:6
2	A:7	A:14
3	A:15	A:31
4	A:32	A:37

Duration	%B	Solvent A	Solvent B
0.0	0.0	A2 dichlorometha	B2 methanol
0.5	0.0	A2 dichlorometha	B2 methanol
5.0	5.0	A2 dichlorometha	B2 methanol
10.0	10.0	A2 dichlorometha	B2 methanol
2.0	10.0	A2 dichlorometha	B2 methanol
3.0	15.0	A2 dichlorometha	B2 methanol
4.0	15.0	A2 dichlorometha	B2 methanol
6.0	20.0	A2 dichlorometha	B2 methanol
1.0	100.0	A2 dichlorometha	B2 methanol
14.9	100.0	A2 dichlorometha	B2 methanol

Page 1 of 1

Figure A4. Purification of de-protected lysine. Purified monomer could be found in test tubes 33 to 34 upon removal of the solvent using rotary evaporator and drying under vacuum.

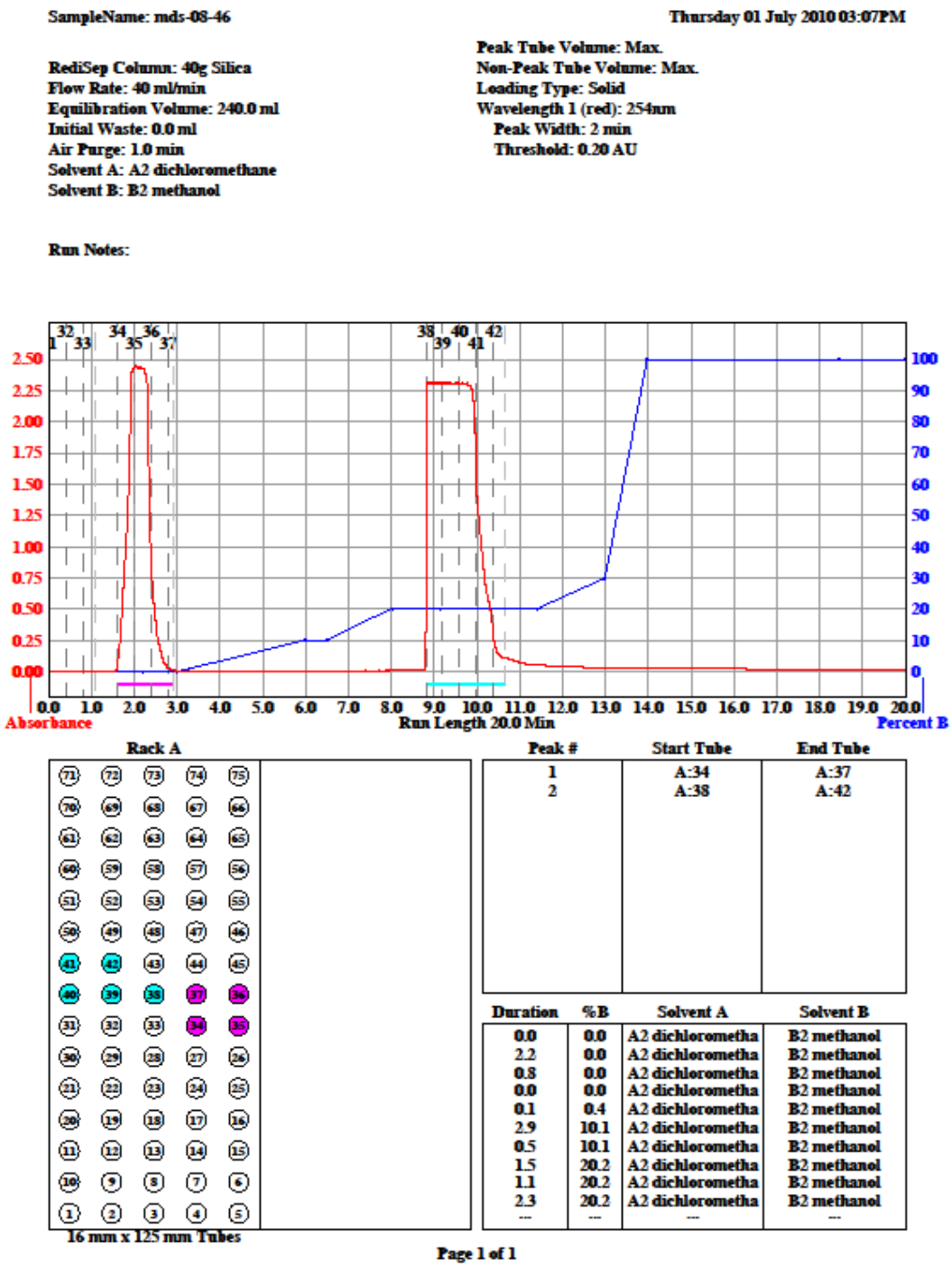

Figure A5. Purification of 2-amino-1,3-diol. Purified monomer was found in test tubes 38 to 42 upon removal of the solvent using a rotary evaporator and drying under vacuum.

APPENDIX B. OTHER MONOMER SYNTHESIS

Alanine Monomer Synthesis

Protected alanine monomer was synthesized by coupling 4-vinylbenzoic acid ($C_9H_8O_2$; MW = 148.16 g/mol) to L-alanine t-butyl ester hydrochloride (H-Ala-OtBu·HCl; MW = 181.7 g/mol). To perform this coupling reaction (**Scheme B1**) 1.040 g (7 mmol) of $C_9H_8O_2$, 1.286 g (7 mmol) of H-Ala-OtBu·HCl, 0.958 g (7 mmol) of 1-hydroxybenzotriazole (HOBT), 2.663 g (7 mmol) of O-benzotriazole-N,N,N'N'-tetra-methyluronium hexafluorophosphate (HBTU) was added to 30 mL of dichloromethane (CH_2Cl_2). This reaction mixture was stirred under nitrogen at room temperature for 15 minutes before addition of 2.4 mL (14 mmol) of N-ethyldiisopropylamine (iPr_2NEt).

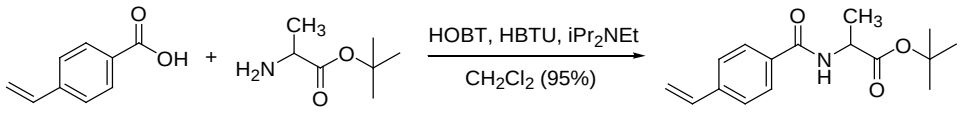

Scheme B1. Synthesis of protected alanine monomer.

This reaction continued to stir under nitrogen at room temperature overnight. The next morning, the reaction was worked up by washing in a separation funnel. It was washed once with 15% brine, twice with distilled water, four times with 20% citric acid solution, and 4 times with 7% sodium bicarbonate. The remaining dichloromethane was dried over sodium sulfate and then removed using a rotary evaporator at 38ºC.

^{1}H NMR spectrum suggested it was clean enough for deprotection without further purification. Protected alanine monomer had a product yield of 1.929 g or 95% yield. ^{1}H NMR (500 MHz, CHLOROFORM-*d*) δ ppm 1.48 (s, 3 H) 1.50 (s, 9 H) 4.67 (quin, *J*=7.0 Hz, 1 H) 5.35 (d, *J*=10.9 Hz, 1 H) 5.84 (d, *J*=17.5 Hz, 1 H) 6.70 - 6.77 (m, 1 H) 7.46 (m, *J*=8.1 Hz, 2 H) 7.77

(m, *J*=8.3 Hz, 2 H). ^{13}C NMR (125 MHz, CHLOROFORM-*d*) δ ppm 18.87 27.97 49.01 82.22 115.90 126.26 127.29 133.18 135.94 140.70 166.19 172.54. This compound was then stored in the freezer.

To deprotect, 1.929 g of protected alanine monomer was mixed with 10 mL trifluoroacetic acid (TFA) and 0.5 mL of triisopropylsilane (TIPS) under nitrogen at room temperature for 2 to 3 hours **(Scheme B2)**. The TFA was removed from the round bottom flask using a rotary evaporator at 38ºC.

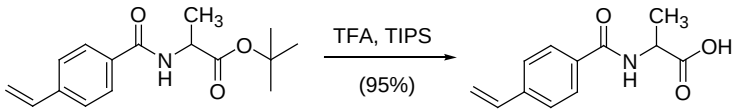

Scheme B2. Synthesis of de-protected alanine monomer.

The remaining mixture was dissolved in methanol (MeOH) and loaded into silica gel. This silica gel was then used to perform automated flash chromatography using CombiFlash Rf system from Teledyne Isco. A solvent system of dichloromethane and methanol (R_f = 0.1; 90% dichloromethane/10% methanol) was used with the CombiFlash to successfully remove the TIPS from the reaction mixture and then allowed for the purification of the product. The solvent was again removed from the system using a rotary evaporator at 38ºC. Final purified alanine monomer had a product yield of 1.720 g, 95%. ^{1}H NMR (500 MHz, DMSO-d_6) δ ppm 1.39 (d, *J*=4.8 Hz, 3 H) 4.42 (br s, 1 H) 5.38 (d, *J*=10.5 Hz, 1 H) 5.96 (d, *J*=17.6 Hz, 1 H) 6.79 (dd, *J*=15.8, 12.1 Hz, 1 H) 7.57 (d, *J*=6.2 Hz, 2 H) 7.87 (d, *J*=6.2 Hz, 2 H) 8.65 (br s, 1 H).

Glycine Monomer Synthesis

The protected glycine monomer was synthesized by coupling 4-vinylbenzoic acid ($C_9H_8O_2$; MW = 148.16 g/mol) to glycine t-butyl ester hydrochloride [H-Gly-OtBu·HCl; MW = 167.6 g/mol]. To perform this coupling reaction (**Scheme B3**) we added 1.025 g (7 mmol) of $C_9H_8O_2$, 1.499 g (7 mmol) of H-Gly-OtBu·HCl, 0.947 g (7 mmol) of 1-hydroxybenzotriazole (HOBT), 2.660 g (7 mmol) of O-benzotriazole-N,N,N'N'-tetra-methyluronium hexafluorophosphate (HBTU) to 30 mL of dichloromethane (CH_2Cl_2). This reaction mixture was stirred under nitrogen at room temperature for 15 minutes before the addition of 2.45 mL (14 mmol) of N-ethyldiisopropylamine (iPr_2NEt).

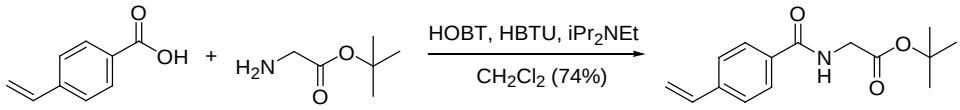

Scheme B3. Synthesis of protected glycine monomer.

This reaction was stirred under nitrogen at room temperature overnight. The next morning the reaction was worked up by washing in a separation funnel. It was washed twice with distilled water, seven times with 20% citric acid solution, and eight times with 7% sodium bicarbonate. The remaining dichloromethane was dried over sodium sulfate and then removed using a rotary evaporator at 38ºC.

^{1}H NMR suggested it was clean enough for deprotection without further purification. Protected glycine monomer had a product yield of 1.283 g or 74% yield. ^{1}H NMR (400 MHz, CHLOROFORM-*d*) δ ppm 1.52 (s, 9 H) 4.15 (d, *J*=4.8 Hz, 2 H) 5.37 (d, *J*=11.1 Hz, 1 H) 5.85 (d, *J*=17.6 Hz, 1 H) 6.64 (br s, 1 H) 6.75 (dd, *J*=17.5, 11.0 Hz, 1 H) 7.47 (m, *J*=8.3 Hz, 2 H) 7.79

(m, *J*=8.0 Hz, 2 H). ^{13}C NMR (100 MHz, CHLOROFORM-*d*) δ ppm 28.07 42.51 82.57 115.99 126.32 127.33 132.94 135.94 140.82 166.82 169.28.

To deprotect, 0.736 g of protected glycine monomer was mixed with 7 mL trifluoroacetic acid (TFA) and 0.33 mL of triisopropylsilane (TIPS) under nitrogen at room temperature for 2 to 3 hours **(Scheme B4)**. The TFA was removed from the round bottom, using a rotary evaporator at 38ºC.

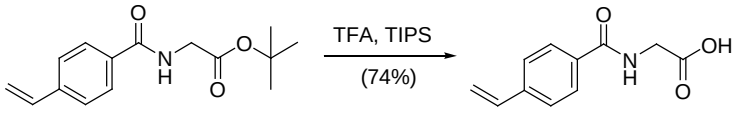

Scheme B4. Synthesis of de-protected glycine monomer.

The remaining mixture was dissolved in methanol (MeOH) and loaded into silica gel. This silica gel was then used to perform automated flash chromatography using CombiFlash Rf system from Teledyne Isco. Using a solvent system of dichloromethane and methanol, the CombiFlash was successful in the removal of the TIPS from the reaction mixture and allowed for the purification of the product. The solvent was again removed from the system with a rotary evaporator at 38ºC. Final purified glycine monomer had a product yield of 0.596 g, 74%.

Isoleucine Monomer Synthesis

The protected isoleucine monomer was synthesized by coupling 4-vinylbenzoic acid ($C_9H_8O_2$; MW = 148.16 g/mol) to L-isoleucine t-butyl ester hydrochloride [H-Ile-OtBu·HCl; MW = 223.7 g/mol]. To perform this amino acid coupling reaction (**Scheme B5**), 0.511 g (3.4 mmol) of $C_9H_8O_2$, 0.764 g (3.4 mmol) of H-Ile-OtBu·HCl, 0.459 g (3.4 mmol) of 1-hydroxybenzotriazole (HOBT), 1.290 g (3.4 mmol) of O-benzotriazole-N,N,N'N'-tetra-

methyluronium hexafluorophosphate (HBTU) was added to 25 mL of dichloromethane (CH_2Cl_2). This reaction mixture was stirred under nitrogen at room temperature for 15 minutes before the addition of 1.15 mL (7 mmol) of N-ethyldiisopropylamine (iPr_2NEt).

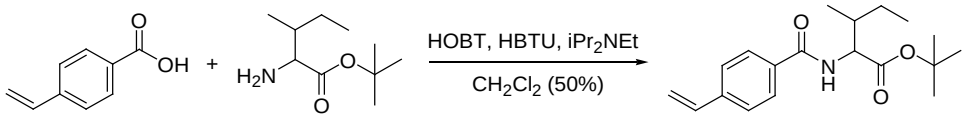

Scheme B5. Synthesis of protected isoleucine monomer.

This reaction was stirred under nitrogen at room temperature overnight. The next morning, the reaction was worked up by washing in a separation funnel. It was washed twice with distilled water, four times with 20% citric acid solution, and four times with 7% sodium bicarbonate. The remaining dichloromethane was dried over sodium sulfate and then removed with a rotary evaporator at 38ºC.

^{1}H NMR spectrum suggested it was clean enough for deprotection without further purification. Protected isoleucine monomer had a product yield of 0.544 g, 50%. ^{1}H NMR (400 MHz, CHLOROFORM-*d*) δ ppm 0.83 - 1.07 (m, 7 H) 1.18 - 1.36 (m, 1 H) 1.50 (s, 9 H) 2.00 (ddt, *J*=9.0, 6.8, 4.7, 4.7 Hz, 1 H) 4.71 (dd, *J*=8.2, 4.5 Hz, 1 H) 5.35 (d, *J*=10.9 Hz, 1 H) 5.83 (d, *J*=17.6 Hz, 1 H) 6.63 - 6.83 (m, 2 H) 7.46 (m, *J*=8.2 Hz, 2 H) 7.77 (m, *J*=8.2 Hz, 2 H). ^{13}C NMR (125 MHz, CHLOROFORM-*d*) δ ppm 11.74 15.32 25.51 28.04 38.49 57.00 82.28 115.90 126.24 127.28 133.27 135.89 140.73 166.60 171.26.

To deprotect, 0.544 g of protected isoleucine monomer was mixed with 10 mL trifluoroacetic acid (TFA) and 0.4 mL of triisopropylsilane (TIPS) under nitrogen at room temperature for 2 to 3 hours **(Scheme B6)**. The TFA was removed from the round-bottom flask with a rotary evaporator at 38ºC.

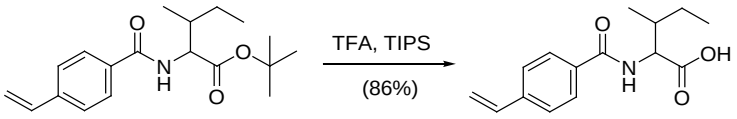

Scheme B6. Synthesis of de-protected isoleucine monomer.

The remaining mixture was dissolved in methanol (MeOH) and loaded into silica gel. This silica gel was then used to perform an automated flash chromatography with the CombiFlash Rf system from Teledyne Isco. A solvent system of dichloromethane and methanol was used with the CombiFlash to successfully remove the TIPS from the reaction mixture and allowed for separation of purified product. The solvent was again removed from the system using a rotary evaporator at 38ºC. Final purified isoleucine monomer had a product yield of 0.386 g, 86%.

Leucine Monomer Synthesis

The protected leucine monomer was synthesized by coupling 4-vinylbenzoic acid ($C_9H_8O_2$; MW = 148.16 g/mol) to leucine t-butyl ester hydrochloride [H-Leu-OtBu·HCl; MW = 223.7 g/mol]. To perform this coupling reaction (**Scheme B7**) 0.512 g (3.4 mmol) of $C_9H_8O_2$, 0.762 g (3.4 mmol) of H-Leu-OtBu·HCl, 0.462 g (3.4 mmol) of 1-hydroxybenzotriazole (HOBT), 1.290 g (3.4 mmol) of O-benzotriazole-N,N,N'N'-tetra-methyluronium hexafluorophosphate (HBTU) was added to 25 mL of dichloromethane (CH_2Cl_2). This reaction mixture was stirred under nitrogen at room temperature for 15 minutes before 1.2 mL (7 mmol) of N-ethyldiisopropylamine (iPr_2NEt) was added.

This reaction was stirred under nitrogen at room temperature overnight. The next morning, the reaction was worked up by washing in a separation funnel. It was washed twice

with distilled water, four times with 20% citric acid solution, and four times with 7% sodium bicarbonate. The remaining dichloromethane was dried over sodium sulfate and then removed with a rotary evaporator at 38ºC.

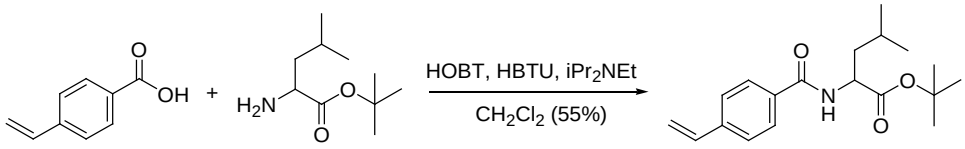

Scheme B7. Synthesis of protected leucine monomer.

^{1}H NMR spectrum suggested it was clean enough for deprotection without further purification. Protected leucine monomer had a product yield was 0.588 g, 55%. ^{1}H NMR (500 MHz, CHLOROFORM-*d*) δ ppm 0.99 (t, *J*=6.9 Hz, 6 H) 1.49 (s, 9 H) 1.58 - 1.68 (m, 1 H) 1.69 - 1.81 (m, 2 H) 4.71 - 4.79 (m, 1 H) 5.35 (d, *J*=10.9 Hz, 1 H) 5.83 (d, *J*=17.6 Hz, 1 H) 6.60 (d, *J*=7.8 Hz, 1 H) 6.74 (dd, *J*=17.8, 10.9 Hz, 1 H) 7.45 (m, *J*=7.8 Hz, 2 H) 7.76 (m, *J*=8.0 Hz, 2 H). ^{13}C NMR (125 MHz, CHLOROFORM-*d*) δ ppm 22.28 22.83 25.06 28.01 42.23 51.70 82.09 115.90 126.26 127.30 133.24 135.94 140.72 166.45 172.50.

To deprotect, 0.700 g of protected leucine monomer was mixed with 15 mL trifluoroacetic acid (TFA) and 0.6 mL of triisopropylsilane (TIPS) under nitrogen at room temperature for 2 to 3 hours **(Scheme B8)**. The TFA was removed from the round-bottom flask with a rotary evaporator at 38ºC.

The remaining mixture was dissolved in methanol (MeOH) and loaded into silica gel. This silica gel was then used to perform automated flash chromatography using CombiFlash Rf system from Teledyne Isco. A solvent system of dichloromethane and methanol was used with the CombiFlash to successfully remove the TIPS from the reaction mixture and allowed for the

purification of the product. The solvent was again removed from the system using a rotary evaporator at 38ºC. Final purified leucine monomer had a product yield of 0.379 g, 66%.

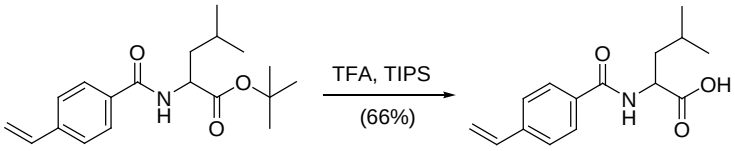

Scheme B8. Synthesis of de-protected leucine monomer.

Phenylalanine Monomer Synthesis

The protected phenylalanine monomer was synthesized by coupling 4-vinylbenzoic acid ($C_9H_8O_2$; MW = 148.16 g/mol) to L-phenylalanine t-butyl ester hydrochloride [H-Phe-OtBu·HCl; MW = 257.76 g/mol]. This coupling reaction (**Scheme B9**) was performd with the addition of 1.037 g (7 mmol) of $C_9H_8O_2$, 1.804 g (7 mmol) of H-Phe-OtBu·HCl, 0.949 g (7 mmol) of 1-hydroxybenzotriazole (HOBT); 2.648 g (7 mmol) of O-benzotriazole-N,N,N'N'-tetramethyluronium hexafluorophosphate (HBTU) to 25 mL of dichloromethane (CH_2Cl_2). The reaction mixture was stirred under nitrogen at room temperature for 15 minutes before 2.4 mL (14 mmol) of N-ethyldiisopropylamine (iPr_2NEt) was added.

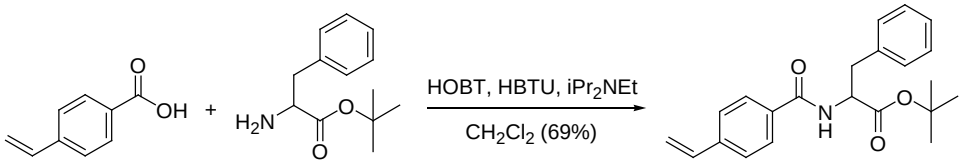

Scheme B9. Synthesis of protected phenylalanine monomer.

This reaction was stirred under nitrogen at room temperature overnight. The next morning, the reaction was worked up by washing with a separation funnel. It was washed once with 15% brine, twice with distilled water, four times with 20% citric acid solution, and four

times with 7% sodium bicarbonate. The dichloromethane was dried over sodium sulfate and then removed using a rotary evaporator at 38ºC.

The crude protected compound was then dissolved in methanol (MeOH) and loaded into silica gel. This silica gel was used to perform an automated flash chromatography with the CombiFlash Rf system from Teledyne Isco. A solvent system of dichloromethane and methanol (R_f = 0.9% dichloromethane/10% methanol) was used with the CombiFlash for successful purification. The solvent was removed from the system using a rotary evaporator at 38ºC. Final purified protected phenylalanine monomer had a product yield of 1.699 g, 69%. ^{1}H NMR (300 MHz, CHLOROFORM-*d*) δ ppm 1.35 - 1.40 (m, 2 H) 1.44 (s, 9 H) 3.24 (d, *J*=5.8 Hz, 2 H) 4.91 - 5.01 (m, 1 H) 5.36 (d, *J*=11.0 Hz, 1 H) 5.84 (d, *J*=17.6 Hz, 1 H) 6.64 (d, *J*=7.1 Hz, 1 H) 6.74 (dd, *J*=17.6, 10.7 Hz, 1 H) 7.22 - 7.31 (m, 5 H) 7.45 (d, *J*=8.2 Hz, 2 H) 7.71 (d, *J*=8.2 Hz, 2 H).

To deprotect, 1.699 g of protected phenylalanine monomer was mixed with 10 mL trifluoroacetic acid (TFA) and 0.5 mL of triisopropylsilane (TIPS) under nitrogen at room temperature for 3 to 4 hours **(Scheme B10)**. The TFA was removed from the round-bottom flask with a rotary evaporator at 38ºC.

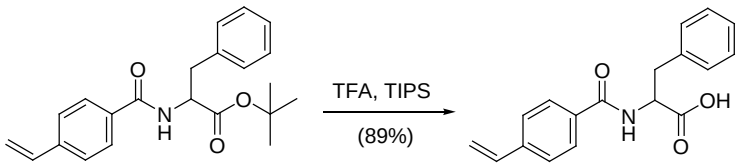

Scheme B10. Synthesis of de-protected phenylalanine monomer.

The remaining mixture was dissolved in methanol (MeOH) and loaded into silica gel. This silica gel was used to perform automated flash chromatography with the CombiFlash Rf system from Teledyne Isco. A solvent system of dichloromethane and methanol (R_f = 0.1; 90% dichloromethane/10% methanol) was used with the CombiFlash to successfully remove the TIPS

from the reaction mixture and allowed for purification of the product. The solvent was removed from the system with a rotary evaporator at 38ºC. Final purified phenylalanine monomer had a product yield of 1.266 g, 89%. It polymerizes above 185ºC. ^{1}H NMR (500 MHz, DMSO-d_6) δ ppm 3.08 (d, *J*=10.8 Hz, 1 H) 3.17 (d, *J*=4.1 Hz, 1 H) 4.61 (ddd, *J*=10.6, 8.1, 4.6 Hz, 1 H) 5.36 (d, *J*=11.0 Hz, 1 H) 5.94 (d, *J*=17.6 Hz, 1 H) 6.77 (dd, *J*=17.9, 11.0 Hz, 1 H) 7.15 - 7.19 (m, 1 H) 7.24 - 7.32 (m, 4 H) 7.54 (m, *J*=8.2 Hz, 2 H) 7.77 (m, *J*=8.2 Hz, 2 H) 8.69 (d, *J*=8.2 Hz, 1 H).

Proline Monomer Synthesis

The protected proline monomer was synthesized by coupling 4-vinylbenzoic acid ($C_9H_8O_2$; MW = 148.16 g/mol) to L-proline t-butyl ester hydrochloride [H-Pro-OtBu·HCl; MW = 207.7 g/mol]. To perform this amino acid coupling reaction (**Scheme B11**) we added 1.038 g (7 mmol) of $C_9H_8O_2$, 1.451 g (7 mmol) of H-Pro-OtBu·HCl, 0.948 g (7 mmol) of 1-hydroxybenzotriazole (HOBT), 2.660 g (7 mmol) of O-benzotriazole-N,N,N'N'-tetramethyluronium hexafluorophosphate (HBTU) was added to 25 mL of dichloromethane (CH_2Cl_2). This reaction mixture was stirred under nitrogen at room temperature for 15 minutes before 2.4 mL (14 mmol) of N-ethyldiisopropylamine (iPr_2NEt) was added.

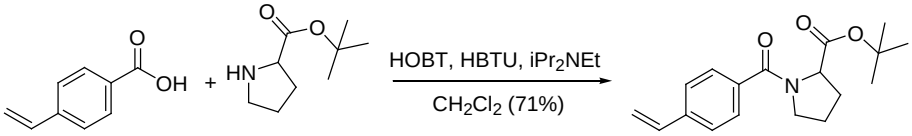

Scheme B11. Synthesis of protected proline monomer.

This reaction was stirred under nitrogen at room temperature overnight. The next morning, the reaction was worked up by washing in a separation funnel. It was washed once with 15% brine, twice with distilled water, four times with 20% citric acid solution, and four

times with 7% sodium bicarbonate. The remaining dichloromethane was dried over sodium sulfate and removed with a rotary evaporator at 38ºC.

^{1}H NMR spectrum suggested it need further purification. The crude protected compound was dissolved in methanol (MeOH) and loaded into silica gel. This silica gel was used to perform an automated flash chromatography with a CombiFlash Rf system from Teledyne Isco. A solvent system of dichloromethane and methanol (R_f= 0.9% dichloromethane/10% methanol) was used with the CombiFlash to successfully purify the product. The solvent was removed from the system with a rotary evaporator at 38ºC. Final purified protected proline monomer had a product yield of 1.499 g, 71%.

To deprotect the protected proline monomer, 1.499 g of protected proline monomer was mixed with 10 mL trifluoroacetic acid (TFA) and 0.4 mL of triisopropylsilane (TIPS) under nitrogen gas at room temperature for 3 to 4 hours **(Scheme B12)**. The TFA was removed from the round-bottom flask with a rotary evaporator at 38ºC.

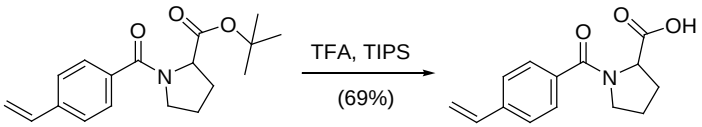

Scheme B12. Synthesis of de-protected proline monomer.

The remaining mixture was dissolved in methanol (MeOH) and loaded into silica gel. This silica gel was used to perform automated flash chromatography with the CombiFlash Rf system from Teledyne Isco. A solvent system of dichloromethane and methanol (R_f = 0.1; 90% dichloromethane/10% methanol) was used with the CombiFlash and was successful in TIPS removal from the reaction mixture and allowed for purification of the product. The solvent was

removed from the system with a rotary evaporator at 38ºC. Final purified proline monomer had a product yield of 0.846 g, 69%.

Valine Monomer Synthesis

The protected valine monomer was synthesized by coupling 4-vinylbenzoic acid ($C_9H_8O_2$; MW = 148.16 g/mol) to L-valine t-butyl ester hydrochloride [H-Val-OtBu·HCl; MW = 209.7 g/mol]. To perform this coupling reaction (**Scheme B13**) was performed by addition of 1.038 g (7 mmol) of $C_9H_8O_2$, 1.470 g (7 mmol) of H-Val-OtBu·HCl, 0.952 g (7 mmol) of 1-hydroxybenzotriazole (HOBT), 2.660 g (7 mmol) of O-benzotriazole-N,N,N'N'-tetramethyluronium hexafluorophosphate (HBTU) to 25 mL of dichloromethane (CH_2Cl_2). This reaction mixture was stirred under nitrogen at room temperature for 15 minutes before 2.4 mL (14 mmol) of N-ethyldiisopropylamine (iPr_2NEt) was added.

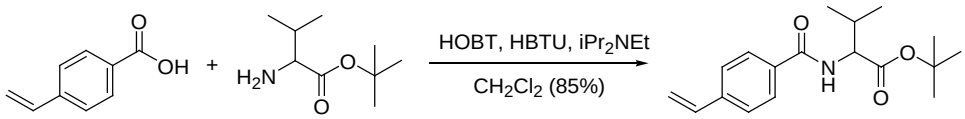

Scheme B13. Synthesis of protected valine monomer.

This reaction was stirred under nitrogen at room temperature overnight. The next morning, the reaction was worked up by washing in a separation funnel. It was washed once with 15% brine, twice with distilled water, four times with 20% citric acid solution, and four times with 7% sodium bicarbonate. The remaining dichloromethane was dried over sodium sulfate and removed with a rotary evaporator at 38ºC.

^{1}H NMR spectrum suggested it need further purification. The crude protected compound was dissolved in methanol (MeOH) and loaded into silica gel. This silica gel was then used to

perform an automated flash chromatography with the CombiFlash Rf system from Teledyne Isco. A solvent system of dichloromethane and methanol (R_f = 0.9% dichloromethane/10% methanol) was used with the CombiFlash and successfully separated the purified product. The solvent was removed from the system with the rotary evaporator at 38ºC. The final purified protected valine monomer had a product yield of 1.797 g, 85%.

To deprotect, 0.915 g of protected valine monomer was mixed with 10 mL trifluoroacetic acid (TFA) and 0.5 mL of triisopropylsilane (TIPS) under nitrogen at room temperature for 3 to 4 hours **(Scheme B14)**. The TFA was removed from the round-bottom flask with a rotary evaporator at 38ºC.

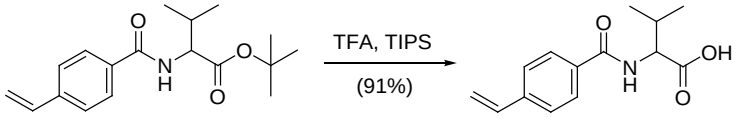

Scheme B14. Synthesis of de-protected valine monomer.

The remaining mixture was dissolved in methanol (MeOH) and loaded into silica gel. This silica gel was then used to perform automated flash chromatography using CombiFlash Rf system from Teledyne Isco. A solvent system of dichloromethane and methanol (R_f = 0.1; 90% dichloromethane/10% methanol) was used with the CombiFlash to successfully remove the TIPS from the reaction mixture and allowed for the purification of the product. The solvent was removed from the system with a rotary evaporator at 38ºC. Final purified valine monomer had a product yield of 0.679 g, 91%. It polymerizes above 170ºC.

Ethylamine Monomer Synthesis

A solution of 4-vinylbenzoic acid (1.333 g, 3 mmol), ethanolamine (0.550 g, 9 mmol), BOP (3.981 g, 9 mmol), N,N-diisopropyletthylamine (2.908 g, 22.5 mmol) in dichloromethane was stirred under nitrogen at room temperature for 3 hours (**Scheme B15**). Solvent was then removed under reduced pressure. The product was purified using automated flash chromotrography over silica gel using dichloromethane/methanol (R_f= 0.5; 90% dichloromethane/10% methanol) as the mobile phase. Final purified ethylamine monomer had a product yield of 0.265 g, 40%. mp: 119-122ºC. ^{1}H NMR (400 MHz, DMSO-d_6) δ ppm 3.26 - 3.37 (m, 2 H) 3.51 (q, *J*=6.0 Hz, 2 H) 4.75 (t, *J*=5.5 Hz, 1 H) 5.35 (d, *J*=11.1 Hz, 1 H) 5.93 (d, *J*=17.8 Hz, 1 H) 6.77 (dd, *J*=17.6, 10.9 Hz, 1 H) 7.54 (d, *J*=8.2 Hz, 2 H) 7.84 (d, *J*=8.2 Hz, 2 H) 8.43 (t, *J*=5.0 Hz, 1 H). ^{13}C NMR (125 MHz, DMSO-d_6) δ ppm 42.30 59.82 116.43 126.17 127.77 133.82 136.10 139.94 166.38.

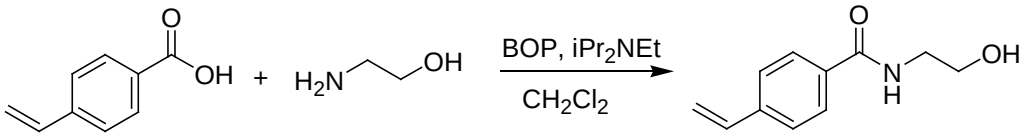

Scheme B15. Synthesis of ethanolamine monomer.